11-1-2007

On the plasma induced degradation of organosilicate glass (OSG) as an interlevel dielectric for sub 90 nm CMOS

Amy Huang

On the Plasma Induced Degradation of Organosilicate Glass (OSG) as an Interlevel Dielectric for Sub 90 nm CMOS

By Amy Huang

A Thesis Submitted in

Partial Fulfillment

of the Requirements for the Degree of

Masters of Science

In Materials Science

Approved by:

Professor _____

Dr. KSV Santhanam

Professor _____

Dr. Santosh Kurinec

Professor _____

Dr. Karl Hirschman

External Advisor _____

Phil Hecker DMOS 6 Plasma Manager

Department of Materials Science

College of Science

Rochester Institute of Technology

Rochester, New York

November 2007

Preface

When there's a will, there's a way. My thirst for innovation is signified by this simple slogan. I once believed that the technological world was about solely inventing something revolutionary but maturity and modern times emphasize synergy as a requirement to achieve one's goals of innovation. No one person may claim absolute greatness for it is the sum of bits and pieces of what everyone contributes that equate to greatness. With that message delivered, I'd like to thank all the people who made this thesis research possible: my manager Phil Hecker for being a great resource, Terry Richardson for helping me take the initiative to work on these experiments, and DMOS6 as a whole in Texas Instruments for allowing me to using the top of the line semiconductor equipment and process flow analysis methods to obtain my goals. I'd also like to thank Dr. Santosh Kurinec, Dr. KSV Santhanam, and Dr. Karl Hirschman at Rochester Institute of Technology for supporting my external studies. My parents and husband have also influenced me to strive and think outside of the box. This list almost feels infinite because everyone I've encountered in my life has had some impact on my existence, great or small. The journey I took to write something of my very own has been very fulfilling.

Study of Low-K Back End of Line OSG Film Degradation Through Resist Strip and Clean

I, Amy Huang, hereby grant permission to the Wallace Memorial Library, of the Rochester Institute of Technology, to reproduce my thesis, in whole or in part, with the knowledge that any reproduction will not be for commercial use or profit.

Student _____

Amy Huang

Abstract

The fabrication of integrated circuits (ICs) in a semiconductor manufacturing environment is governed by two main categories: Front End of the Line (FEOL) processing and Back End of the Line (BEOL) processing. Transistors are formed in active regions in FEOL while BEOL processing focuses on creation of metal interconnects and interlevel dielectrics (ILDs). These dielectrics patterned in BEOL are required to have low permittivity or *k* values in order to mitigate parasitic capacitance. This reduction in capacitance between metal layers diminishes dynamic power dissipation, crosstalk noise, and interconnect delay issues as IC technology nodes continue to scale down in size. Dielectric constants between 2.0 to 2.7 are required for sub 90nm CMOS technology. Organosilicate glass (OSG) has been chosen as a candidate in this thesis study due to its *k* value being within the required range. OSG film was deposited on pilot wafers via Plasma Enhanced Chemical Vapor Deposition (PECVD) using a reaction between organosilane and oxygen gases. A challenge that has been identified in patterning OSG as an interlevel dielectric film occurs during the photoresist removal or ash process. Two types of plasma ash chemistries have been used to test OSG film integrity: O_2 and H_2Ar. The quality of OSG film is compromised due to plasma damage observed by carbon depletion or hydrogen species. Pre- and post-resist removal of OSG film composition has been characterized using materials analytic methods such as Fourier Transform Infrared (FTIR) spectrometry, X-ray Photoelectron Spectroscopy (XPS), Dynamic Secondary Ion Mass Spectrometry (DSIMS), and Surface Photovoltage (SPV). Wafer test chips were also fabricated and probed at Metal 1 and Metal 2 levels for serpentine line resistances and comb capacitances to characterize the performance of the OSG film as an ILD. The H_2Ar plasma chemistry has been proven to be a better candidate for maintaining OSG composition.

Table of Contents

List of Figures

List of Acronyms

BEOL (Back End of Line)

CMOS (Complimentary Metal Oxide Semiconductor)

DSIMS (Dynamic Secondary Ion Mass Spectrometry)

FEOL (Front End of Line)

FTIR (Fourier Transform Infrared Spectrometry)

ILD (Interlevel Dielectric)

1. Introduction

1.1 Background

In the semiconductor industry, the development of new IC technology using single and dual-damascene (Fig. 1) [1] processes involves the process integration of a difficult and critical step of copper interconnects and low-k dielectrics. New materials used in interconnect layers are essential for achieving the higher speed operations that are required for advanced computing and communications applications. Copper serves as a better conductor than aluminum and the interline capacitance of low-k materials is lower than that of silicon dioxide [2]. The combination of lower resistance from copper metal lines and the lower capacitance from low-k dielectrics has greatly reduced the RC delay in interconnect circuitry allowing further reduction in geometry without a loss in performance. RC delay caused by interconnects plays a major role in device performance.

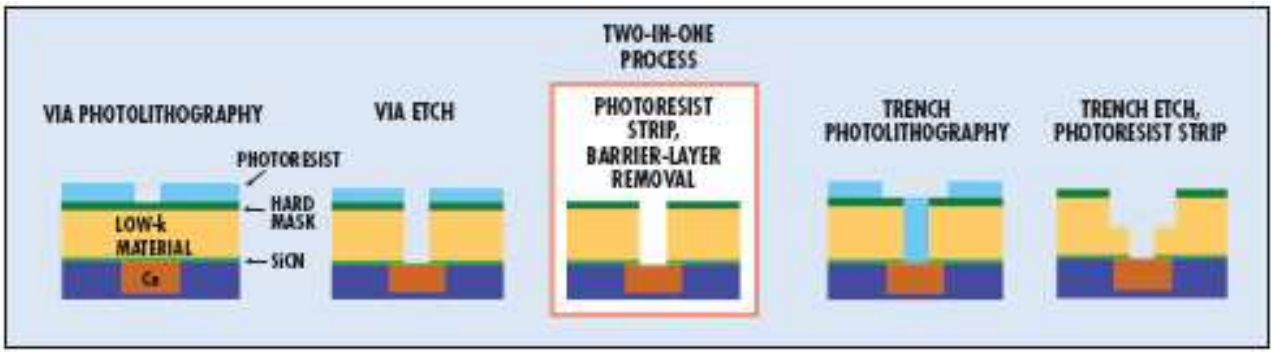

Figure 1. Dual Damascene Process Flow [1]

For the 65 nm generation and on, various studies show that dielectric constants of $k < 3.0$ are required to reduce this delay [1-15]. The demands of decreasing chip size and fabricating higher speed chips are answered by fabricating smaller transistors and placing them closer together. Thus the insulating dielectric layers between metal interconnects of the same layer

become thinner and thinner laterally. Low-k dielectrics such as OSG films are required for faster clock speeds, reducing cross-talk and parasitic capacitance, lower power consumption, and lower heat dissipation to enable faster switching speeds [3]. Dielectric materials with lower k values are porous making their insulating properties closer to air. This attribute, however, makes them more susceptible to modification by plasma etching and photoresist stripping. There is also very little published data on the microstructure study of organic low-k materials.

1.2 Thesis Research at Texas Instruments

Two parts of the copper/low-k integration process such as stripping photoresist and cleaning wafers without damaging the low-k materials, have been significant challenges. Advanced 300mm semiconductor facilities have met this challenge in production, and work has progressed on the development of next generation ultra-low-k dielectrics (particularly nanoporous materials) to further reduce the dielectric constant [4].

OSG film degradation after resist strip has been characterized using various analytic film techniques provided by Texas Instruments. A lot of 24 test chip wafers using several resist strip and wafer clean methods was processed based on the observations noted from film composition of OSG pilot wafers to define a process window in the low-k integration process. Analysis of electrical data in the Metal 1 and 2 layers are included as a direct comparison to the realization of these process parameters.

2. Theory

2.1 Current Low-K Photoresist Strip and Clean Options for OSG Films

During photolithography, a layer of film is patterned after photoresist deposition to define topography. When resist is no longer needed after etch, it is stripped inside a plasma chamber. Studies have shown that the quality of resist removal generally depends on power, pressure, temperature, gas flows, and time [1-8]. The gas species inside the chamber react with the resist that is exposed to downstream plasma. The reactive species, usually oxygen and fluorine, recombine with resist forming ash bi-products which are then removed through a vacuum pump.

Plasma damage that is incorporated into the low-k films raises the overall dielectric constant of the film. There are currently several popular low-k PR strip options available in industry and development research including exsitu low temperature/low pressure O_2 ash [2,3], exsitu high temperature/high pressure H based ash [4], H and N resist strip options [5], exsitu high pressure/high temperature H based resist strip with a low amount of O_2 [6], insitu low temperature/low pressure O_2 ash [7]. O_2 is known to deplete carbon and thus two approaches are taken: a H_2Ar based ash at higher temperatures without O_2 and a low temperature/low pressure O_2 based ash, where the lower pressure/temperature is used to reduce carbon depletion. The H_2Ar process was patented at Texas Instruments by Patricia Smith and Phillip Matz of the SiTD group [8]. Low ambient temperatures are typically used to prevent damage of porous low-k materials.

Once resist stripping is complete, the wafer requires a clean step to remove residual particles left from the ash process. The two options that were tested are batch and single wafer cleans. Both cleans have fluoride containing chemistries formulated for removal of inorganic

and highly oxidized etch residues and controlled etching of contaminated oxide surfaces. Clean processing may sometimes, though rarely, cause mechanical damage such as OSG cracking [9].

2.2 OSG Film

In the semiconductor industry, a low-k film is designed to have low density and porosity is also introduced. Organosilicate glass (OSG) is a popular candidate for back-end low-k dielectrics because of its terminal CH_3 groups that cannot network. OSG films can deliver k values lower than 2.7 [10-17]. They are generally deposited via PECVD. The molecular structure is displayed in Figure 2.

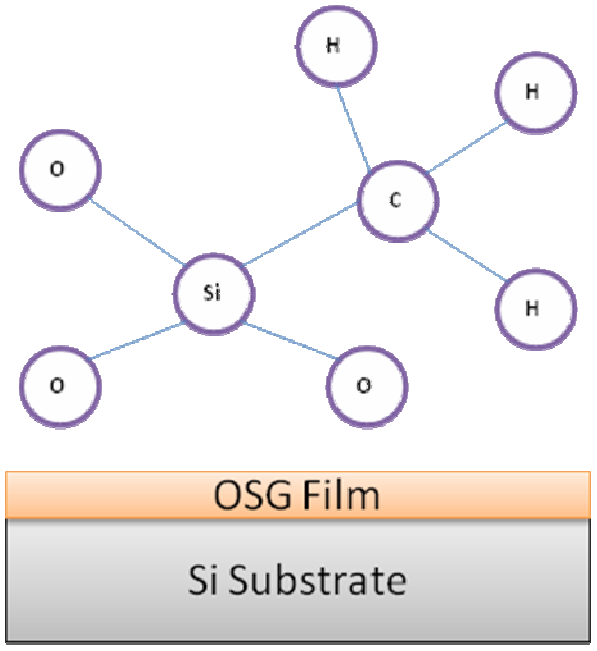

Figure 2. Schematic of OSG deposited film on Si and its molecular structure

2.3 Film Characterization Methods

2.3.1 Dynamic Secondary Ion Mass Spectrometry (DSIMS)

SIMS is a valuable analytical technique that has developed into an established method for characterizing semiconductors. Some advantages regarding the applications of SIMS in the semiconductor industry include surveying implanted dopant profile, determination of doping composition, location of trace contaminants across device features, and identification of inorganic contaminants [18-20].

The technique can be used to analyze any element and its isotope in the periodic table. It has a relatively high sensitivity (10^{14} – 10^{18} cm^{-3}) depending on the element being analyzed. SIMS also has good lateral resolution of about 1 µm. However, some disadvantages include complex instrumentation, its destructive nature of testing, and the requirement of calibration standards for quantitative estimation [19]. Another disadvantage present is the dependence of the secondary ion yield on the matrix of the sample. This effect, known as the matrix effect, can cause the secondary ion signal from the same element in different matrices to be different. Matrix effects can complicate quantitative estimation of the impurity species in the sample.

In SIMS, a primary ion beam is incident upon a sample. The ions used for the primary beam may be argon, cesium, or oxygen, and the energies are typically in the 1-30 keV range [20]. This causes material to be sputtered off the surface of the sample. Most of the sputtered material is composed of neutral atoms, and these are lost and go undetected. However, a small fraction (about 1%) of the ejected material is in the form of either positive or negative ions. These ions, called secondary ions, of either polarity are then extracted and analyzed by passing them through a mass spectrometer. The analyzed ion signal is then recorded and both the substrate and

contaminant atoms of the sample at the primary beam location can be analyzed. Figure 3 [18] is a schematic of a SIMS instrument and its components.

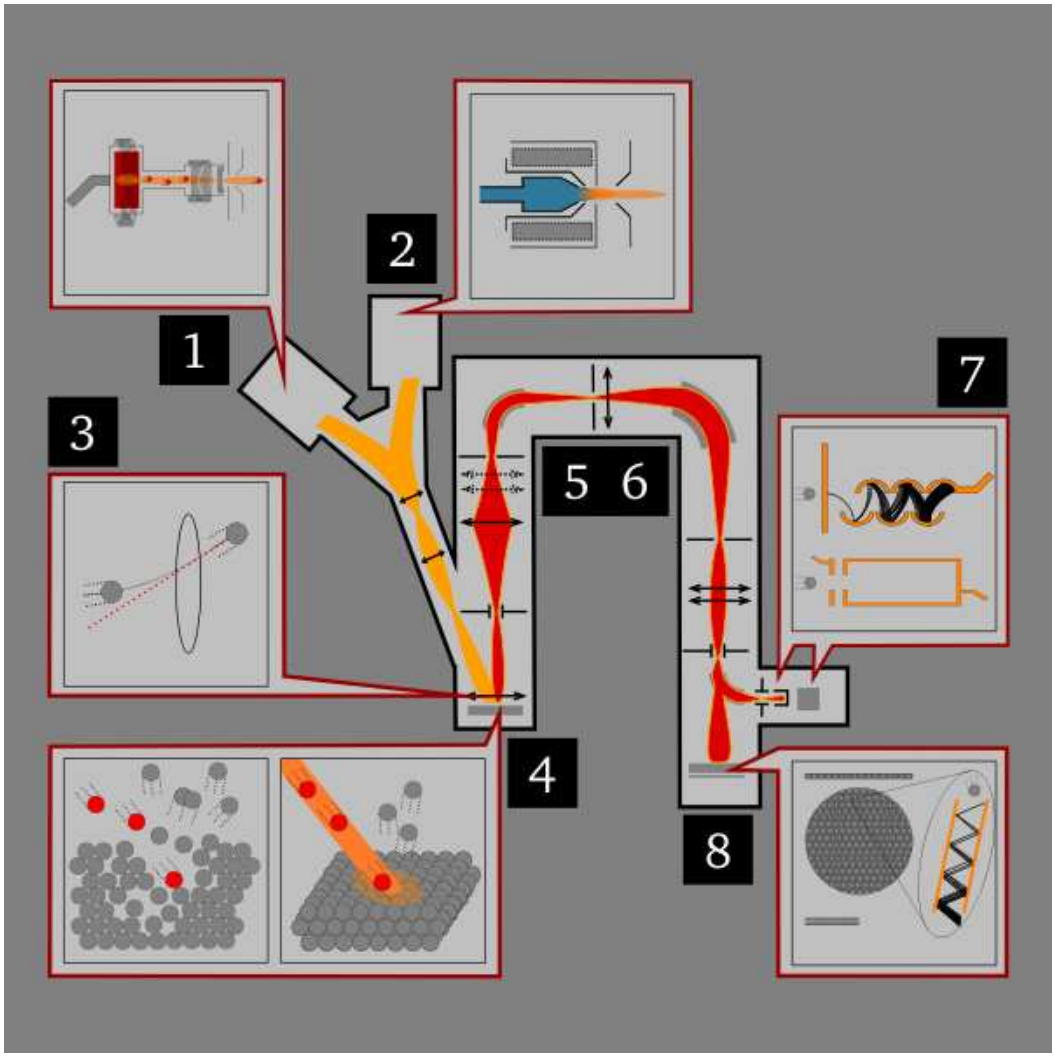

Figure 3. Schematic of a SIMS Instrument: 1) Cesium ion source. 2) Duoplasmatron. 3) Electrostatic lens. 4) Sample. 5) Electrostatic sector - ion energy analyzer. 6) Electromagnet - mass analyzer. 7) Electron multiplier / Faraday cup. 8) Channel-plate / Fluorescent screen - ion image detector. [18]

SIMS can be operated in three modes: static, dynamic, and imaging. In order to obtain a depth profile, dynamic mode (DSIMS) was used [18]. The sputtering rate is approximately 10 µm/hr and causes erosion of the sample where a crater develops at the primary beam location [20]. The depth of the crater correlates to the sputtering time. The mass spectrometer is locked

on to a single mass-to-charge ratio, and the analyzed ion signal intensity is monitored as a function of sputtering time. One of the main applications of DSIMS is the analysis of trace element depth distribution (i.e. dopants in semiconductors). Impact ion energy is adjusted depending on the applications. Low energy (down to 200-300 eV) is used to reduce atomic mixing due to the collision cascade and improve depth resolution to the nanometer level whilst high energy (up to 20-30 keV) is chosen to go deeper (10-20 microns), faster (µm/min), and improve detection limits and image resolution [18]. DSIMS is the preferred method in analyzing the composition of OSG post-ash and clean processes.

2.3.2 Fourier Transform Infrared Spectroscopy (FTIR)

In FTIR, infrared radiation is passed through an analyzed sample. Some of the infrared radiation is absorbed by the sample and also transmitted. The resulting spectrum represents the molecular absorption and transmission, creating a molecular blueprint of the sample. Like a fingerprint, no two unique molecular structures produce the same infrared spectrum. This attribute makes FTIR useful for several types of analysis. FTIR can identify bond peaks of unknown materials, determine the quality or consistency of a sample, and determine the amount of components in a mixture [21].

When converting spectra from time domain to frequency domain in FTIR, the following equation is used:

$$S(t) = \int_{-\infty}^{\infty} I(\nu)\, e^{-i\nu 2\pi t}\, d\nu$$

Equation 1

Where *t* represents time, *I* is the intensity, and *v* is wavenumber. The sum is performed over all contributing frequencies to a given signal *S(t)* in the time domain.

$$I(v) = 2Re \int_{-\infty}^{\infty} S(t)\, e^{2i\pi vt}\, dt$$

Equation 2

Gives non-zero value when *S(t)* contains a component that matches the oscillating function.

An optical device called an interferometer that measures infrared frequencies was developed in order to overcome the limitations of a slow scanning process. It produces a unique type of signal which has all of the infrared frequencies "encoded" into it. The signal is then measured very quickly, usually on the order of one second. Thus the time element per sample is reduced from several minutes to a few seconds [22].

Most interferometers employ a beamsplitter which divides the incoming infrared beam into two optical beams [23]. One beam reflects off a flat mirror which is fixed in place. The other beam reflects off a flat mirror on a mechanism which allows this mirror to move a very short distance (typically a few mm) away from the beamsplitter. Because the path that one beam travels is a fixed length and the other is constantly changing as its mirror moves, the signal which exits the interferometer is the result of these two beams "interfering" with each other. The resulting signal is called an interferogram which has the unique property that every data point (a function of the moving mirror position) up the signal has information about every infrared frequency that comes from the source. A standard spectrometer layout is show in Figure 4 [22].

A plot of the intensity at each individual frequency or frequency spectrum is required in order to make identify a sample since the measured interferogram signal cannot be interpreted

directly. Decoding the individual frequencies is accomplished via Fourier transformation, which is performed by a computer that produces the desired spectral information for analysis.

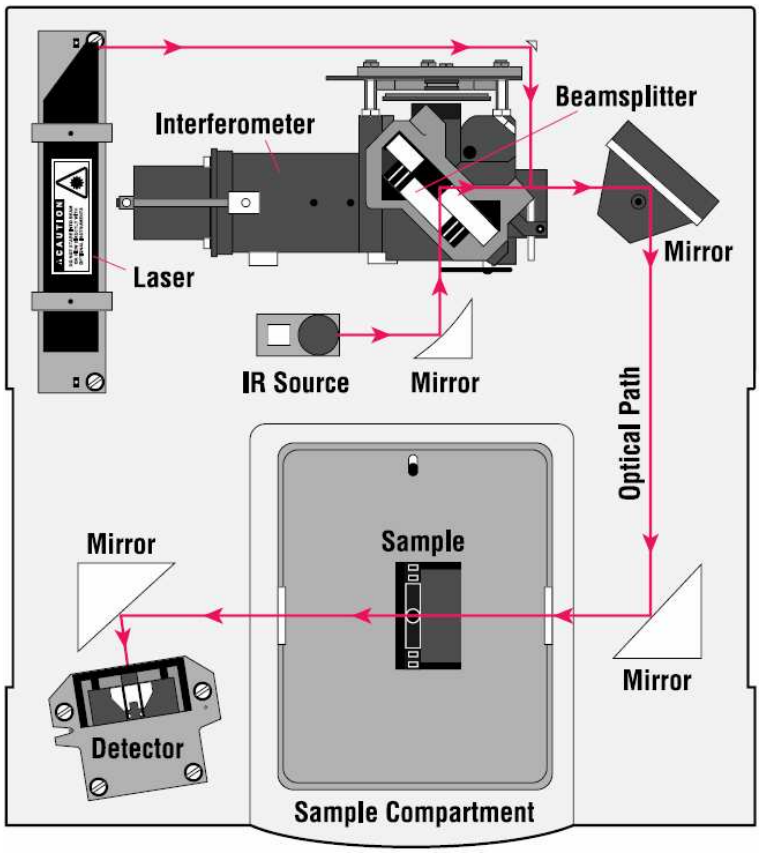

Figure 4. Simple FTIR spectrometer layout [22]

Some advantages of FTIR include speed, sensitivity, mechanical simplicity, and self-calibration. Measurements made by FTIR are extremely accurate and reproducible due to these advantages. Thus, it is a very reliable technique for identification of virtually any sample. The sensitivity benefits enable identification of even the smallest contaminants. A lot of 24 OSG3 and OSG4 pilots are analyzed with FTIR to find refractive indices and dielectric constant post-deposition.

2.3.3 X-ray Photoelectron Spectroscopy (XPS)

XPS is a method used to determine various elements and their quantities present within 10 nm of the sample surface, the density of electron states, binding energies, and the existence of contamination that exists on a sample. The energy of an X-ray wavelength can be used to excite an electron to determine the electron binding energy of emitted electrons using the equation:

$$E_{binding} = E_{photon} - E_{kinetic} - \emptyset \quad \text{Equation 3}$$

where $E_{binding}$ is the energy of the electron emitted from one electron configuration within an atom, E_{photon} is the energy of the X-ray photons being used, $E_{kinetic}$ is the kinetic energy of the emitted electron as measured by the instrument, and $\emptyset$ is the work function of the spectrometer. Raw XPS signals are converted to atomic values through dividing signal intensity by a relative sensitivity factor (RSF) and normalized over every elemented detected.

A typical XPS system consists of a moderate vacuum sample introduction chamber, a sample stage, sample mounts, a set of stage manipulators, a source of X-rays, an ultra-high vacuum (UHV) chamber with UHV pumps, an electron energy analyzer, an electron collection lens, a moderate vacuum sample introduction chamber, and a magnetic field shielding [24]. Figure 5 demonstrates the schematic of a typical XPS system.

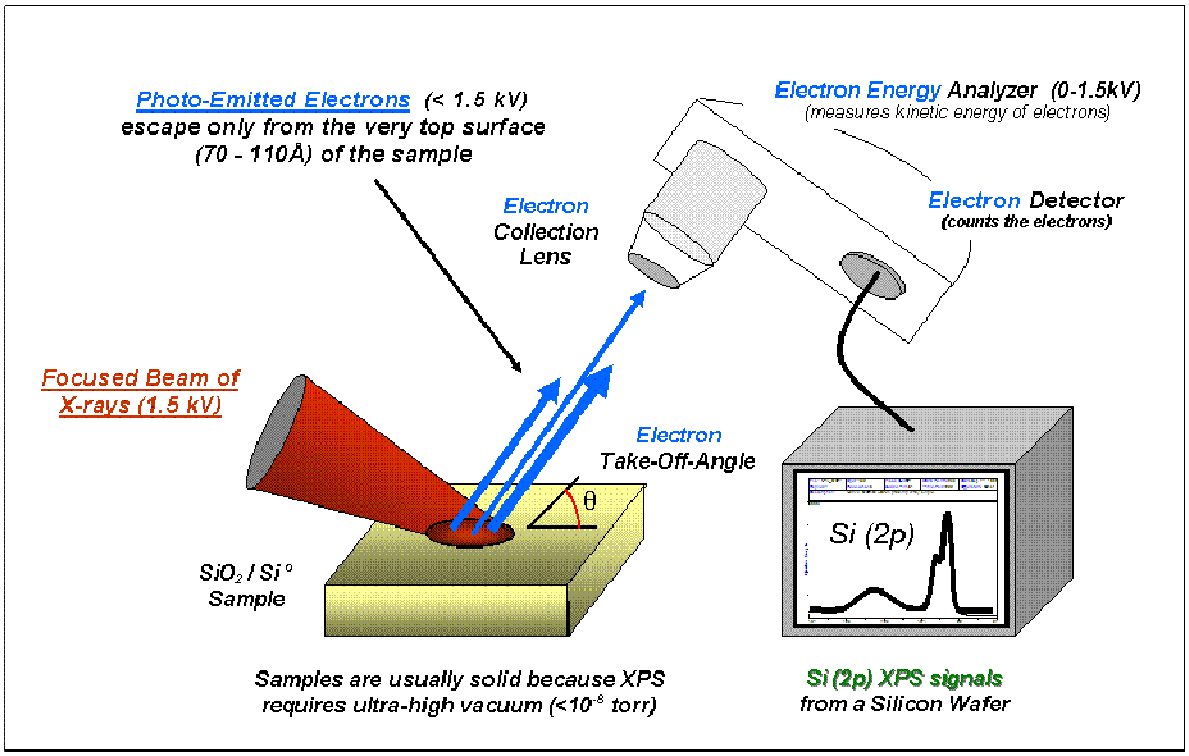

Figure 5. Schematic of an XPS System [24]

XPS is limited in that it cannot detect hydrogen or helium elements. The detection limit for most elements is within the parts per thousands range. With ideal samples and operation conditions, a quantitative accuracy of atom percent values close to 95% may be achieved. Parameters such as correction for electron transmission function, correction for energy dependency of electron mean free path, surface volume homogeneity, signal to noise ratio, accuracy of relative sensitivity factors, and degree of sample degradation may all affect the quantitative accuracy. In terms of determining OSG film composition, elements such as nitrogen, fluorine, oxygen, silicon, and carbon are expected to be found inside the film. However, its inability to detect hydrogen content is somewhat of a hindrance in characterizing OSG films.

2.3.4 Surface Photovoltage

Surface photovoltage is a method used in the semiconductor industry for detecting the surface potential of a semiconductor through the use of a light source that acts as an illumination [25-27]. Electron-hole pairs are produced from the bulk of the semiconductor diffuse through to the surface depletion region. This diffusive process is determined by the following expression:

$$L = \sqrt{D\tau_{bulk}} \qquad \text{Equation 4}$$

where L is the diffusion length, D is the diffusion coefficient, and τ_{bulk} is the bulk carrier lifetime. This expression is adjusted in a real semiconductor in the next two expressions:

$$L_{meas} = \sqrt{D\tau_{eff}} \qquad \text{Equation 5}$$

$$\frac{1}{\tau_{eff}} = \frac{1}{\tau_{bulk}} + \frac{2}{d} \qquad \text{Equation 6}$$

where τ_{eff} is the effective carrier lifetime, s is the surface recombination velocity, and d is the film or wafer thickness. The electric field inside a film or semiconductor layer is expressed by

$$E = \frac{eN}{\epsilon} \qquad \text{Equation 7}$$

where e is the charge of an electron, N is the dipole density, and ε is the dielectric constant. The surface voltage of a film is determined by

$$|\Delta\emptyset_s| = Ed(cos(\theta)) \qquad \text{Equation 8}$$

where *d* is the film thickness. Equations 5 and 6 may be combined to form:

$$\Delta \emptyset_s = Ned(cos(\theta))$$ Equation 9

Through this methodology, the dielectric constant can be extrapolated with SPV measurements.

Figure 6 represents a schematic of a SPV tool. A light source is illuminated and scanned upon a monochromator. A chopper is used to filter the light source onto the wafer surface whilst it sits on a grounded stage with a kelvin probe is positioned above it. The kelvin probe observes the work function of the surface and captures the catalytic activity that occurs on the atomic level. The lock-in amplifier measures the contact potential as the kelvin probe inputs data that is referenced out through the chopper.

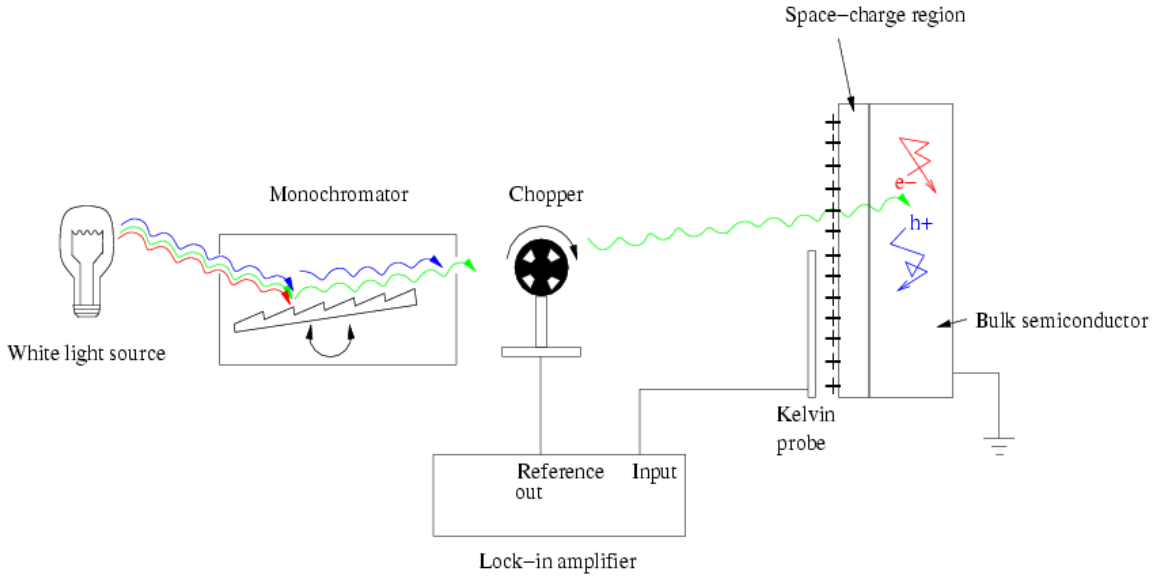

Figure 6. Schematic of a SPV tool [25]

2.4 Electrical Data

Serpentine line and comb test structures can be designed for analyzing the low-k film quality. Serpentine lines are used to measure Cu line resistance and trench dimensions. Combs are used to measure the capacitance of the low-k dielectric between Cu lines. Similar tests have

been performed by Xu et. Al. [28]. Via stress migration tests were also performed to test the voltage migration during an oven bake over a long period of time.

A Kelvin probe method used for device testing consists of a reference electrode tip suspended above and parallel to a stationary specimen electrode. Their positioning creates a simple capacitor and once an electrical contact is made between the two electrodes, their Fermi levels equalize. The resulting flow of electrons from metal with the lower work function produces a potential difference, V_{CPD} given by:

$$eV_{CPD} = \emptyset_{specimen} - \emptyset_{tip} \qquad \text{Equation 10}$$

Where e is the electron charge, $\emptyset_{specimen}$ is the work function of the stationary electrode, and $\emptyset_{tip}$ is the work function of the tip electrode.

3. Pilot Wafer Tests

3.1 Investigation of a Post Etch Treatment Step

The birth of this thesis began with a preliminary investigation to remove surface polymer during the etch process. Bevel polymer buildup has been an issue in movable magnet etchers that still exists after an ash process. Bevel polymers can damage the surface edge integrity of a wafer, reducing the edge exclusion for fabricating devices. One possible solution is to have the problem contained before a wafer is processed at the next step.

Bare silicon pilots were used to run a DOE to see how a PET step, pins up, and ash time can affect the amount of polymer removal around the edge. The first pass experiment involved taking a qualitative approach using an edge inspection tool to capturing images around the edge

of the wafer. Theoretically, it was predicted that a longer PET step, longer pins up step, and ash time would decrease the amount of polymer. However, finding a treatment combination that takes the least amount of time for the polymer to clear was also important to investigate. The wafers were etched from 1 through 21 in that order. The pilot wafers were etched with longer PET steps last to reduce run order effects. The insitu-ash was performed in a movable magnet etcher. A standard O_2 ash recipe was processed with two varying factors: ash time and pins up or pins down. During the pins up step, the wafer was supported by three pins and elevated closer to the plasma for a more aggressive ash and better polymer edge removal. Table 1 describes how each wafer was processed with a varying PET step along with varied ash steps.

(a) Wafer	PET (sec)	Ash Recipe #
1	none	no ash
2	none	2
3	none	1
4	none	4
5	none	no ash
6	none	5
7	none	2
8	none	no ash
9	none	no ash
10	5	2
11	5	4
12	5	3
13	10	5
14	10	no ash
15	15	1
16	15	5
17	15	3
18	20	3
19	20	no ash
20	insitu Ash 20	1
21	insitu Ash 20	no ash

(b) Ash Recipe #	Ash Time (sec)	Pins Up (sec)
1	2	10
2	2	30

3	**180**	**0**
4	**180**	**10**
5	**180**	**30**

Table 1. (a) Shows how each wafer was processed and (b) describes the detailed ash steps.

An edge inspection tool was used to analyze the results of polymer edge buildup and removal of each wafer depending on the process conditions. Edge images were taken at 0° (at notch), 90°, 180°, and 270° to obtain comparable inspections on the same wafer bevel positions. The inspection tool is capable of finding a position relative to the notch as close as ±0.667°. The findings for each wafer are shown below. Polymer buildup is represented by the beige streak typically visible along the lower half of the bevel.

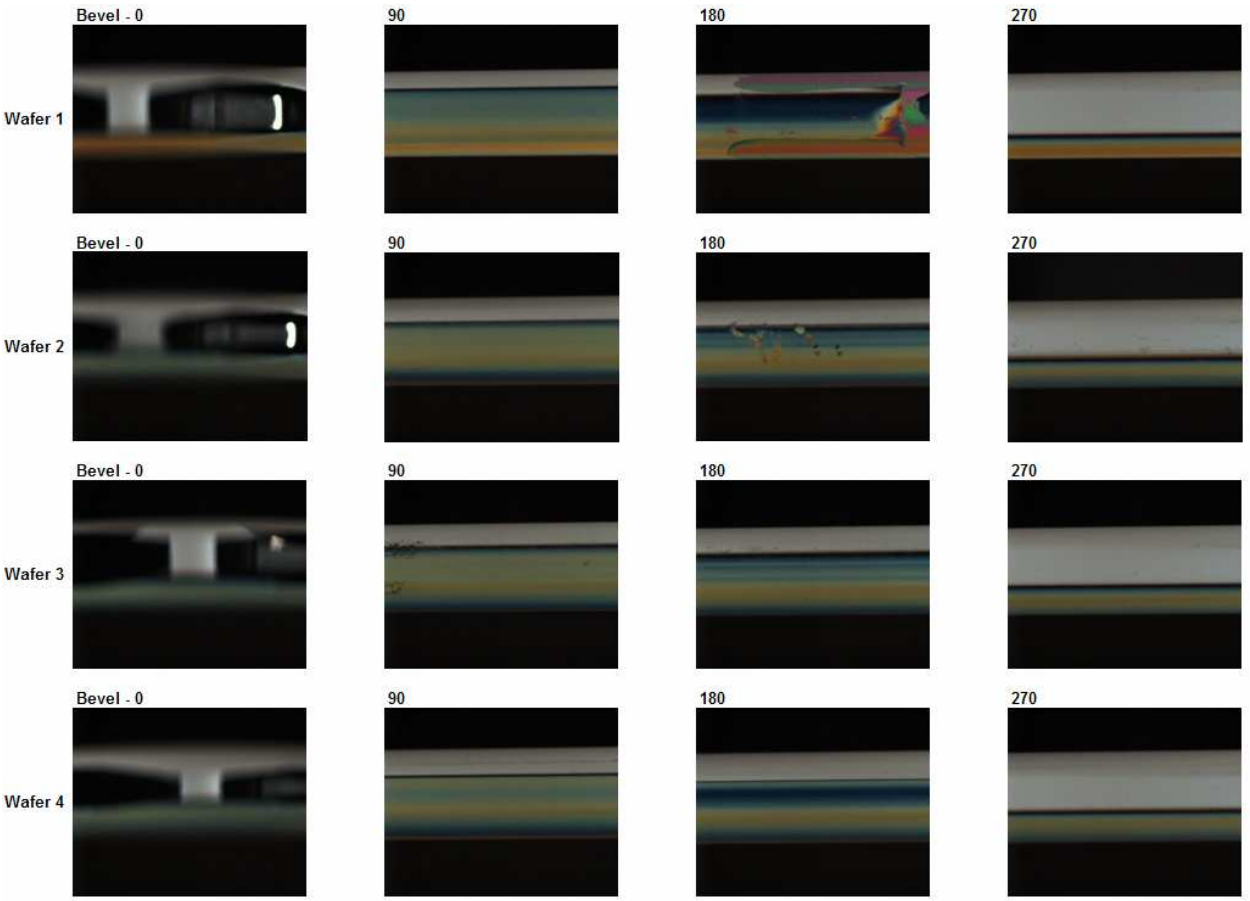

Figure 7. Resulting edge images of PET/Ash experiment for Wafers 1 through 4

Wafers 1 through 4 did not process with a post-etch treatment and results revealed the presence of polymer buildup after etch and ash in Figure 7. Wafer 1 being the etched control wafer exhibited the worst polymer buildup. Not much variation is seen between wafers 2 through 4 despite their varying ash recipes.

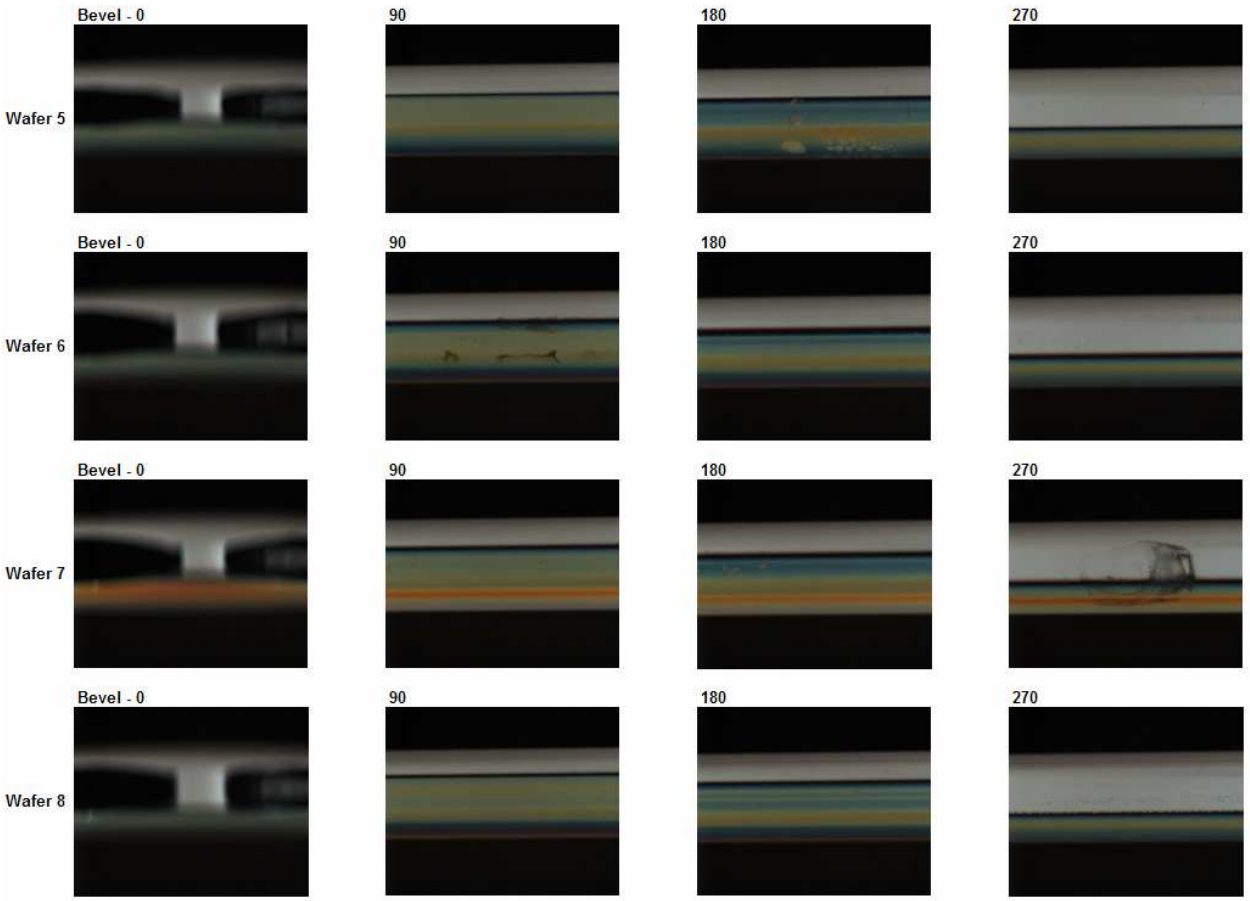

Figure 8. Resulting edge images of PET/Ash experiment for Wafers 5 through 8

Similarly, wafers 5 through 8 shown in Figure 8 also exhibited polymer edge buildup. All wafers that did not receive a PET step were faced with this problem. Figures 9 and 10 also do not represent much improvement. It was observed that the least amount of buildup was found at a position 270° away from the notch. This indicates a slight non-uniformity of edge buildup most likely due to the design of the etch process chambers.

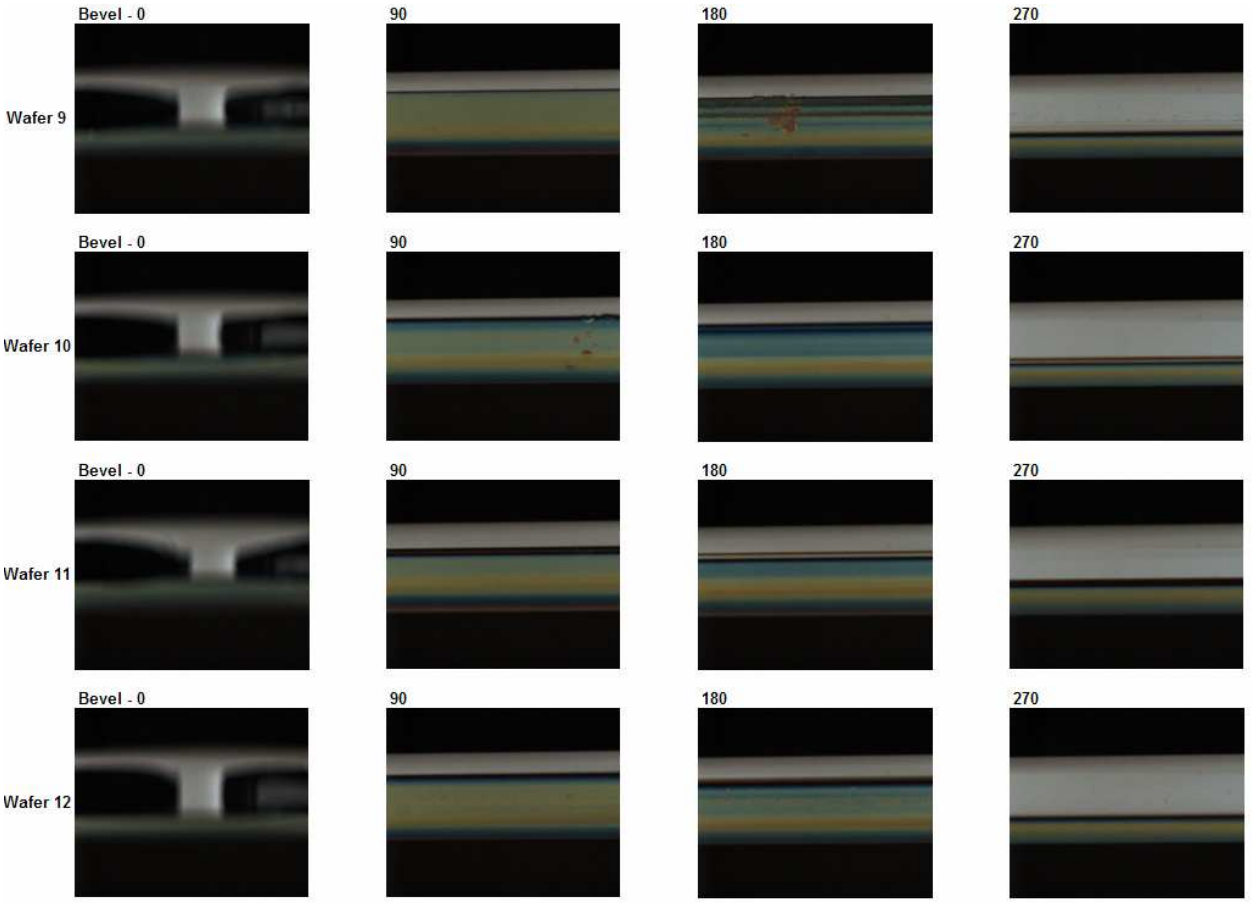

Figure 9. Resulting edge images of PET/Ash experiment for Wafers 9 through 12

In Figure 9, wafers 9 through 12 did not exhibit much improvement in terms of polymer removal. This was probably due to the PET step not being aggressive enough even on wafer 12. Each wafer exhibits the beige polymer ring around the bevel. Wafers 13 through 16 in Figure 10 look similar to Figure 9. This evidence shows that a longer, more aggressive PET step is necessary in removing the polymer buildup inside the etch chamber. Wafer 16, which did receive a 20 second PET step, has slightly less buildup compared to the previous 15 wafers.

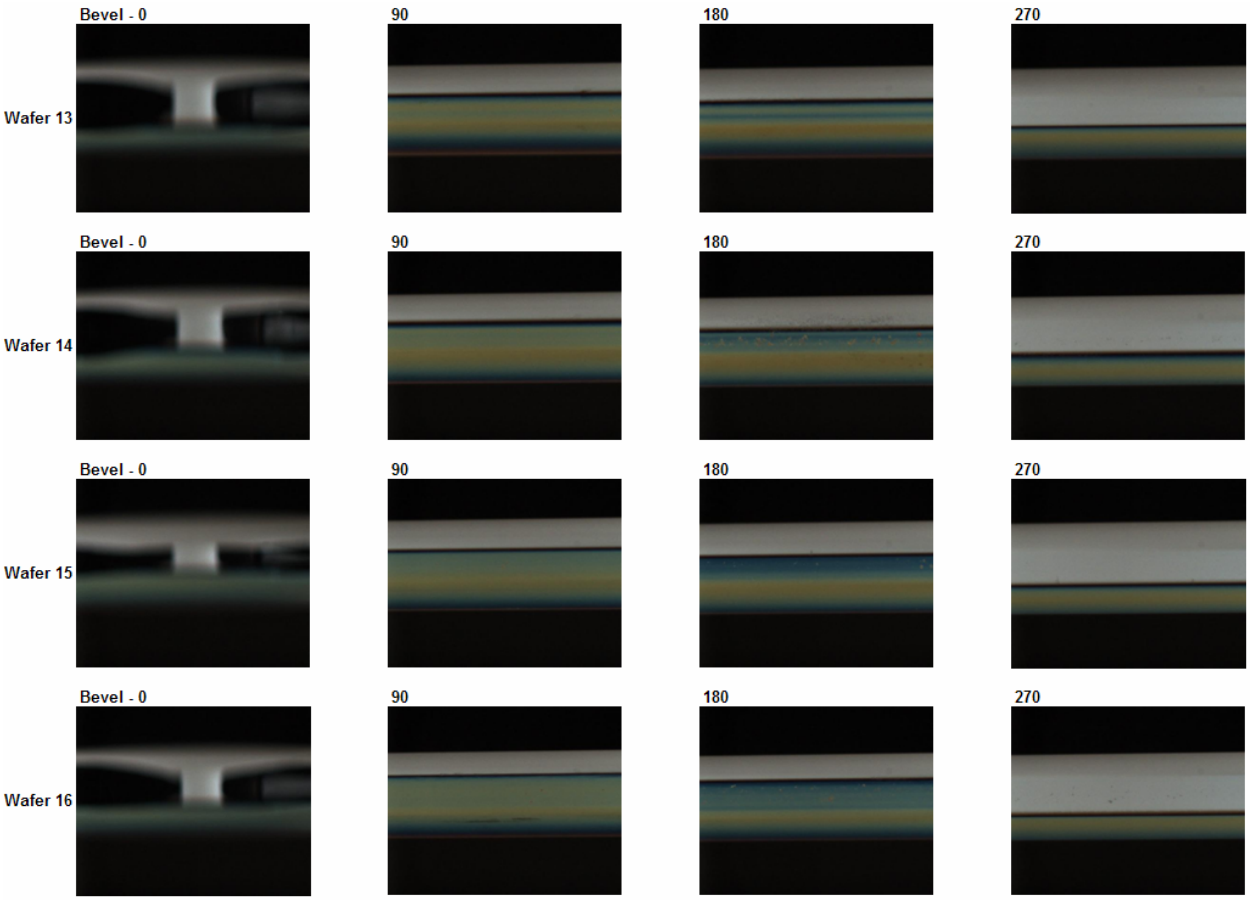

Figure 10. Resulting edge images of PET/Ash experiment for Wafers 13 through 16

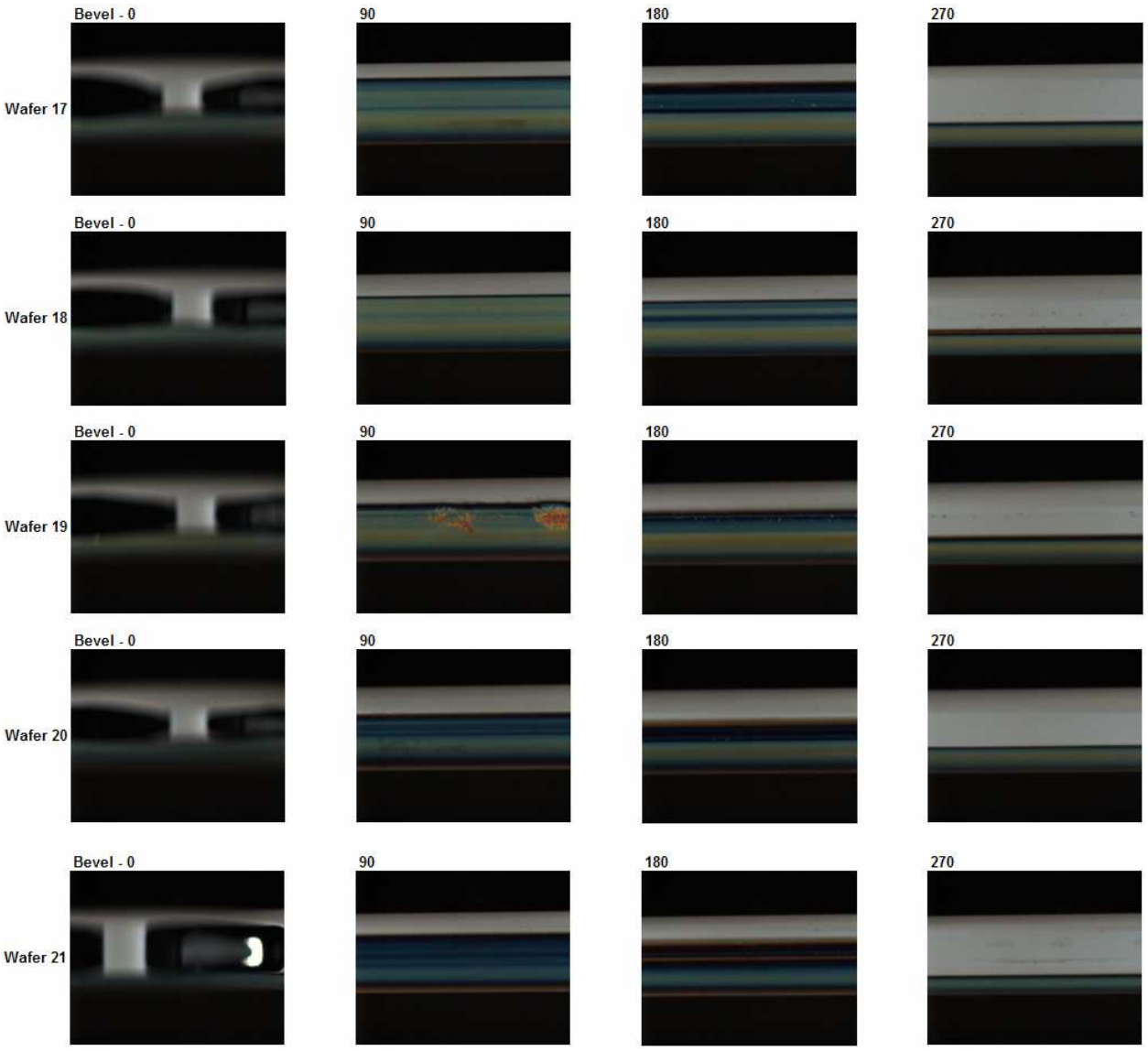

Figure 11. Resulting edge images of PET/Ash experiment for Wafers 17 through 21

Overall, the most notable improvement was found in wafers 17, 18, 20, and 21 which all underwent a long PET/Ash time or an insitu-ash step in the etch chamber in Figure 11. These preliminary studies sparked the interest in understanding the interactions between back end etch and ash processes. However, the bulk of the thesis research is concentrated on resist strip effects on dielectric film.

3.2 Pilot Tests Performed With OSG Film Deposition

Understanding the effects of changes in materials composition is vital for process integration. A lot of 24 bare Si pilot wafers were deposited with 2,700 Å OSG3 and OSG4 film. OSG4 has slightly lower dielectric constant compared to OSG3. The thickness and index of refraction of all wafers were measured using a thin films metrology tool. Two control wafers that were not processed through ash were measured on the FTIR tool to capture SiCOH bond peaks. Wafers were then be ashed without photoresist using two types of chemistries (H_2Ar and O_2) as shown above for 120 seconds.

Several wafers were cleaned in a hood using either a batch process or single wafer clean (SWC). In the batch process, wafers are dipped inside a bath whereas each wafer is cleaned with sprayed chemistry in single wafer clean. After the wafers have been ashed/cleaned, they were analyzed with FTIR, DSIMS, and XPS to detect the OSG damage. An SPV tool will be used to measure the k value. Table 2 shows the wafer splits that were used. Baseline processes were used in this experiment. Only pressure and temperature have been tweaked for the O_2 process. The H_2Ar process did not receive any treatment combinations. The interactions between plasma ash and clean processes have been studied via thickness delta before and after processing, SPV, FTIR, XPS, and DSIMS in that order.

Wafer	Dep Film	Ash Recipe			NE14 Clean	Analysis
		Gas	Temp (C)	Pressure (mT)		
1	OSG3	NA	NA	NA	NA	Thick delta, k, FTIR, DSIMS, XPS
2	OSG3	H_2Ar	BL	BL	BL	Thick delta, k, FTIR, DSIMS, XPS
3	OSG3	O_2	25	10	BL	Thick delta, k, FTIR, DSIMS, XPS
4	OSG3	O_2	25	20	BL	Thick delta, k, FTIR, DSIMS, XPS
5	OSG3	O_2	25	30	BL	Thick delta, k, FTIR, DSIMS, XPS
6	OSG3	O_2	50	10	BL	Thick delta, k, FTIR, DSIMS, XPS
7	OSG3	O_2	50	20	BL	Thick delta, k, FTIR, DSIMS, XPS
8	OSG3	O_2	50	30	BL	Thick delta, k, FTIR, DSIMS, XPS
9	OSG3	H_2Ar	BL	BL	Batch	Thick delta, k, FTIR, DSIMS, XPS
10	OSG3	O_2	25	20	Batch	Thick delta, k, FTIR, DSIMS, XPS
11	OSG3	H_2Ar	BL	BL	SWC	Thick delta, k, FTIR, DSIMS, XPS
12	OSG3	O_2	25	20	SWC	Thick delta, k, FTIR, DSIMS, XPS
13	OSG4	NA	NA	NA	NA	Thick delta, k, FTIR, DSIMS, XPS
14	OSG4	H_2Ar	BL	BL	BL	Thick delta, k, FTIR, DSIMS, XPS
15	OSG4	O_2	25	10	BL	Thick delta, k, FTIR, DSIMS, XPS
16	OSG4	O_2	25	20	BL	Thick delta, k, FTIR, DSIMS, XPS
17	OSG4	O_2	25	30	BL	Thick delta, k, FTIR, DSIMS, XPS
18	OSG4	O_2	50	10	BL	Thick delta, k, FTIR, DSIMS, XPS
19	OSG4	O_2	50	20	BL	Thick delta, k, FTIR, DSIMS, XPS
20	OSG4	O_2	50	30	BL	Thick delta, k, FTIR, DSIMS, XPS
21	OSG4	H_2Ar	BL	BL	Batch	Thick delta, k, FTIR, DSIMS, XPS
22	OSG4	O_2	25	20mT	Batch	Thick delta, k, FTIR, DSIMS, XPS
23	OSG4	H_2Ar	BL	BL	SWC	Thick delta, k, FTIR, DSIMS, XPS
24	OSG4	O_2	25	20mT	SWC	Thick delta, k, FTIR, DSIMS, XPS

Table 2. OSG Pilot Wafer Processing

4. Materials Analysis of OSG Wafer Pilots Using Spectroscopy Methods

Each OSG pilot wafer was processed in a random order during plasma ash and wet clean to reduce run order effects. Thickness delta has been calculated and compared to the dielectric damage. The dielectric damage was measured using an SPV tool. FTIR analysis was performed to detect the band spectra to capture the difference between non-treated OSG films and plasma ashed OSG films. XPS data was collected to collect the surface concentration of fluorine, nitrogen, carbon, silicon, and oxygen. Finally, DSIMS was performed on each OSG wafer to detect the depth concentration of element, as it is the most invasive method of determining film composition.

4.1 SPV Analysis

Since the wafers have been processed in back-end resist processes, the risk of metal contamination was eliminated through a backside clean prior to measuring them on the SPV tool. The refractive indices delta, thickness deltas, and dielectric constant results are displayed in Table 3. The sigma value represents k value non-uniformity. The wafers processed using H_2Ar gas flow had the least amount of film degradation compared to O_2 gas flow. This degradation was characterized by the increase in k value and the amount of thickness loss of the film. The k value is relative to control wafers 1 (OSG3 film) and 13 (OSG4 film) that did not process through ash or clean.

Wafer	Delta Thick	k relative	sigma
1	0	1	0.034491
2	13.89769	1.0189829	0.034869
3	264.3814	1.4509347	0.086844
4	216.6487	1.3979877	0.052517
5	166.2793	1.3551414	0.054736
6	272.0142	1.4419736	0.084734
7	214.5962	1.409782	0.063403
8	168.2567	1.3577779	0.049426
9	11.71454	1.1081506	0.036211
10	259.6763	1.4759493	0.094494
11	16.51221	1.0670099	0.036994
12	224.136	1.4332251	0.059956
13	0	1	0.035535
14	18.96033	1.0140444	0.038028
15	242.6855	1.3570392	0.082034
16	186.0708	1.330399	0.058677
17	145.1783	1.3063374	0.055077
18	239.1917	1.3718311	0.084212
19	192.4855	1.3220922	0.058015
20	147.6838	1.3054531	0.045743
21	16.60646	1.065455	0.036873
22	233.018	1.3868229	0.086106
23	16.59845	1.0441131	0.039019
24	200.7515	1.3630495	0.051544

Table 3. Thickness loss Dielectric Constant Results

This test was the first step in realizing the advantage of using H_2Ar over O_2 gas flows in plasma resist strip. A significant increase in dielectric constant is observed in O_2 ash processed at the lowest pressure. Batch clean compared to single wafer clean also exhibited a higher increase in k and greater thickness degradation. OSG3 and OSG4 films behaved similarly to both O_2 ash and batch clean in that a higher thickness degradation correlate to a higher k damage. Figure 12 displays the statistical measure of how well a regression trend line appromixates the correlation between thickness loss and k damage. A correlation of 0.955 represents a strong correlation between the two results.

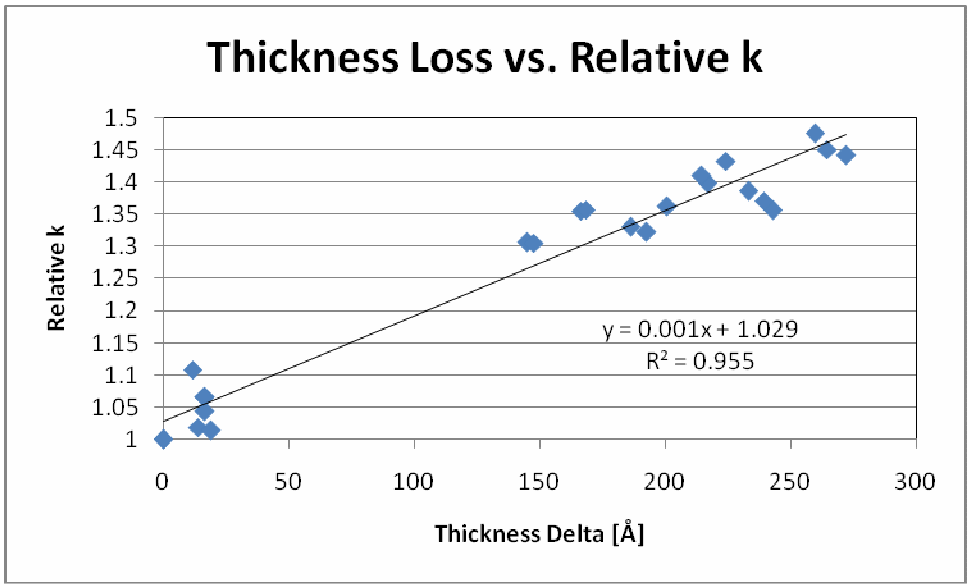

Figure 12. Thickness loss vs relative k value

4.2 FTIR Analysis

The wafers processed according to Table 2 were measured in an FTIR system three times to remove variations within the measurement tool before and after photoresist strip. The peaks present in the FTIR system shown in Figures 13 through 16 confirm the findings of bond peaks present in OSG film. Very little discrepancy was observed between bond peaks before and after ash and clean. FTIR data acts as a strong indicator of the bond peaks inside the OSG film content. However, it is not sensitive enough to capture OSG degradation.

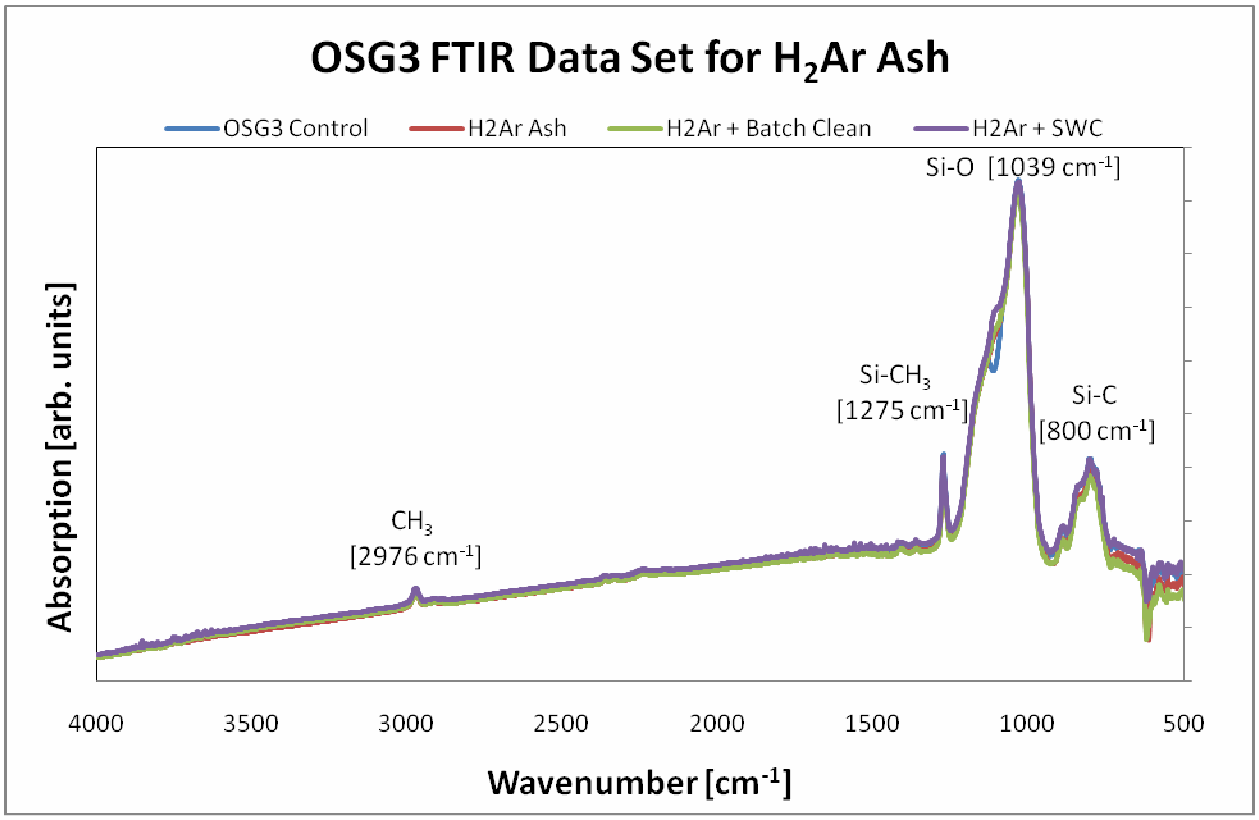

Figure 13. FTIR data for OSG3 film processed with H_2Ar ash vs. Control Wafer

Figure 13 shows the tabulated OSG3 FTIR data set for H_2Ar ash and clean processes. The peaks that have been characterized include Si-C, Si-O, Si-CH_3, and CH_3. When compared to the control wafer, the three processed wafers exhibit a band spectra with a highly uniform overlay of bond peaks.

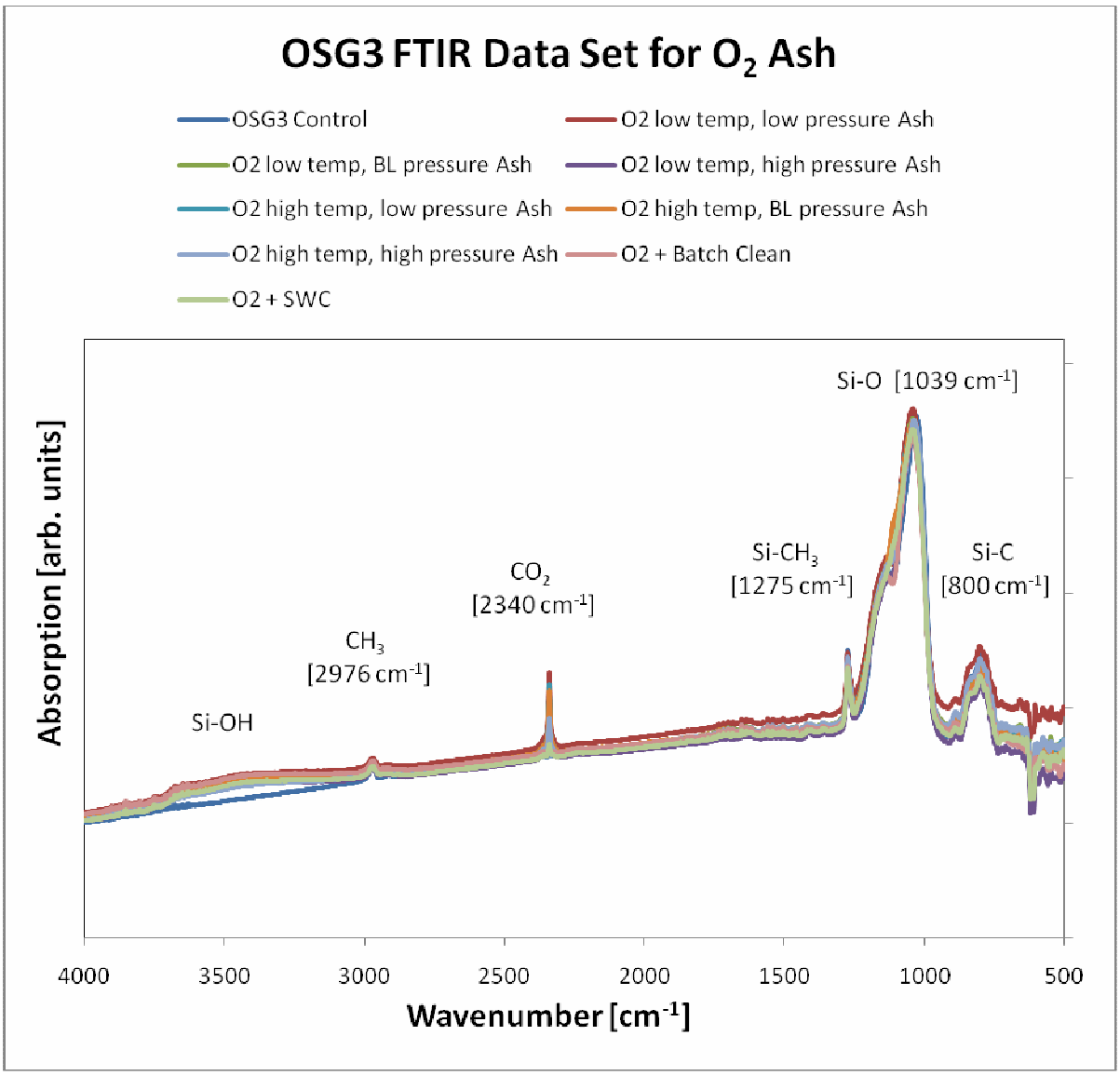

Figure 14. FTIR data for OSG3 film processed with O_2 ash vs. Control Wafer

Figure 14 shows a band spectra of eight OSG3 wafers processed with O_2 ash and clean. The spectra on these wafers exhibit slight alterations such as a new CO_2 bond peak at 2340 cm^{-1} that was not originally present in the control wafer. The presence of a broad Si-OH peak visible at approximately 3500 cm^{-1} gives evidence of OSG degradation. These two peaks observed post O_2 resist strip indicate that plenty of functional groups have been destroyed, causing an increase

in dangling bonds in the OSG. More moisture is absorbed easily by the porous OSG leading to an increase in dielectric constant and leakage current [15].

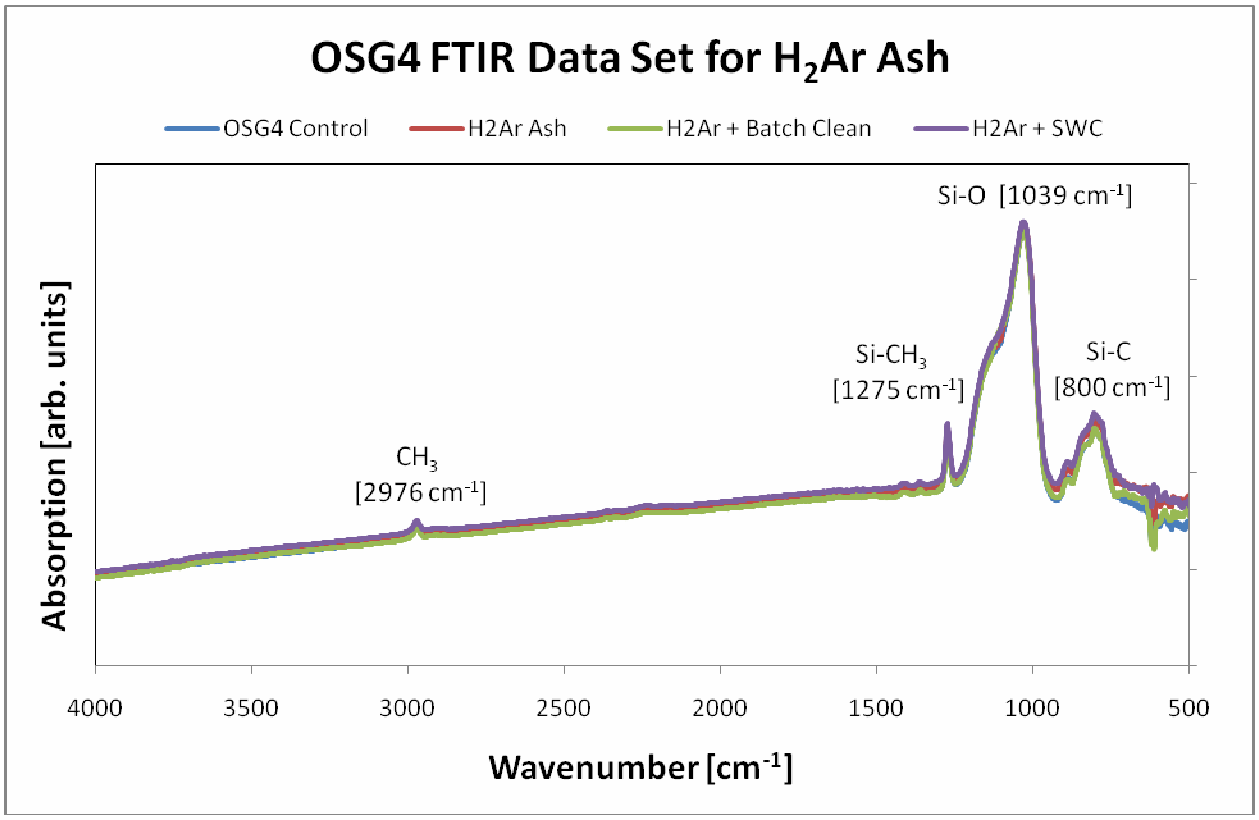

Figure 15. FTIR data for OSG4 film processed with H_2Ar ash vs. Control Wafer

Figures 15 and 16 display the FTIR spectra for OSG4 films ashed with H_2Ar and O_2. The band spectras are similar to Figures 13 and 14 in that OSG wafers processed with H_2Ar ash have much less degradation than O_2 ash process. Broad Si-OH bond peaks and CO_2 bond peaks are not present in wafers processed with H_2Ar and dielectric properties are maintained.

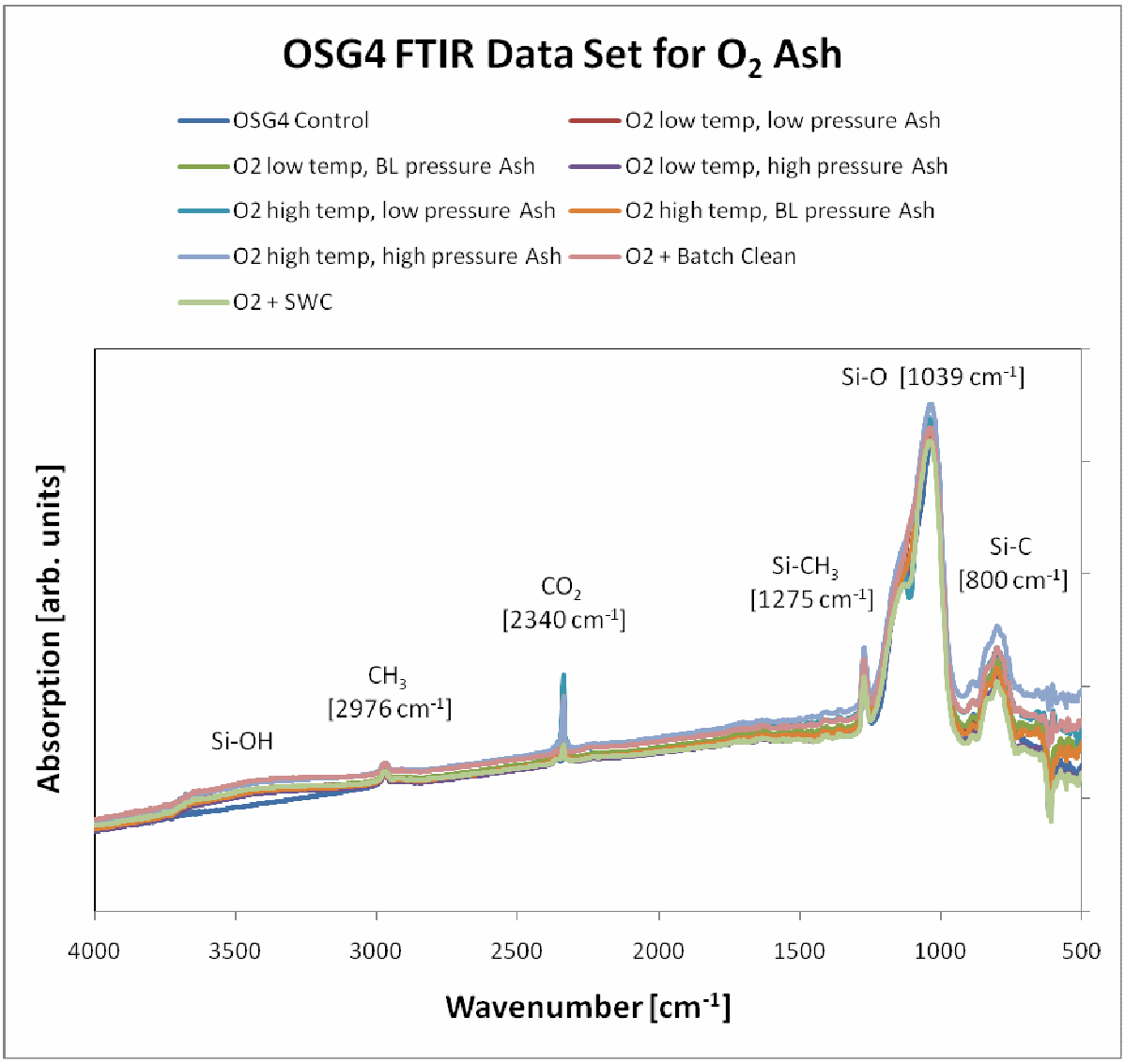

Figure 16. FTIR data for OSG4 film processed with O_2 ash vs. Control Wafer

4.3 XPS Analysis

Surface XPS measurements have been performed on the 24 OSG wafers that were processed through plasma and clean. The relative content of five elements compared to control wafers 1 and 13 are comprised of carbon, nitrogen, oxygen, fluorine, and silicon. These atomic percentages have been tabulated in Table 4.

Atomic Concentration Table (from multiplex)	C-1s relative	N-1s relative	O-1s relative	F-1s relative	Si-2p relative
S-1,OSG control	1	1	1	1	1
S-2,OSG,H2Ar,baseline C,baseline pressure, 120s,no NE14	0.682927	1	1.135117	4.875	1.038534
S-3,OSG O2,25 C,10 pressure,120s,no NE14	0.378469	1	1.348471	3	0.971889
S-4,OSG O2,25 C,20 pressure,120s,no NE14	0.351976	1	1.365333	0.375	0.975047
S-5,OSG O2,25 C,30 pressure,120s,no NE14	0.258621	1	1.396808	2.75	0.994946
S-6,OSG O2,50 C,10 pressure,120s,no NE14	0.258621	1	1.403777	1	0.989893
S-7,OSG O2,50 C,20 pressure,120s,no NE14	0.145921	1	1.442896	1.25	1.018636
S-8,OSG O2,50 C,30 pressure,120s,no NE14	0.108074	1	1.453462	0.125	1.034744
S-9,OSG H2Ar,baseline C,baesline pressure,120s,Batch	0.692178	1.01	1.134667	12.25	1.013582
S-10,OSG O2,25 C,20mT pressure,120s,Batch	0.174516	1	1.443345	0.5	0.998421
S-11,OSG H2Ar,baseline C,baesline pressure,120s,SWC	0.686291	1.28	1.154227	14.125	0.976627
S-12,OSG O2,25 C,20mT pressure,120s,SWC	0.142977	1	1.446268	1.5	1.015161
S-13,OSG control	1	1	1	1	1
S-14,OSG H2Ar,baseline C,baseline prressure,120s,noNE14	0.590573	1.21	1.219644	1.14	1.024945
S-15,OSG O2,25 C,10 prressure,120s,noNE14	0.338138	1	1.41233	1.1	0.977897
S-16,OSG O2,25 C,20 prressure,120s,noNE14	0.370471	1	1.400609	1.04	0.969372
S-17,OSG O2,25 C,30 prressure,120s,noNE14	0.341254	1	1.411392	1.07	0.977266
S-18,OSG O2,50 C,10 prressure,120s,noNE14	0.374757	1	1.391936	1.16	0.973476
S-19,OSG O2,50 C,20 prressure,120s,noNE14	0.402026	1	1.382794	1.17	0.963688
S-20,OSG O2,50 C,30 prressure,120s,noNE14	0.77912	1	1.144632	2	0.952321
S-21,OSG H2Ar,baseline C,baseline prressure,120s,Batch	0.236463	1	1.452414	1.12	1.005684
S-22,OSG O2,25 C,20mT prressure,120s,Batch	0.356447	1	1.421238	1.18	0.948532
S-23,OSG H2Ar,baseline C,baseline prressure,120s,SWC	0.629918	1	1.196906	2	1.003158
S-24,OSG O2,25 C,20mT prressure,120s,SWC	0.209194	1	1.480778	1.1	0.990212

Table 4. Tabulated XPS data where OSG3 wafers 2-12 are compared to control wafer 1 and OSG4 wafers 14-24 are compared to control wafer 13.

Atomic surface concentration data of each element shown in Table 4 are better represented in Figure 17. These data confirm that exposure of OSG films to plasma ash and clean conditions results in a modified surface layer deficient of carbon relative to the original material. The broken bonds of methyl groups from OSG films has been indicated by the XPS data due to the lack of carbon necessary in the formation of methyl groups.

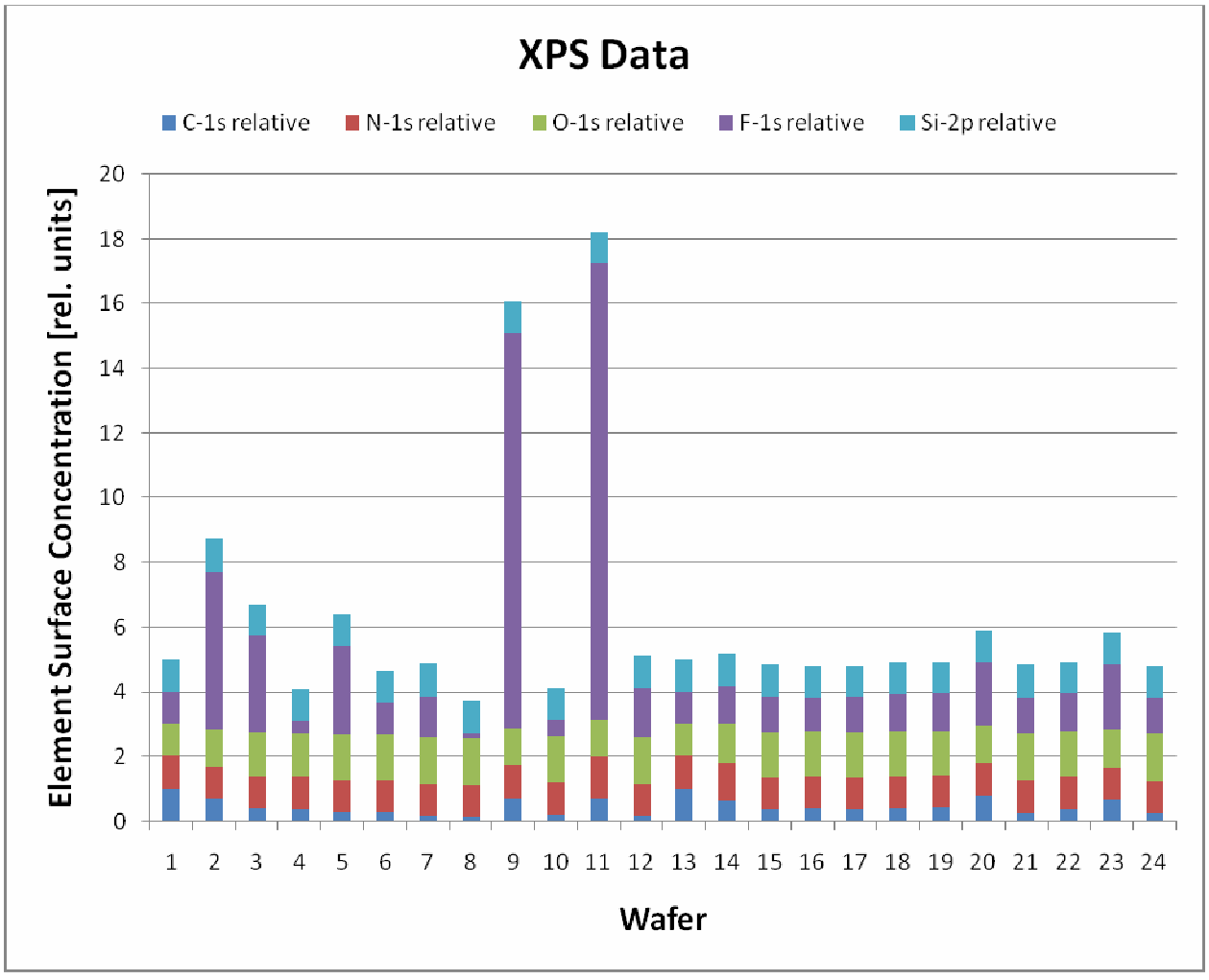

Figure 17. Interpretation of XPS Data for OSG3 and OSG4 Pilots

A high amount of carbon was depleted in OSG3 and OSG4 films that were exposed to O_2 plasma. However, over 60% of the carbon content remained after exposure to H_2Ar plasma on

the film surface. A significant increase in fluorine content was observed for both OSG3 and OSG4 films processed in a batch clean. This may be due to a possible amount of fluorine present in batch clean versus baseline and single wafer clean chemistry. No significant increase or decrease in nitrogen, oxygen, or silicon is observed in the XPS analysis.

4.4 DSIMS Analysis

DSIMS analysis of all 24 wafers with OSG3 and OSG4 films for hydrogen, carbon, nitrogen, oxygen, fluorine, and silicon was performed. The analysis was conducted by the Silicon Technology Development's (SiTD) Process Flow Analysis (PFA) laboratory using the following analytic conditions:

Primary Ions	Cs^+
Primary Impact Energy	3 keV
Impact Angle	< 50º
Cs coverage	>40%
Sputter Rate	<2 nm/s

Table 5. DSIMS Experimental Conditions

The conversion of measured secondary ion counts to concentration was performed using relative sensitivity factors (RSFs). In this case, Rutherford backscattering spectroscopy (RBS) measured values for carbon and fluorine concentrations in a reference sample were used. The precision or sample to sample variation is based on analysis conditions, element monitored, and the sample matrix. The routine analysis precision for the tool is typically 15%. The depth scales were based on a sputter rate calculated from the depths of the analytical crater and the total sputter time. The accuracy of the depth calibration is within ±3-5% or one sigma. However, the depth scale applied to the SIMS profiles presented does not consider the sputter rate differences for the changing matrix materials of ultra low-k and silicon. Differences in the sputter rate among the

various layers are minimal since each layer of OSG film has a reported measured thickness. Figures 18 through 41 depict the atomic concentration depth profiles obtained from DSIMS analysis. Figures 18 and 30 represent OSG3 and OSG4 control wafers. The other depth profiles exhibit carbon and hydrogen depletion of various amounts along with oxidization of film surfaces and introduction of fluorine species.

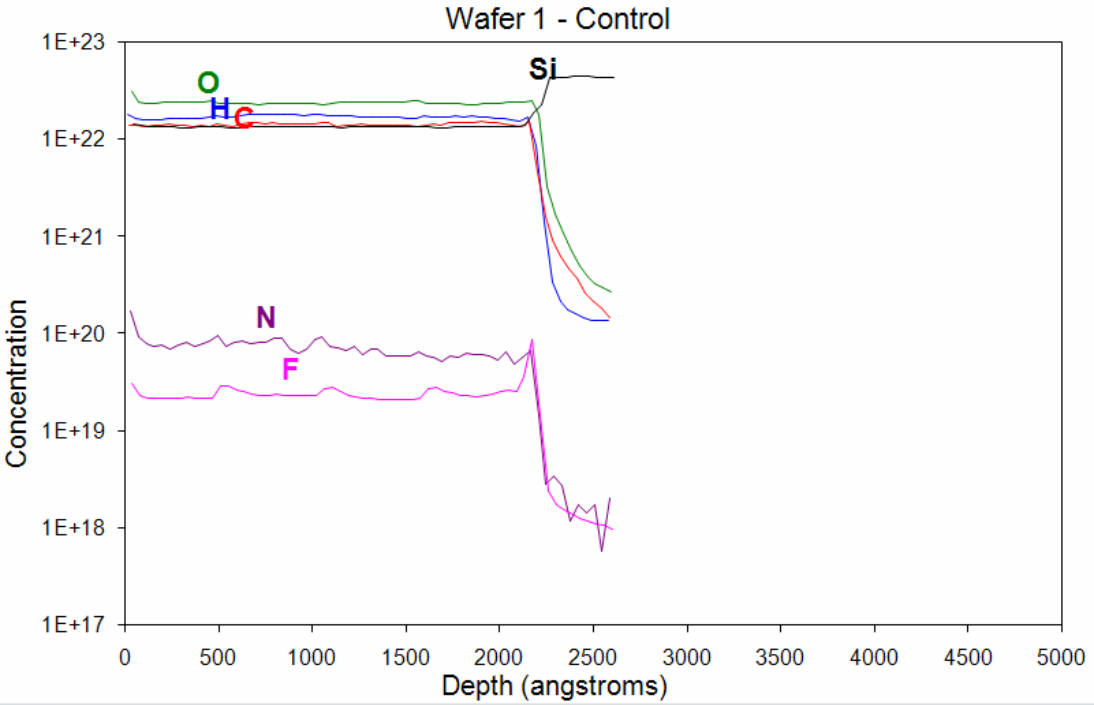

Figure 18. OSG3 Control Wafer Depth Profile

A DSIMS depth profile of an OSG3 control wafer that has not been processed through ash or clean is represented in Figure 18. Atomic concentrations of oxygen, hydrogen, carbon, nitrogen, and fluorine are consistent throughout the depth profile and represent a maintained film integrity. OSG3/Si interface is recorded at a depth of approximately 2250 Å.

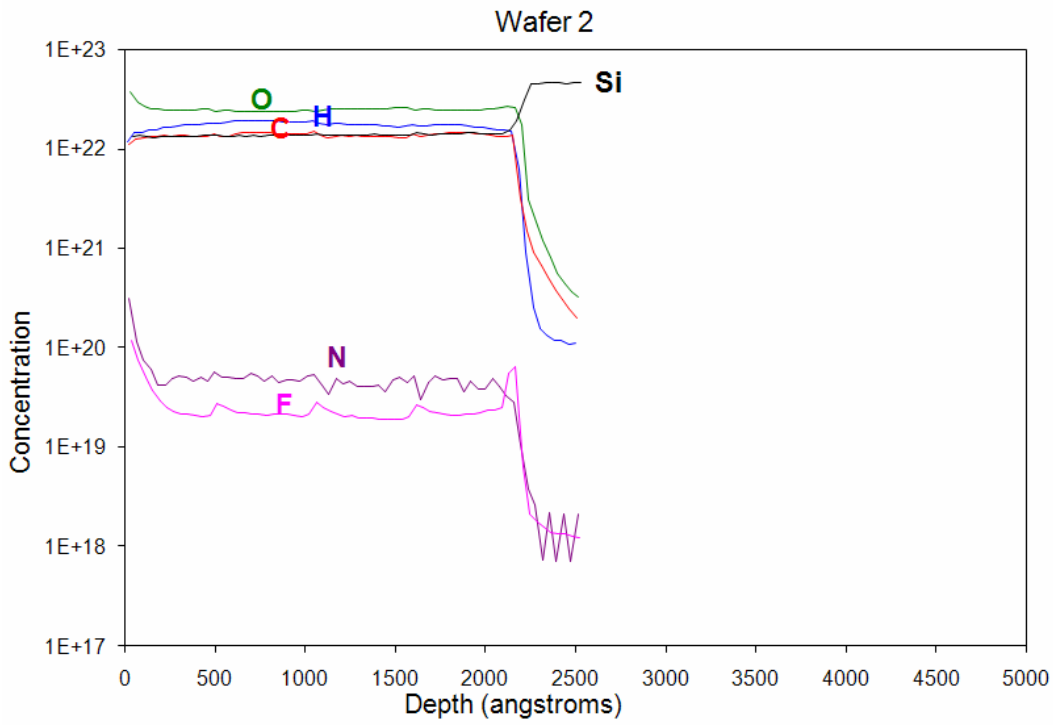

Figure 19. OSG3 Depth Profile ashed with H_2Ar

The depth profile of an OSG3 wafer ashed in H_2Ar plasma exhibits a surface atomic concentration increase in nitrogen and fluorine within 250 Å from the film surface is displayed in Figure 19. A slight decrease in carbon and hydrogen concentration along with a slight increase in oxygen is also visible. Most of the OSG3 film integrity has been maintained in this wafer. Figure 20 represents the DSIMS depth profile of an OSG3 film ashed with O_2 at 10 mT and 25°C. An increase oxygen, fluorine, and nitrogen content represent the introduction of impurities inside the film. The film surface has been oxidized during exposure to O_2 plasma. Carbon and hydrogen depletion is also visible due to the bond breakage of methyl groups.

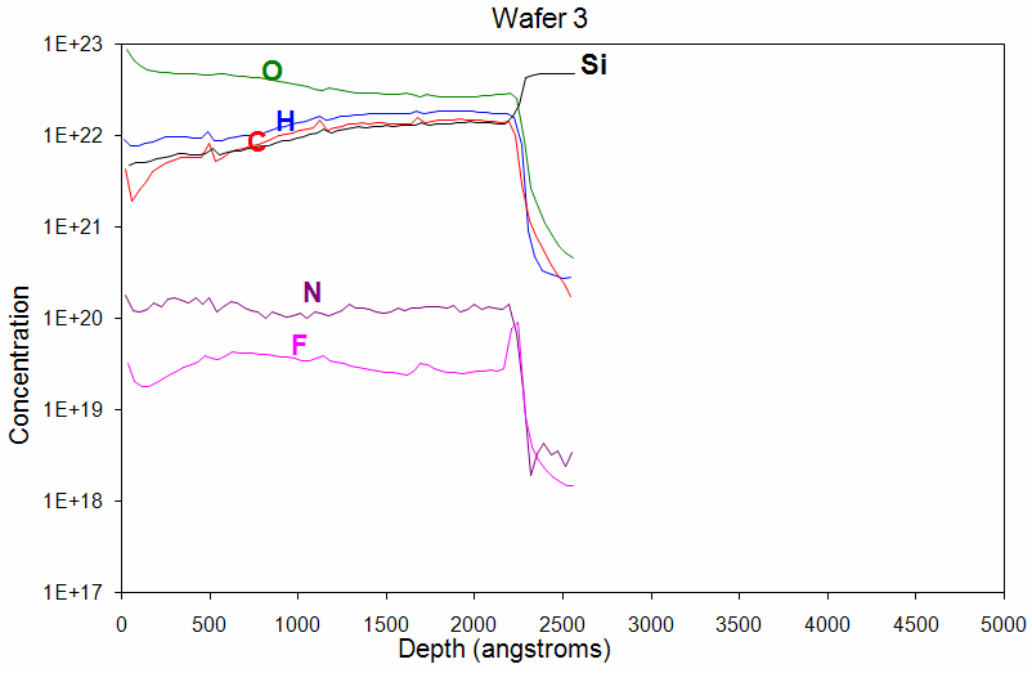

Figure 20. OSG3 Depth Profile processed with O_2 ash at 10 mT and 25°C

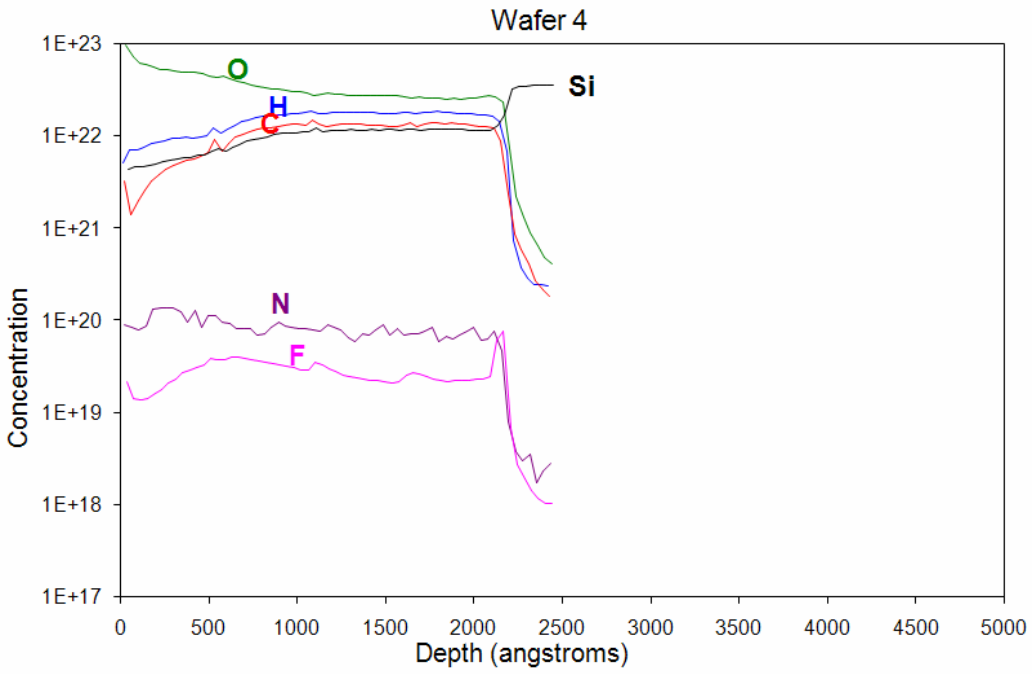

Figure 21. OSG3 Depth Profile processed with O_2 ash at 20 mT and 25°C

Figures 20 through 22 have comparable atomic depth profiles due to the similar processing techniques performed on each. The variation in pressure during the O_2 plasma ash at this temperature did not have a notable effect on OSG3 composition within the depth profile. The depth profile of wafer 5 processed with O_2 plasma at 30 mT and 25°C is captured in Figure 22. A higher process pressure yields slightly less carbon and hydrogen depletion near the film surface compared to OSG3 film concentration in Figure 20. Figures 23 through 25 represent the DSIMS depth profile of O_2 plasma ash processed at 50°C with varying pressures. Figures 26 through 29 depict depth profiles of films that have been processed with plasma ash and clean.

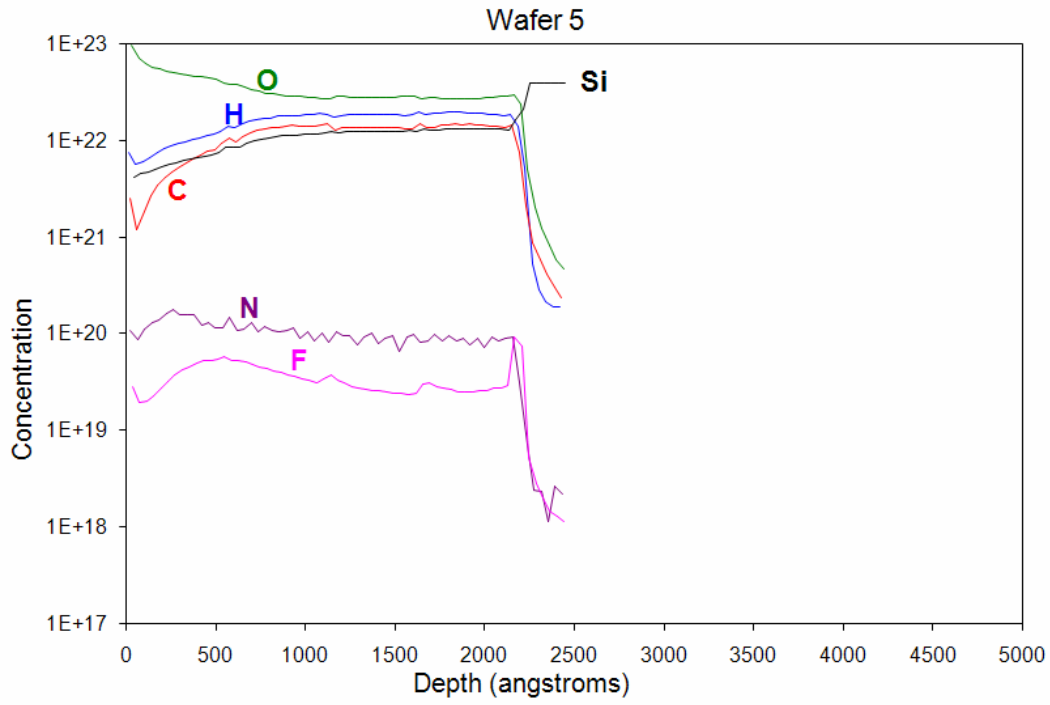

Figure 22. OSG3 Depth Profile ashed with O_2 at 30 mTorr and 25°C

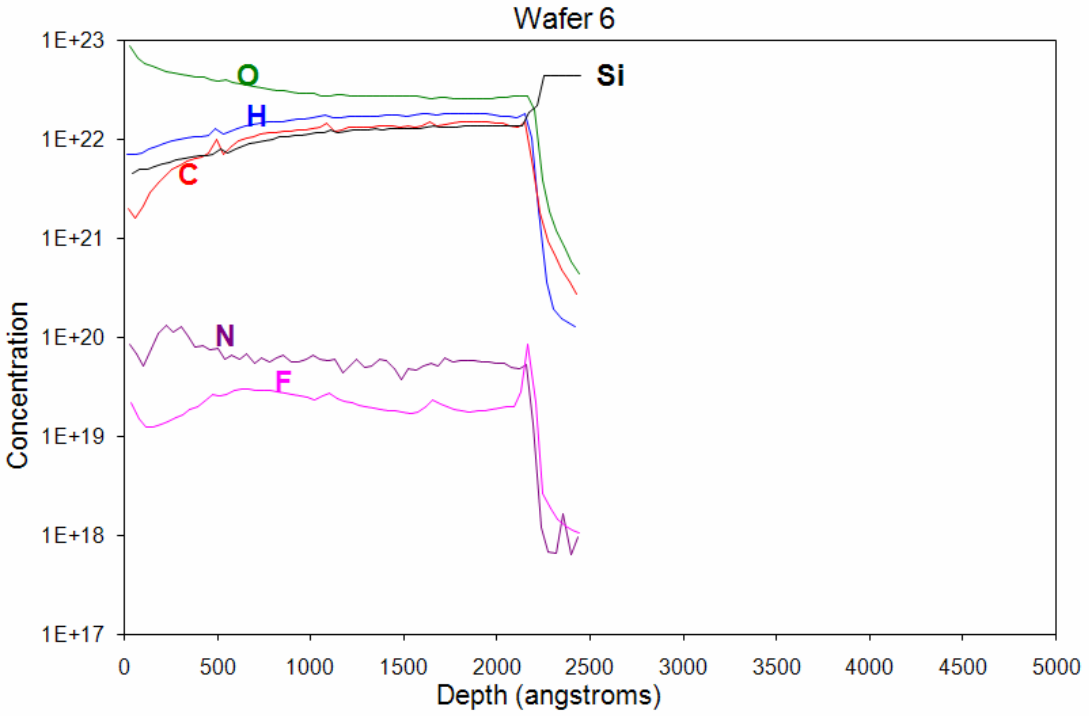

Figure 23. OSG3 Depth Profile ashed with O_2 at 10 mTorr, 120 sec, at 50°C

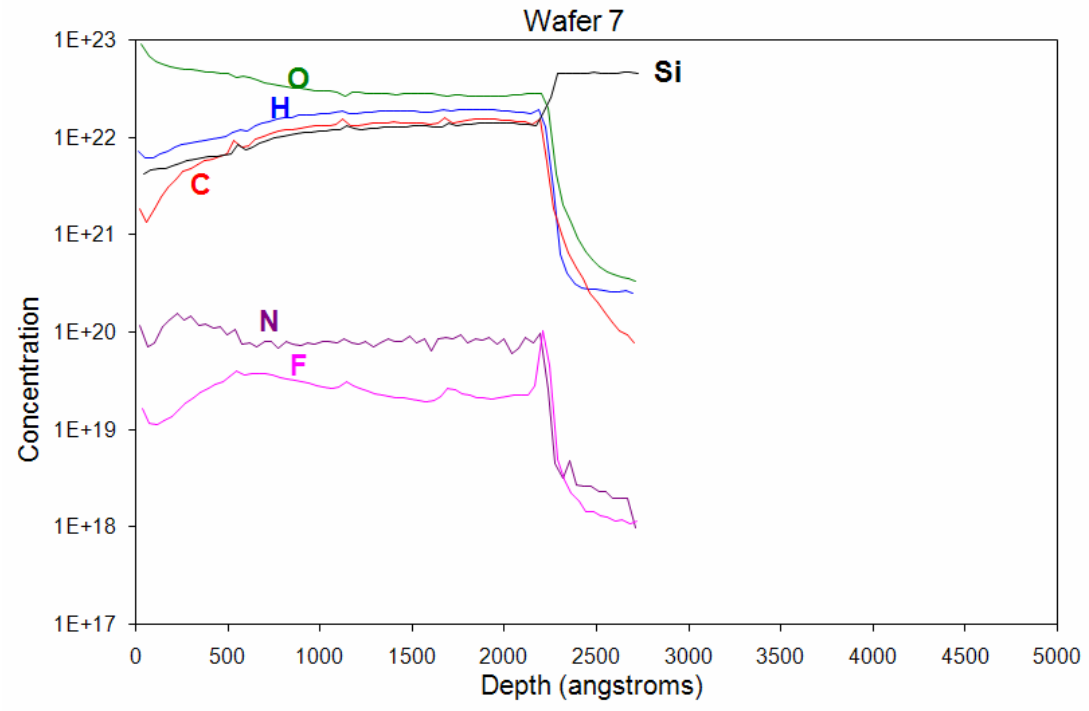

Figure 24. OSG3 Depth Profile ashed with O_2 at 20 mTorr, 120 sec, at 50°C

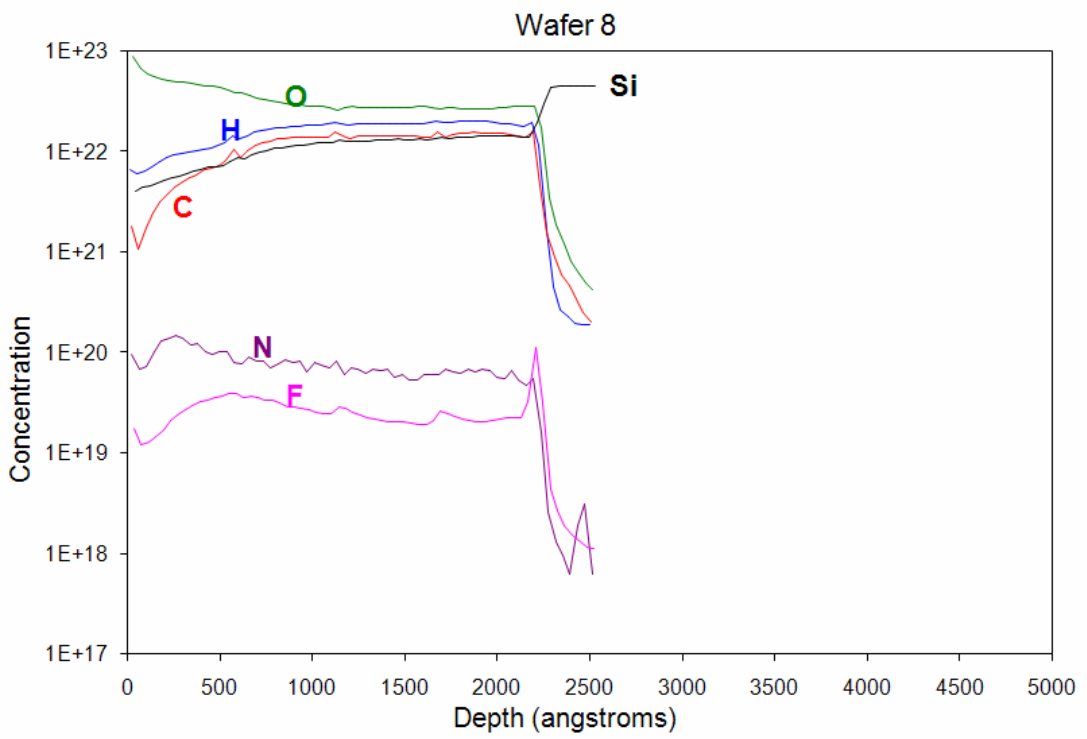

Figure 25. OSG3 Depth Profile ashed with O_2 at 30 mTorr, 120 sec, at 50°C

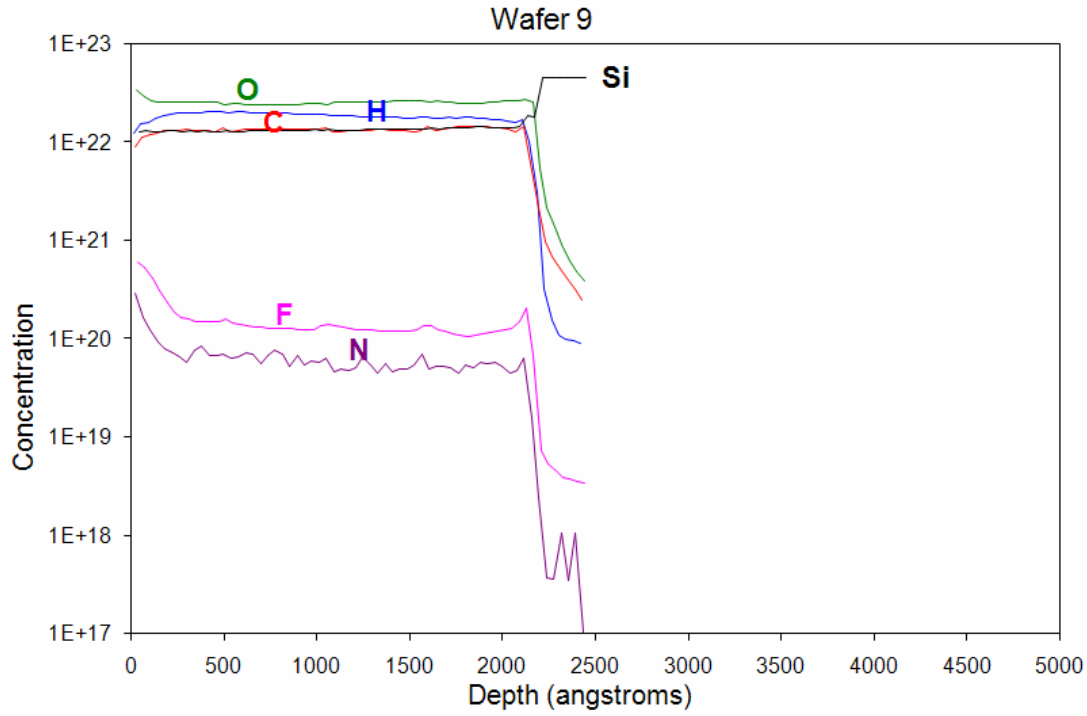

Figure 26. OSG3 Depth Profile ashed with H_2Ar and batch cleaned

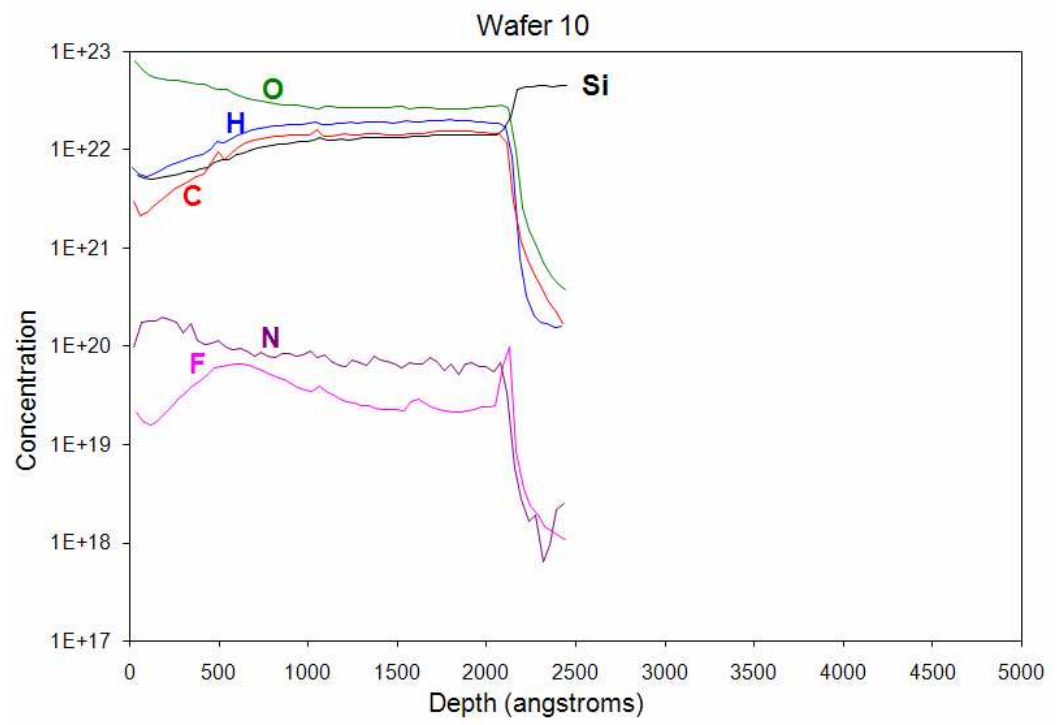

Figure 27. OSG3 Depth Profile ashed with O_2 and batch cleaned

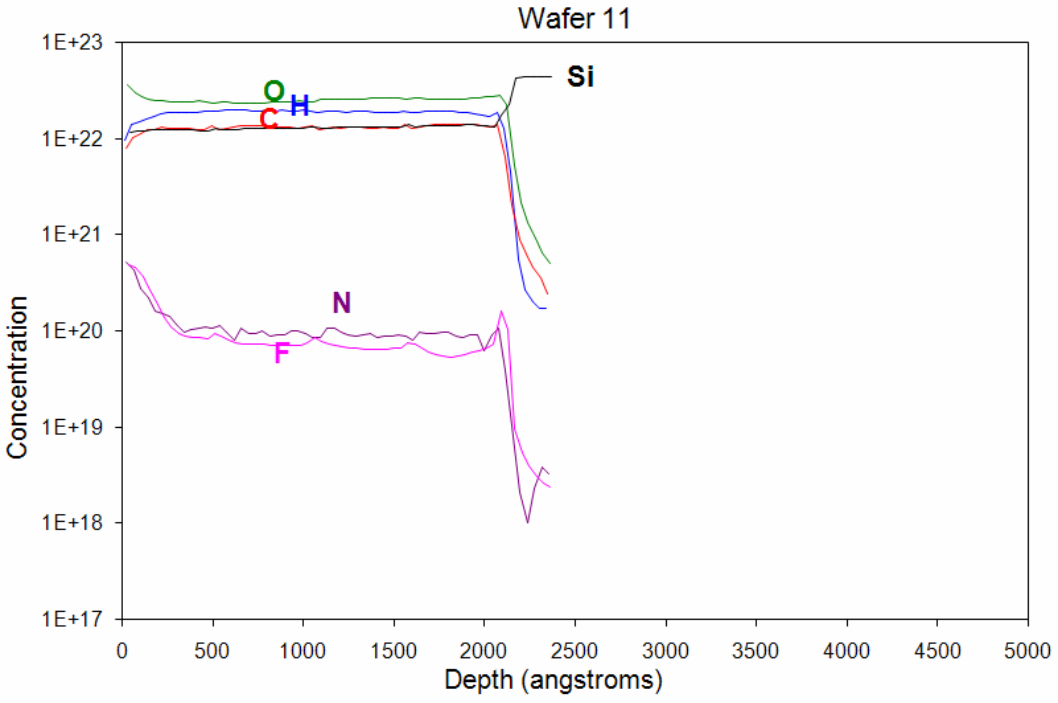

Figure 28. OSG3 Depth Profile ashed with H_2Ar and single wafer cleaned

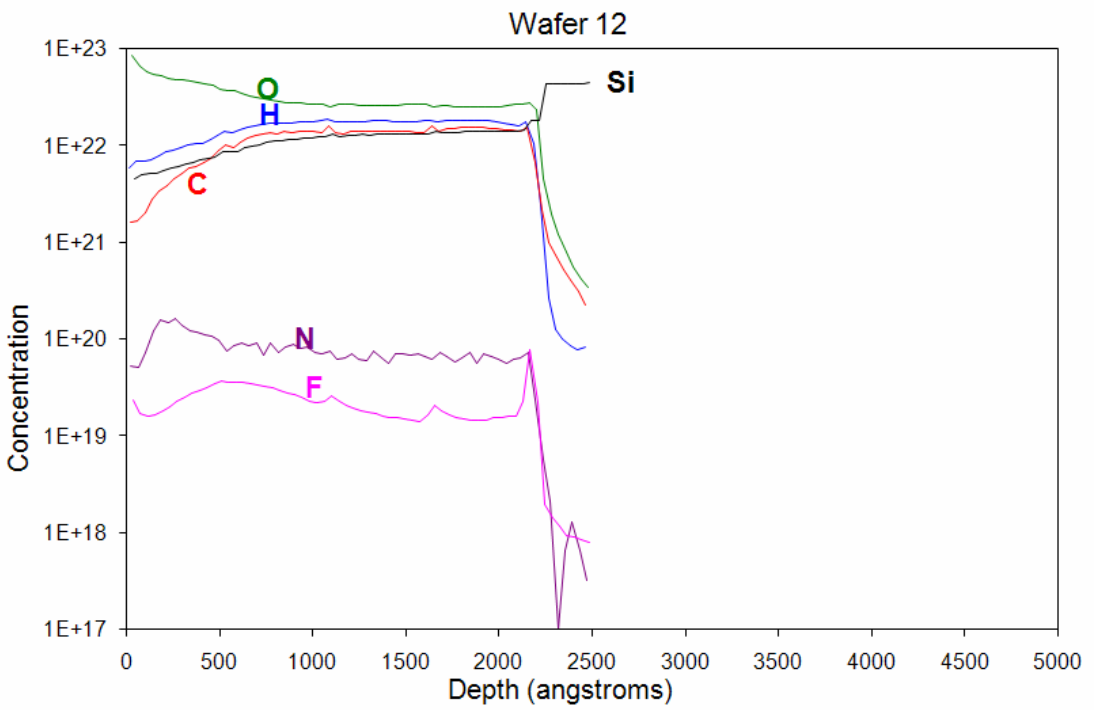

Figure 29. OSG3 Depth Profile ashed with O_2 and single wafer cleaned

Depth concentration profiles of OSG4 films are demonstrated in Figures 30 through 41. Carbon bond breakage and oxidation of O_2 plasma similar to OSG3 films are also observed in wafers deposited with OSG4 films. An increase in fluorine and nitrogen content is noticed as well on wafers processed with both plasma ash and clean. This is mostly due to the fluorine-containing clean chemistry used during processing. High fluorine content was observed in the batch clean than single wafer clean.

Batch clean chemistry exhibits a stronger probability for fluorine contamination since the entire wafer is immersed in a bath, whereas single wafer clean tool uses spray nozzles to dispense the clean chemistry onto the wafer. Single wafer cleans are generally more cost efficient in conserving chemistry compared to batch clean baths.

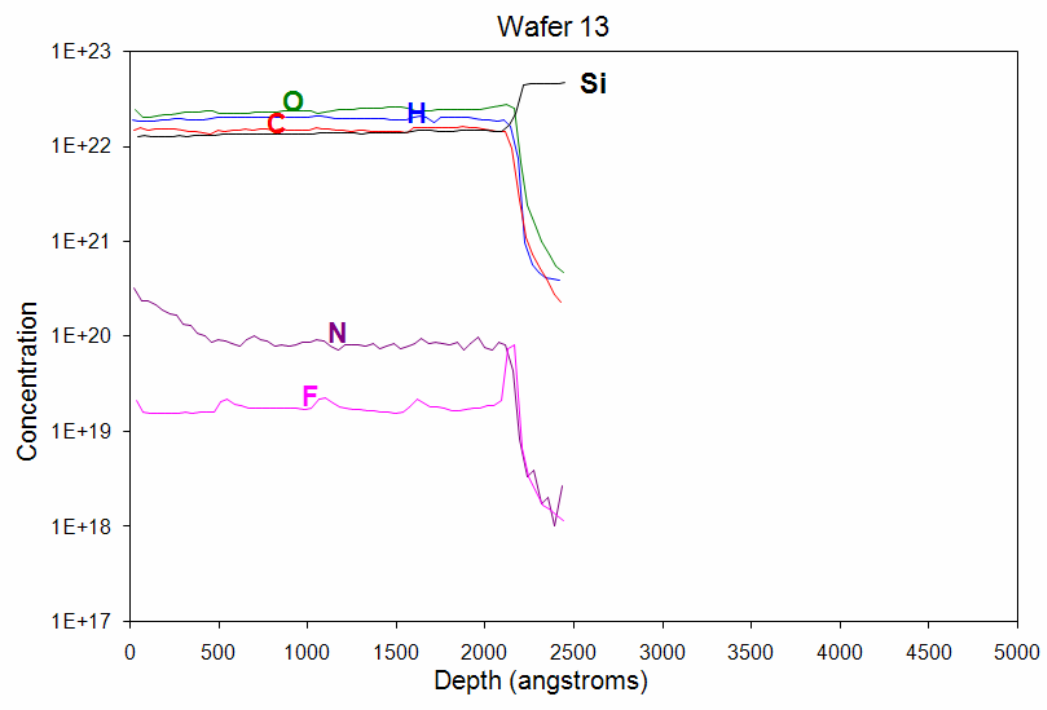

Figure 30. OSG4 Control Wafer Depth Profile

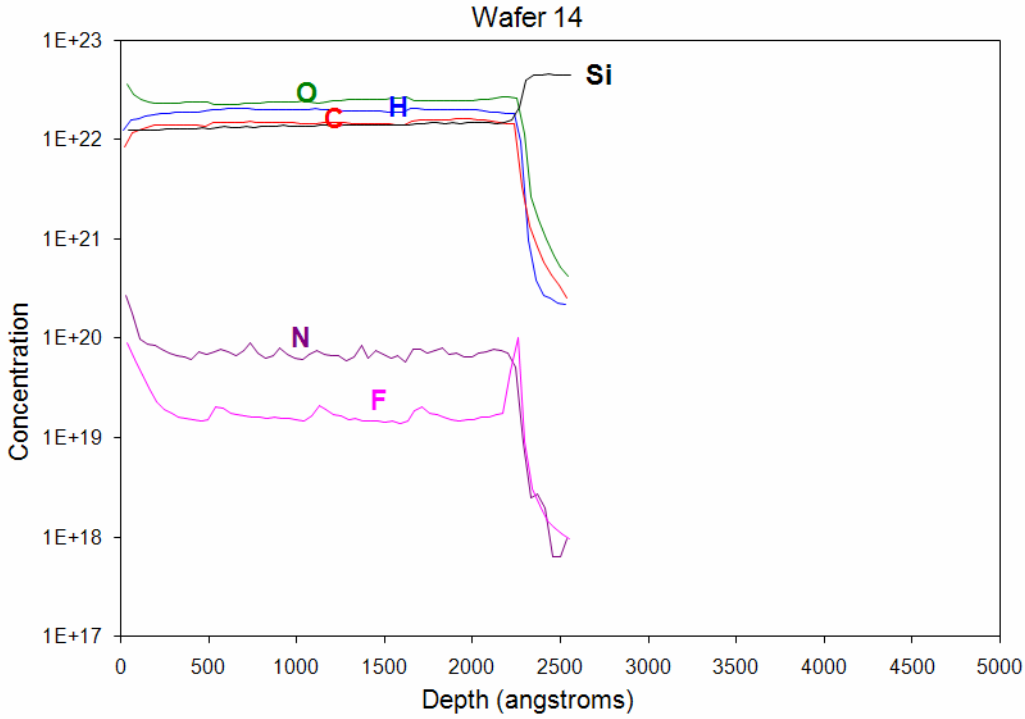

Figure 31. OSG4 Depth Profile ashed with H_2Ar

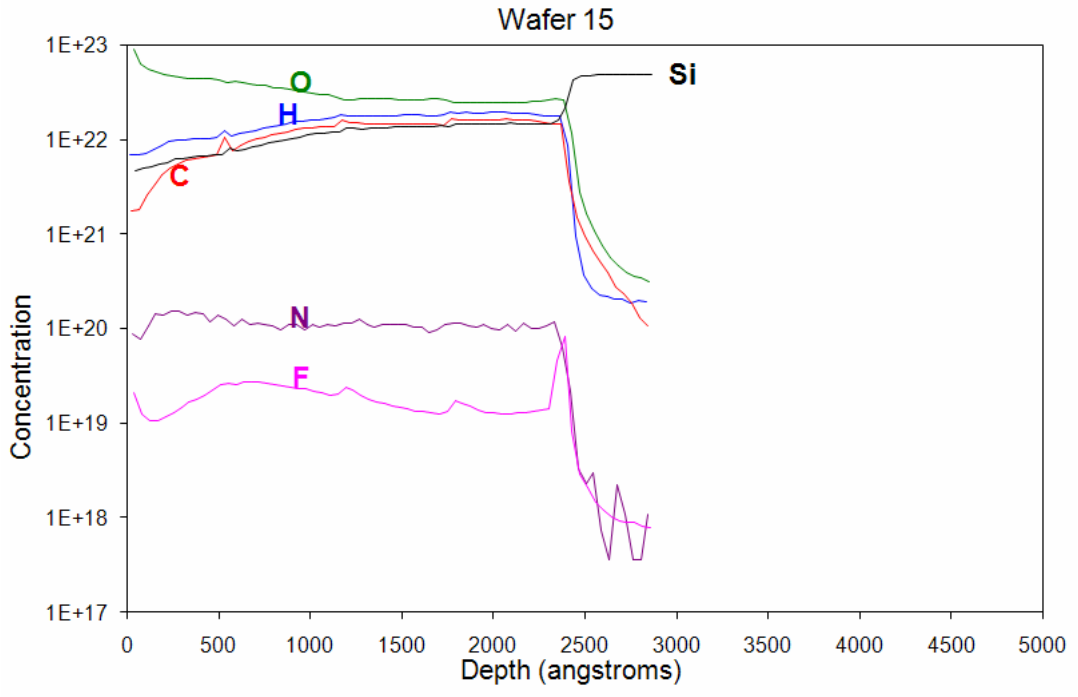

Figure 32. OSG4 Depth Profile ashed with O_2 at 10 mTorr, 120 sec, at 25°C

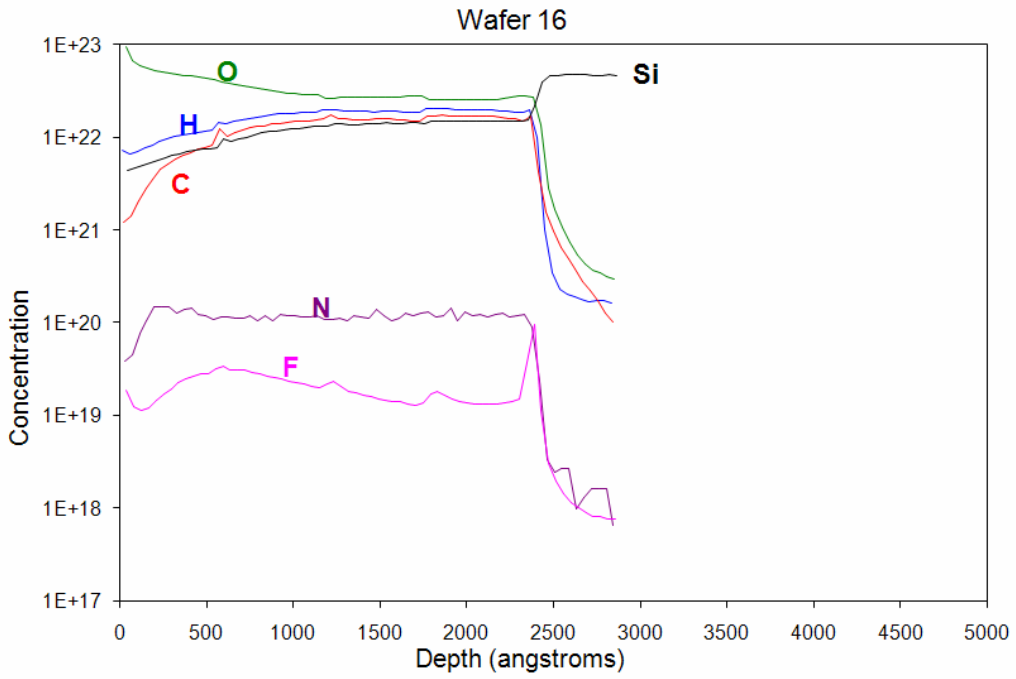

Figure 33. OSG4 Depth Profile ashed with O_2 at 20 mTorr, 120 sec, at 25°C

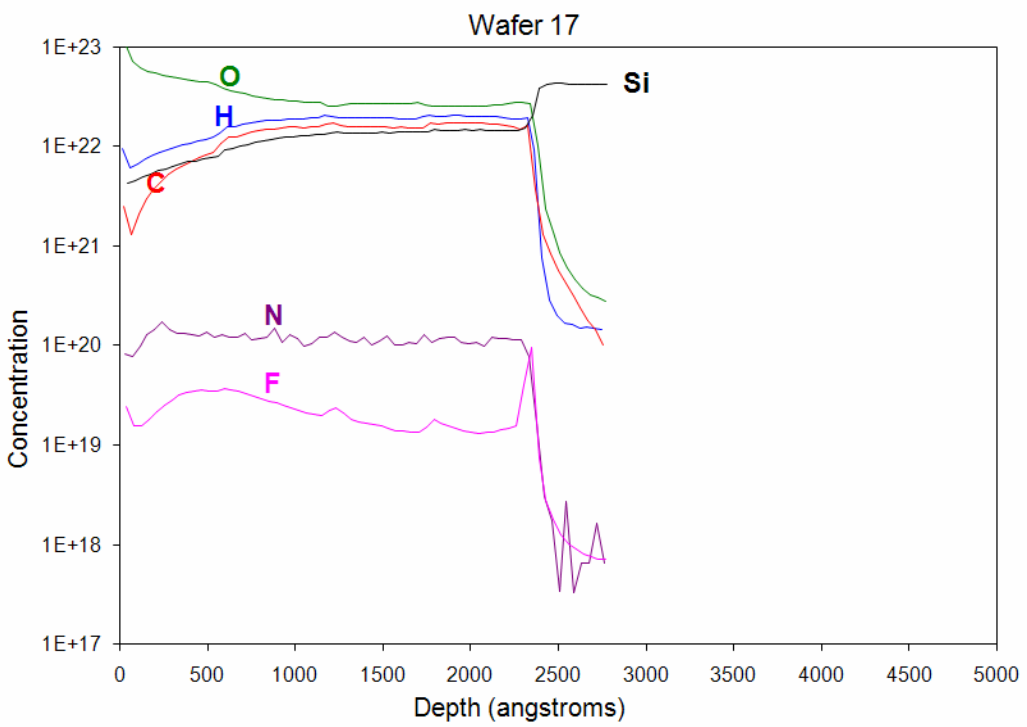

Figure 34. OSG4 Depth Profile ashed with O_2 at 30 mTorr, 120 sec, at 25°C

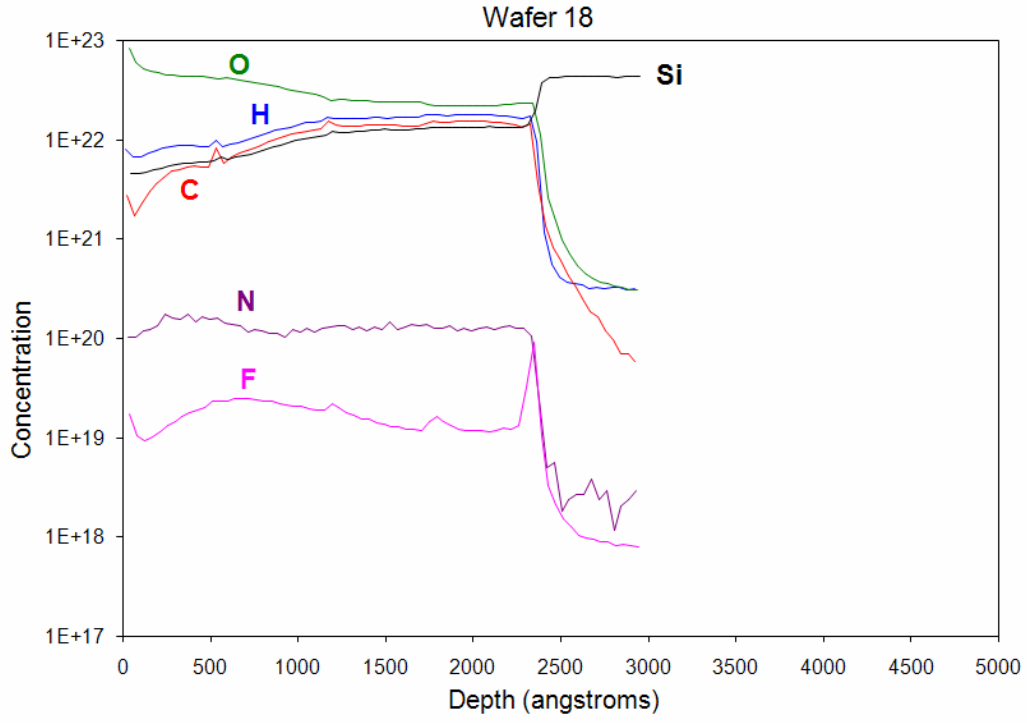

Figure 35. OSG4 Depth Profile ashed with O_2 at 10 mTorr, 120 sec, at 50°C

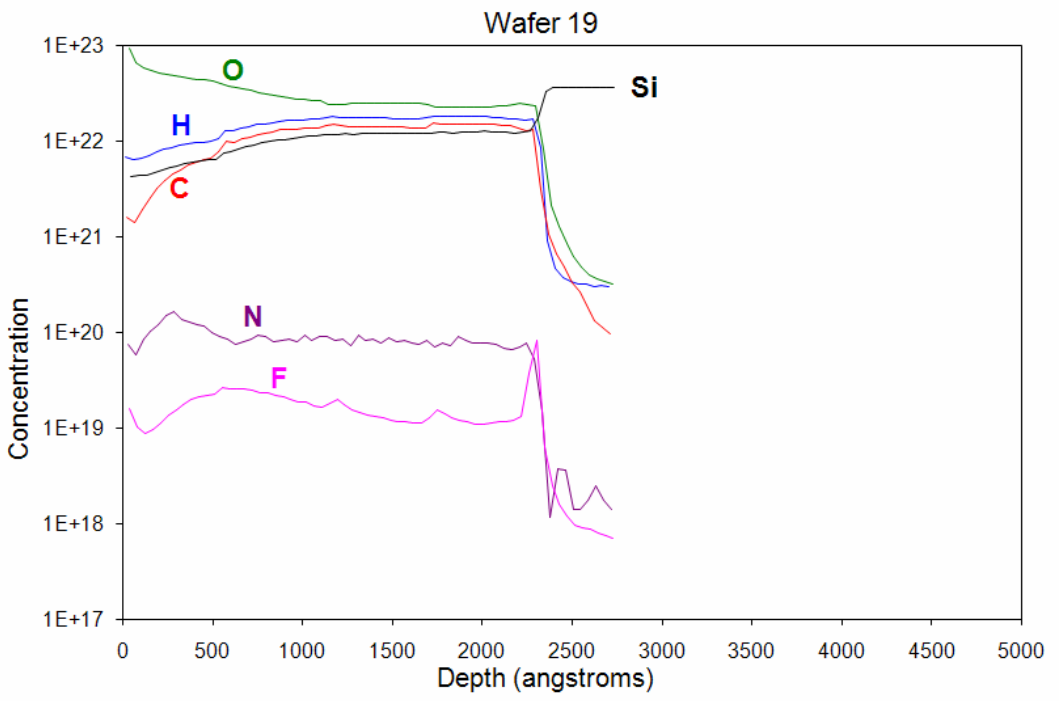

Figure 36. OSG4 Depth Profile ashed with O_2 at 20 mTorr, 120 sec, at 50°C

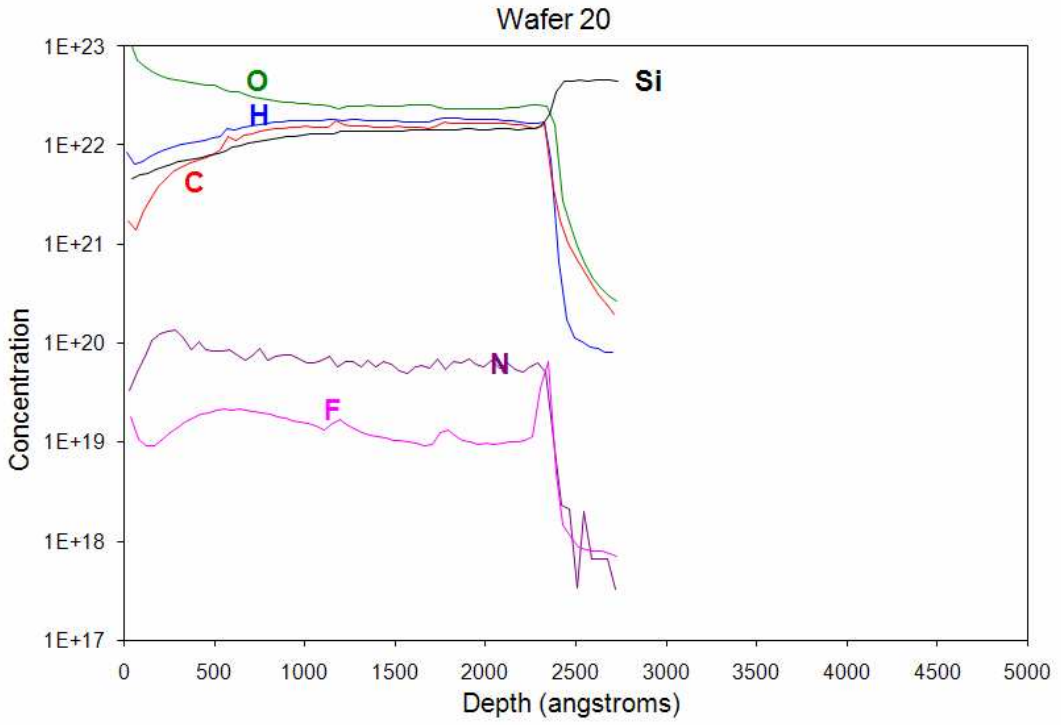

Figure 37. OSG4 Depth Profile ashed with O_2 at 30 mTorr, 120 sec, at 50°C

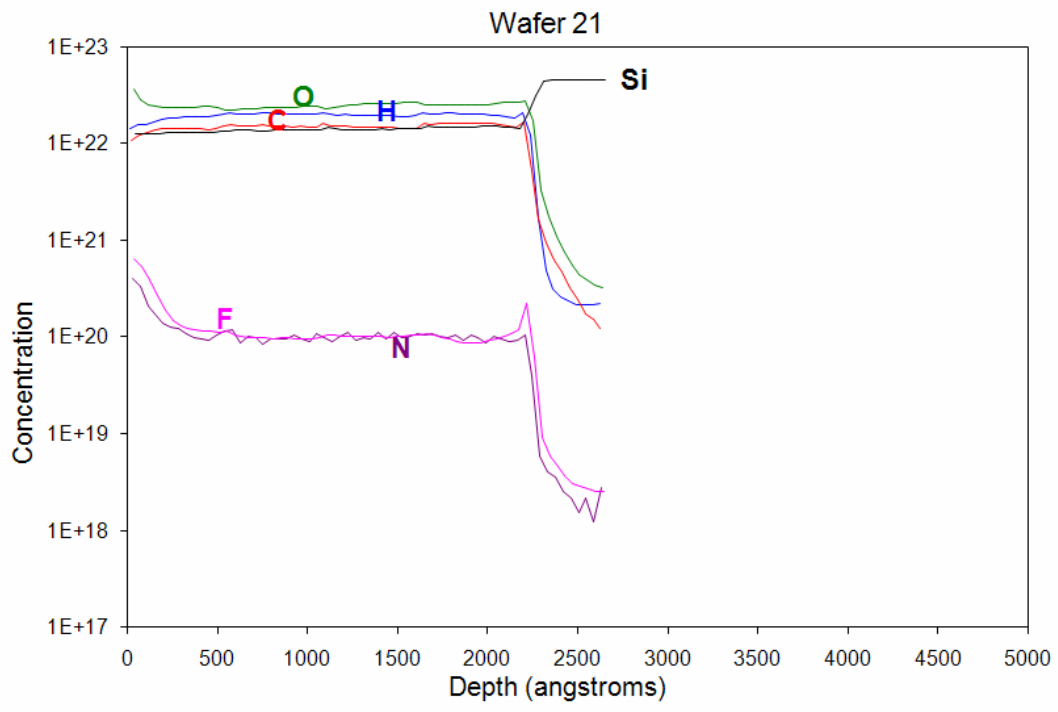

Figure 38. OSG4 Depth Profile ashed with H_2Ar and batch cleaned

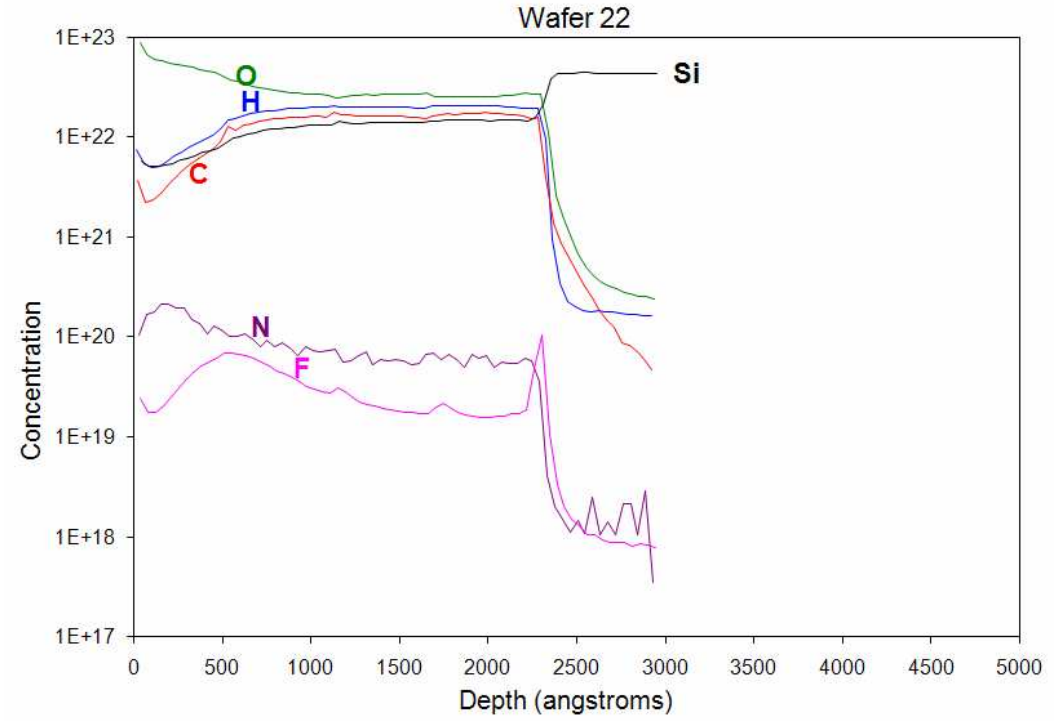

Figure 39. OSG4 Depth Profile ashed with O_2 and batch cleaned

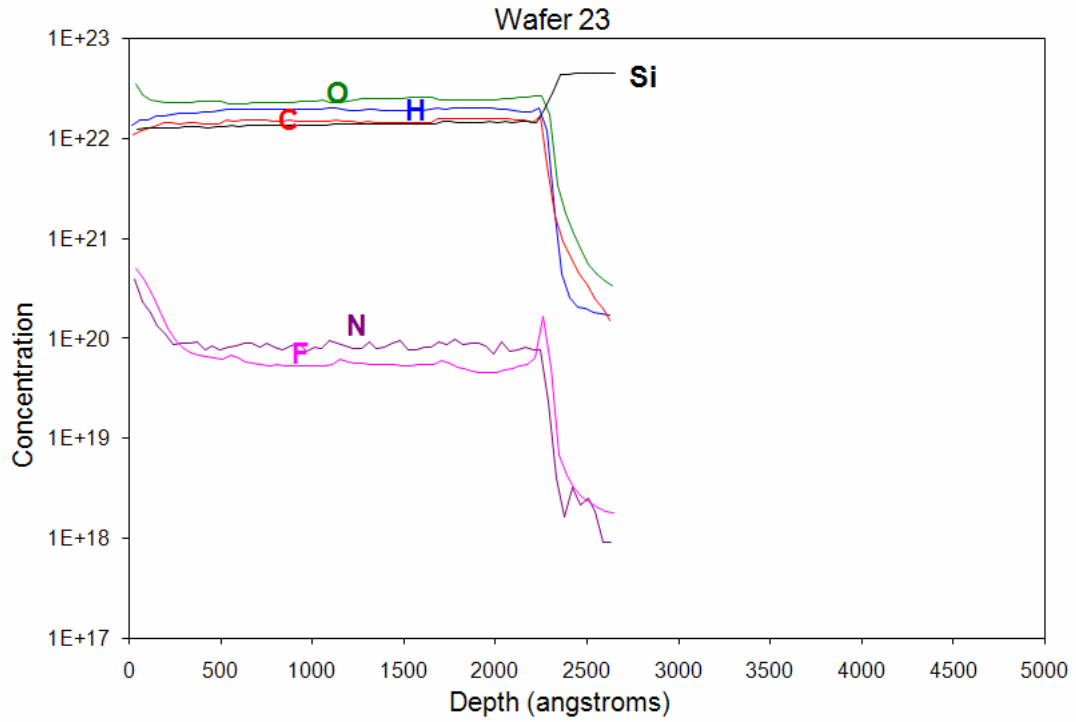

Figure 40. OSG4 Depth Profile ashed with H_2Ar and single wafer cleaned

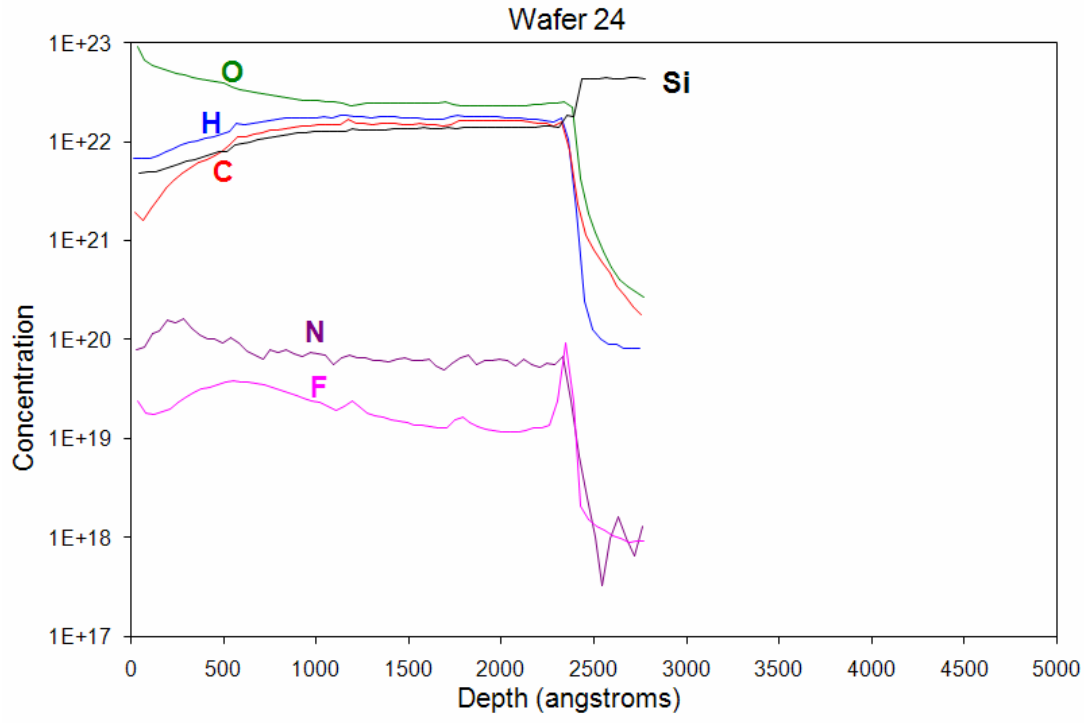

Figure 41. OSG4 Depth Profile ashed with O_2 and single wafer cleaned

Visual depth inspection of each wafer provides a good indication of what has occurred after plasma ash and clean processing within wafer variation. However, it is also necessary to organize the data in a manner that compares wafer to wafer variation. Table 6 lists the average atomic content across the entire depth of both OSG films. The content of each element (hydrogen, carbon, nitrogen, oxygen, fluorine, and silicon) are compared to both OSG3 and OSG4 control wafers.

Wafer	Relative H	Relative C	Relative N	Relative O	Relative F	Relative Si
1	100.00%	100.00%	100.00%	100.00%	100.00%	100.00%
2	102.76%	98.35%	74.47%	107.35%	109.30%	98.90%
3	85.52%	76.78%	186.58%	162.75%	135.81%	81.32%
4	92.41%	78.02%	123.73%	158.82%	119.07%	69.23%
5	97.93%	85.12%	153.52%	155.39%	149.77%	73.63%
6	93.10%	82.64%	93.94%	151.47%	96.28%	78.02%
7	86.90%	76.36%	118.66%	144.12%	104.65%	93.96%
8	99.31%	85.12%	112.77%	151.47%	113.49%	82.42%
9	111.72%	96.69%	95.42%	111.27%	646.51%	93.96%
10	94.48%	84.30%	128.81%	146.08%	145.58%	84.07%
11	115.17%	96.69%	171.85%	112.75%	424.65%	89.01%
12	94.48%	85.95%	116.04%	145.10%	96.28%	82.42%
13	100.00%	100.00%	100.00%	100.00%	100.00%	100.00%
14	98.85%	99.24%	74.59%	105.24%	107.82%	100.00%
15	74.71%	77.86%	103.50%	136.19%	93.30%	100.58%
16	80.46%	83.21%	108.21%	139.52%	102.23%	101.73%
17	82.18%	85.50%	108.43%	140.00%	111.73%	94.80%
18	63.79%	66.87%	113.91%	123.33%	83.24%	96.53%
19	73.56%	75.04%	81.93%	132.86%	85.47%	82.66%
20	77.59%	86.26%	67.47%	133.81%	74.30%	95.38%
21	94.83%	96.18%	106.57%	100.95%	636.87%	108.09%
22	76.44%	80.92%	75.36%	126.19%	143.58%	108.67%
23	94.83%	97.71%	90.91%	101.43%	397.21%	104.62%
24	76.44%	83.21%	72.18%	129.52%	110.61%	93.64%

Table 6. Average atomic content of depth profile calculated relative to control wafers 1 and 13.

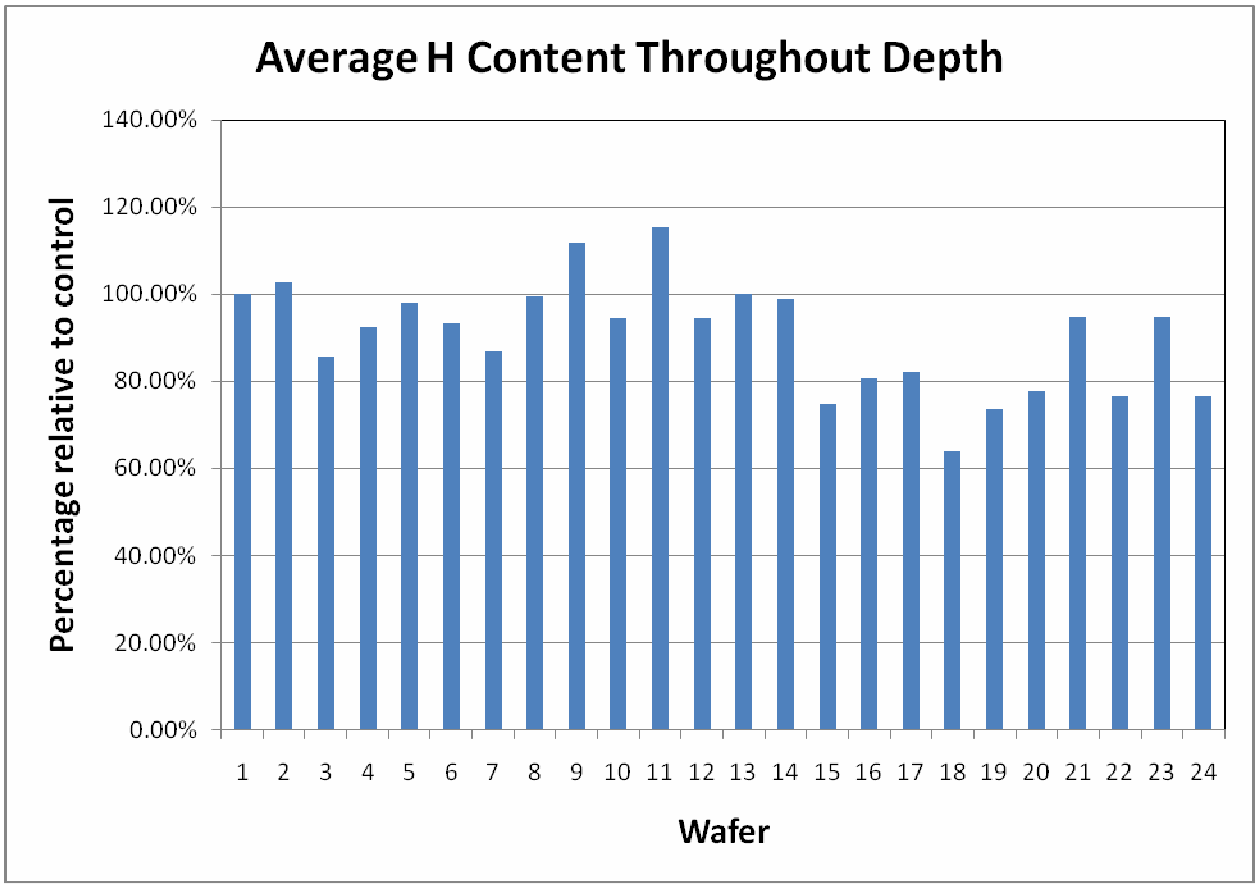

Figure 42. Comparison of H Content across all 24 wafers.

Figure 42 tabulates the comparison of hydrogen content for all 24 wafers. The highest increase in hydrogen content was observed in wafers processed with H_2Ar ash. All wafer ashed with O_2 plasma exhibited a depletion in hydrogen content. The decomposition of functional methyl groups are observed since the O_2 plasma has recombined with hydrogen to form water vapor and Si-OH groups. This consistency matches the XPS and FTIR data that was measured previously.

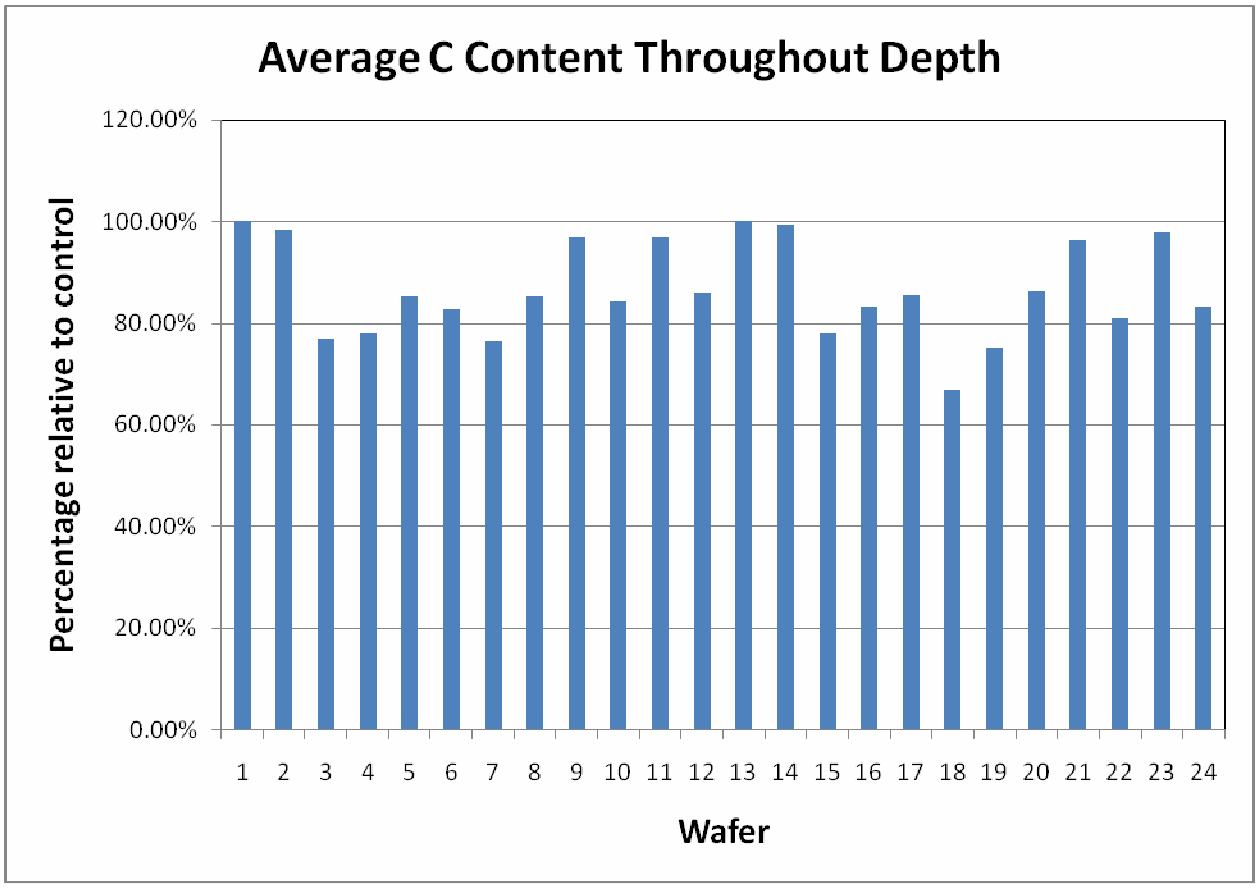

Figure 43. Comparison of C Content across all 24 wafers.

Figure 43 compares the relative carbon depletion across all 24 wafers. Both OSG3 and OSG4 films yield consistent results where the least amount of depletion was observed with a H_2Ar ash. Wafers processed in O_2 plasma at higher pressures compared to lower pressures maintained more functional methyl groups. However, the OSG4 wafer processed with a single wafer clean also retained most of its carbon content.

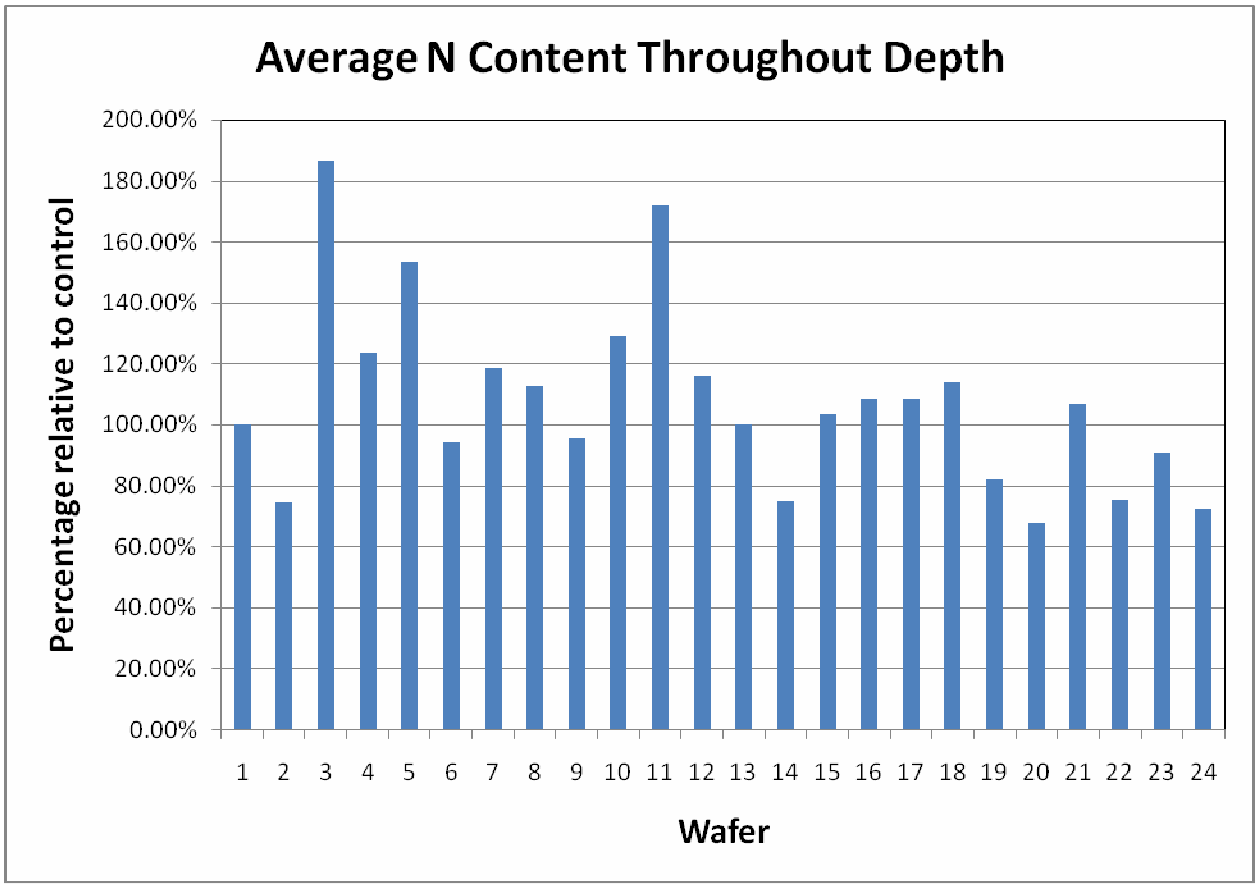

Figure 44. Comparison of N Content across all 24 wafers.

The variation in nitrogen content is depicted in Figure 44. OSG3 wafers showed a higher increase in nitrogen compared to OSG4 wafers. Wafers 2, 6, 9, 13, 14, 19, 20, 22, and 23 all exhibited a decrease in nitrogen relative to control wafers. No strong correlation has been found between the tested process parameters.

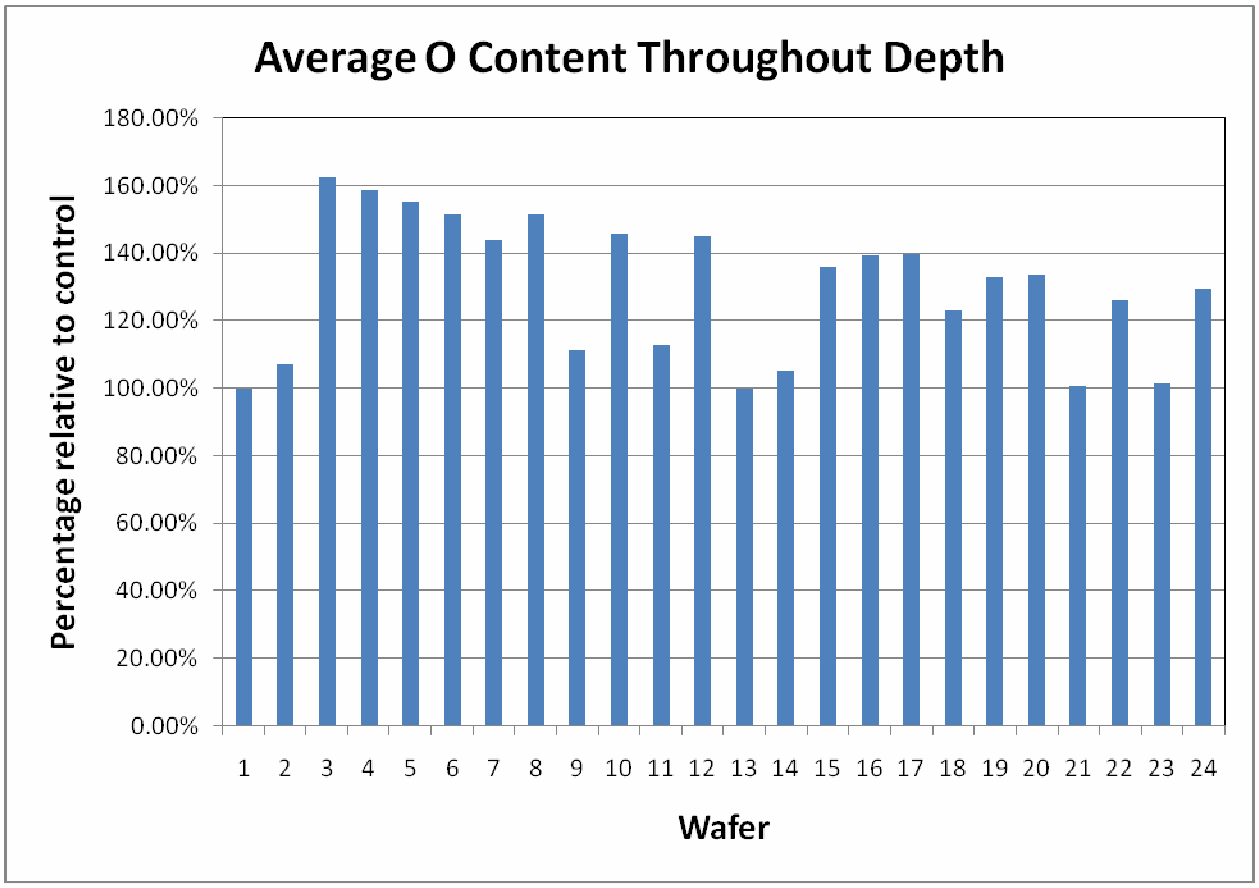

Figure 45. Comparison of O Content across all 24 wafers.

The average calculated oxygen content throughout all OSG films found in Figure 45 confirmed an increase compared to their corresponding control films. OSG3 wafers experienced heavier surface oxidation compared to OSG4 wafers. As expected, wafers processed in H_2Ar plasma show less oxygen buildup near the surface compared to O_2 plasma process.

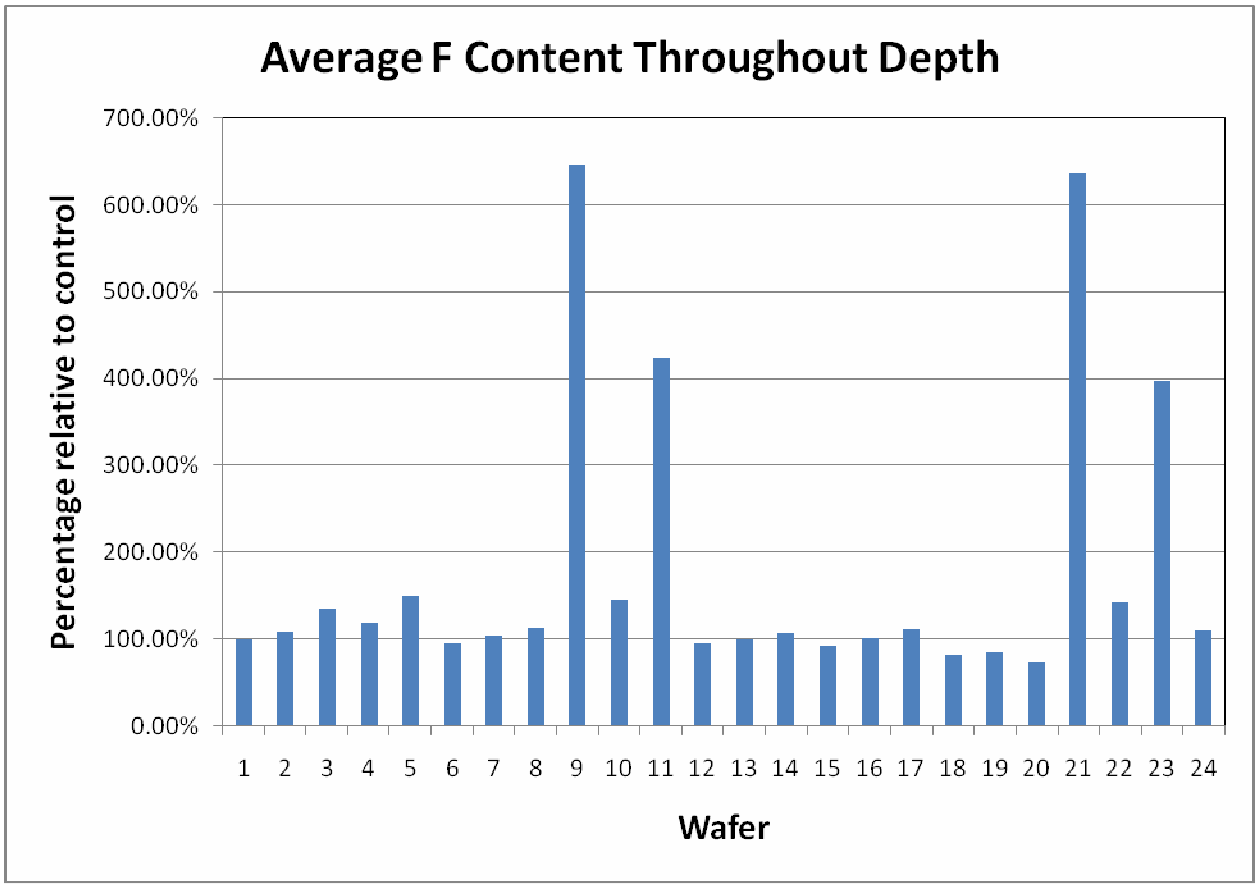

Figure 46. Comparison of F Content across all 24 wafers.

Wafers processed through batch clean exhibited the highest increase in fluorine content. The DSIMS data in Figure 46 is congruent with XPS analysis since the batch clean immerse wafers into a fluorine-containing bath chemistry. Wafers 9, 11, 21, and 23 were processed with batch clean. The rest of the wafers have a comparable amount of fluorine content.

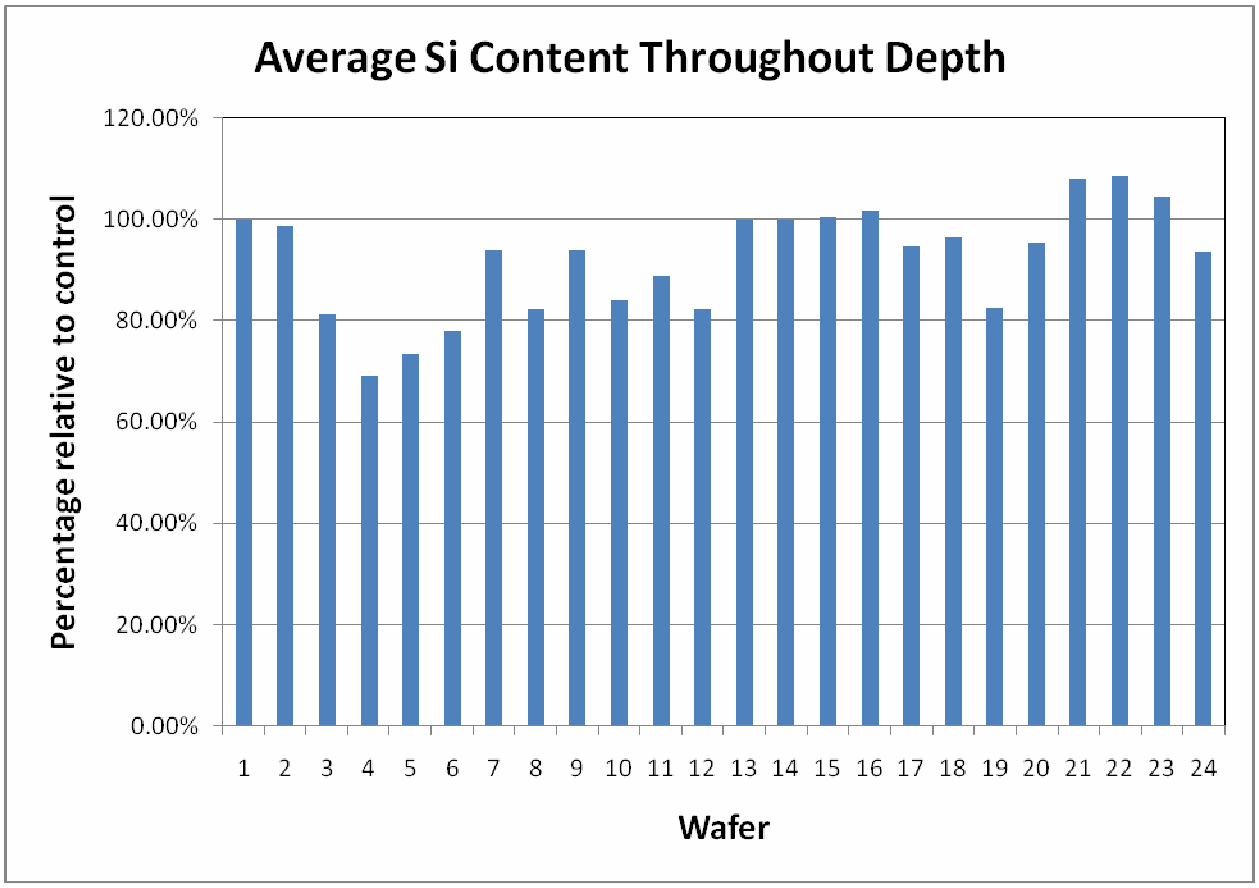

Figure 47. Comparison of Si Content across all 24 wafers.

Silicon bonds exhibited various bond breakages in Figure 47 with no consistent correlation between processes. The amount of silicon is most likely dependent on the location of ion beam sputtered onto the wafer.

5. Developing a Process Window

The development of a process window prior to the fabrication of test chips is necessary in producing the most desired results in formation of copper interconnects and intermetal dielectric layers. JMP software was used to create a prediction profile of all the process parameters analyzed.

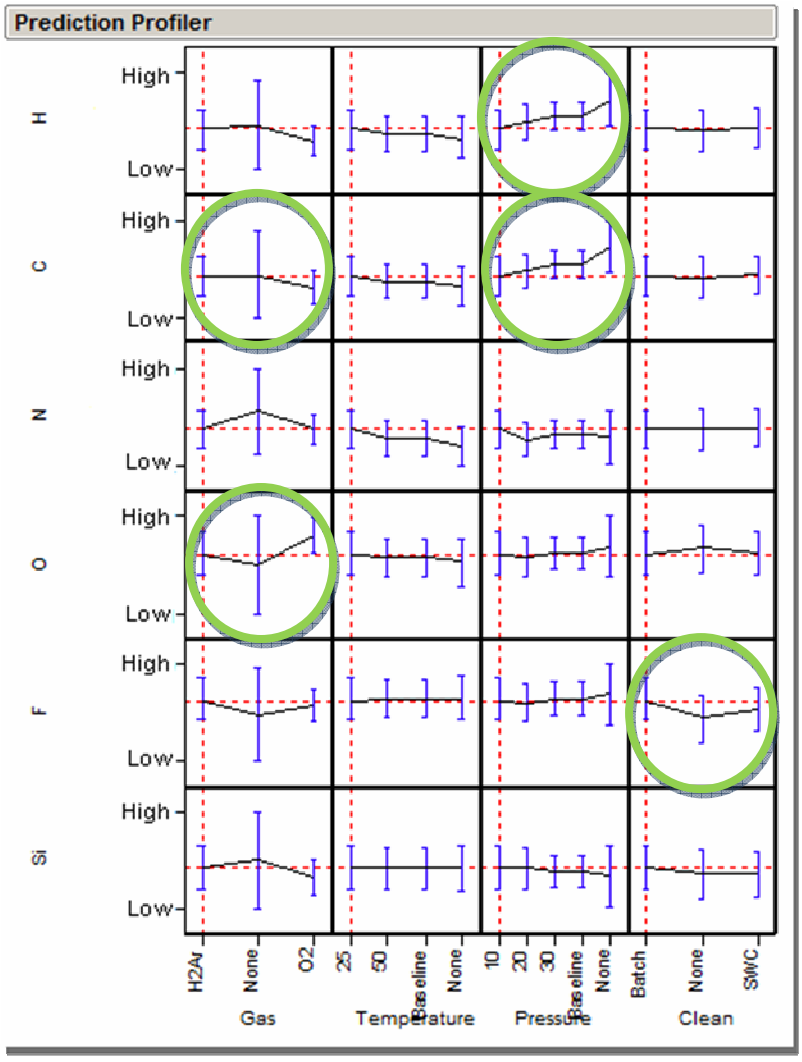

Figure 48. Prediction Profiler of process parameters vs. atomic content

The most notable process parameter interactions are summarized in Figure 48. A higher decrease in carbon species is found with O_2 plasma ash compared to H_2Ar ash. Both hydrogen and carbon species exhibit less depletion as pressure increases. The wafer surface oxidizes in O_2 ash and more oxygen species become present within the OSG film. Single wafer cleans also added less fluorine species compared to the batch clean process. Based on these results, three new plasma ash recipes were designed for chip fabrication: O_2 baseline ash, O_2 margin ash, and H_2Ar ash processes.

6. Test Chip Fabrication

A short flow wafer lot of test chips was obtained for two types of OSG films, two types of clean recipes post-etch (single wafer and batch), and three ash recipes (H_2Ar, O_2 Baseline, O_2 Margin). Each split [OSG3/4 film deposition, H_2Ar/O_2 baseline/O_2 margin ash, fluorine Batch/single wafer clean] occurs in the back end of the line (BEOL) at three levels Trench 1, Via1, and Trench 2.

Two clean regimes will be compared in this short flow. During batch clean, the lot of wafers is immersed into a clean hood. The clean chemistry is set to flow from bottom to top for roughly an hour. The chemistry is generally replaced every 36 hours. In single wafer clean, less chemistry is consumed since it is dispensed from a nozzle onto each individual wafer resulting in a lower cost of ownership. The timed dispense usually lasts one to two minutes and to make up for capacity, single wafer clean hoods contain several chambers to clean multiple wafers simultaneously. Industry is trending toward using single wafer cleans to conserve chemistry and increase capacity. Both clean methodologies were compared.

Three ash regimes were also tested used to process this lot of test wafers. The differences between H_2Ar and O_2 gas flows are mainly ash times and the effects they have on low-k dielectric films. H_2Ar requires a longer ash time but has been found to prevent carbon depletion compared to O_2. This carbon depletion is detected through measuring an increase in the effective dielectric k-values. Ash time is doubled in the O_2 margin recipe compared to the O_2 baseline recipe. The purpose of such an aggressive ash is to prove the yield margin of the ash process window. Table 7 depicts the three possible scenarios that can occur, each of which can potentially provide a wealth of information.

Wafer	Film	Ash	Clean	Split
1	OSG3	H2Ar	Batch NE14	1
2	OSG3	H2Ar	Batch NE14	1
3	OSG3	H2Ar	Batch NE14	1
4	OSG3	H2Ar	Batch NE14	1
5	OSG3	O2 Baseline	Batch NE14	2
6	OSG3	O2 Baseline	Batch NE14	2
7	OSG3	O2 Baseline	Batch NE14	2
8	OSG3	O2 Baseline	Batch NE14	2
9	OSG3	O2 Margin	Batch NE14	3
10	OSG3	O2 Margin	Batch NE14	3
11	OSG3	O2 Baseline	SWC NE14	4
12	OSG3	O2 Baseline	SWC NE14	4
13	OSG4	H2Ar	Batch NE14	5
14	OSG4	H2Ar	Batch NE14	5
15	OSG4	H2Ar	Batch NE14	5
16	OSG4	H2Ar	Batch NE14	5
17	OSG4	O2 Baseline	Batch NE14	6
18	OSG4	O2 Baseline	Batch NE14	6
19	OSG4	O2 Baseline	Batch NE14	6
20	OSG4	O2 Baseline	Batch NE14	6
21	OSG4	O2 Margin	Batch NE14	7
22	OSG4	O2 Margin	Batch NE14	7
23	OSG4	O2 Baseline	SWC NE14	8
24	OSG4	O2 Baseline	SWC NE14	8

Table 7. Treatment combinations for DD chip

The test chip is designed with very large via chains and serpentine/comb structures to facilitate defect detection. It also contains electromigration structures, Kelvin vias and other miscellaneous structures. The wafers were fabricated to compare processes that impact via and trench yields that are generally representative of production. A great advantage in fabricating test chips is the short amount of time it takes to fabricate compared to product wafers. The lot was probed at Metal 2 after its completion of the process flow. Parametric and sameness data was studied according to each treatment combination. After parametric test, electrical breakdown and via stress migration data was also collected.

7. Metal I and II Electrical Data on Test Chip

Fabricated test chips were probed at both Metal 1 and Metal 2. At Metal 1, split 6 exhibited the lowest yields, whereas the other splits were comparable. Two highest yielding splits at Metal 1 include OSG3 film processed with a baseline O_2 ash process and single wafer clean and an OSG4 film processed with a baseline H_2Ar ash process and batch baseline process. At Metal 2 parametric, both O_2 margin splits exhibited zero via yields due to opens whilst splits 1, 4, 5, and 8 have comparable yield. Sample probe measurements were taken and displayed in Figures 49 through 65. The top graph represents the probe time versus value measured and the bottom graph displays the wafer number versus value measured.

Figures 49 through 53 depict a sample of Metal 1 probe data for several comb capacitances and line resistances. Each probe chart has specific targets, lower spec limits, and upper spec limits defined for the process window. All Metal 1 probe data show to be within spec range except for Figure 52 which represents the M1 140 nm Iso Line Resistance. Splits 3, 4, 7, and 8 came close to lower spec limit.

b

Figure 49. Metal 1 Comb CSRP Shorts

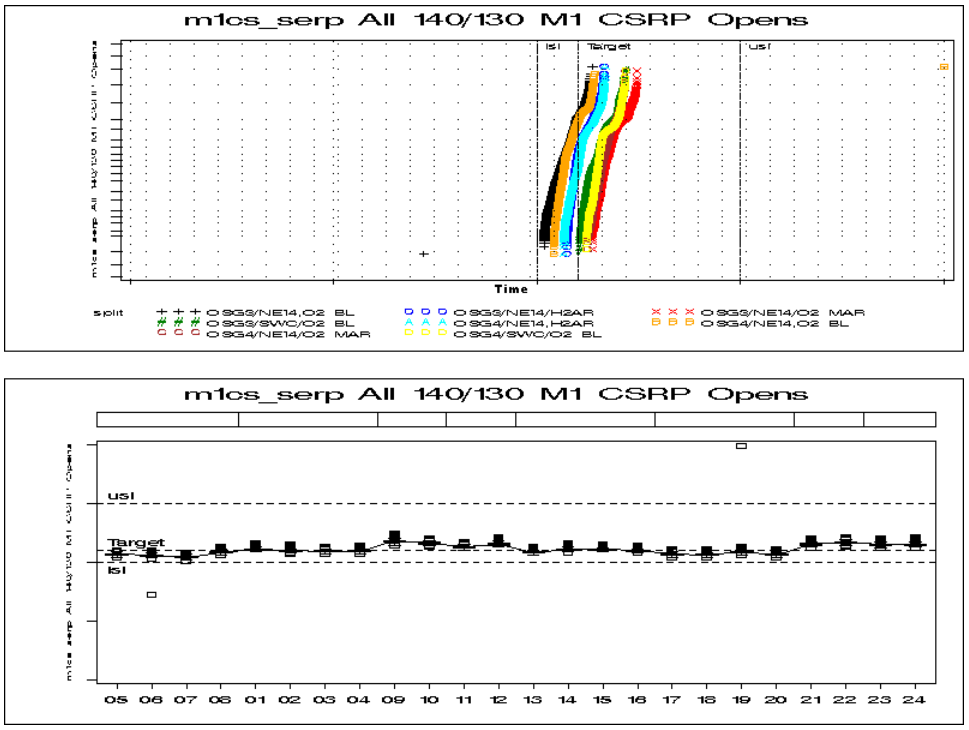

Figure 50. M1 Serpentine CSRP Open

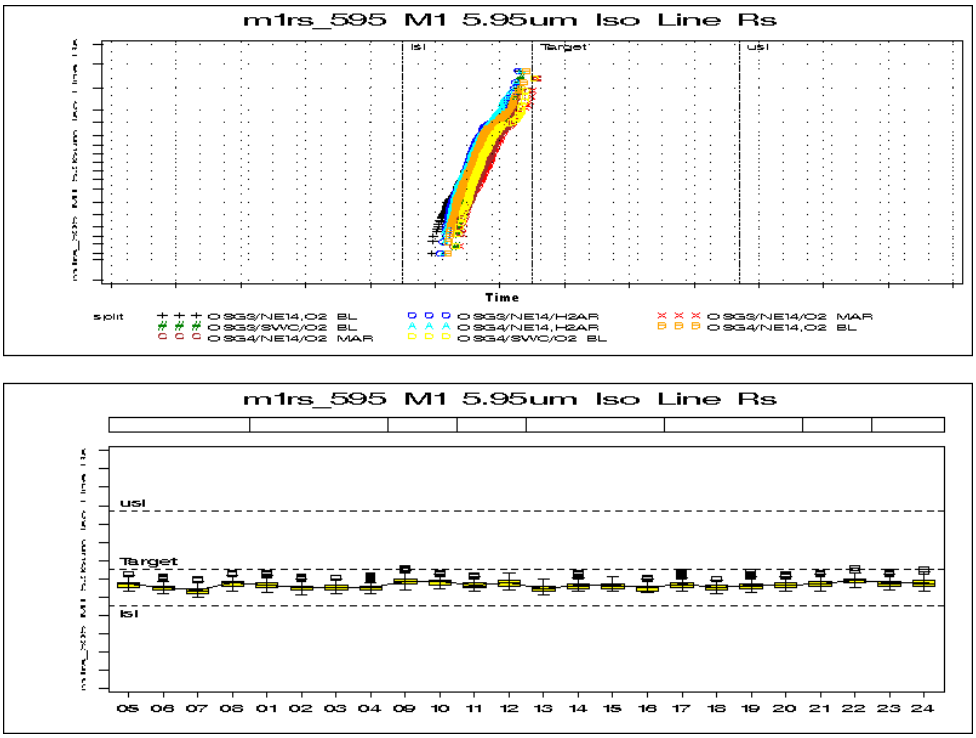

Figure 51. Metal 1 5.95 µm Iso Line Resistance

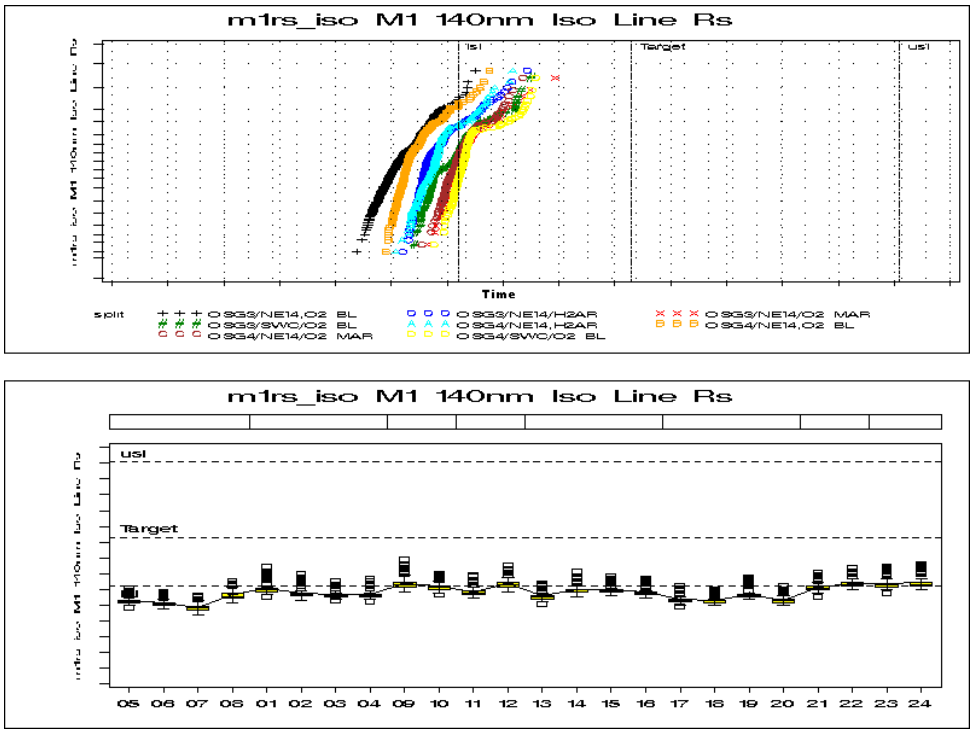

Figure 52. M1 140 nm Iso Line Resistance

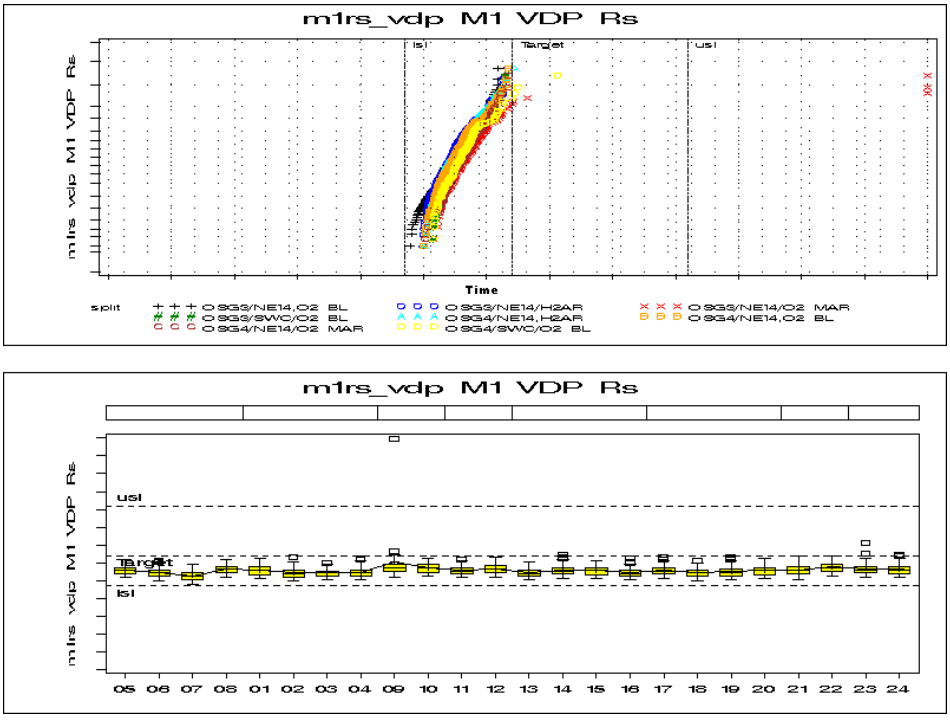

Figure 53. M1 V_{dp} Resistance

Figures 54 through 56 represent line resistances probed at Metal 2. Figure 55 similar to Figure 52 has line resistances below the specified lower spec limit for the same 140 nm structure. This is most likely due to other processes not related to the plasma ash and wet clean splits since every wafer experiences approximately the same line resistance.

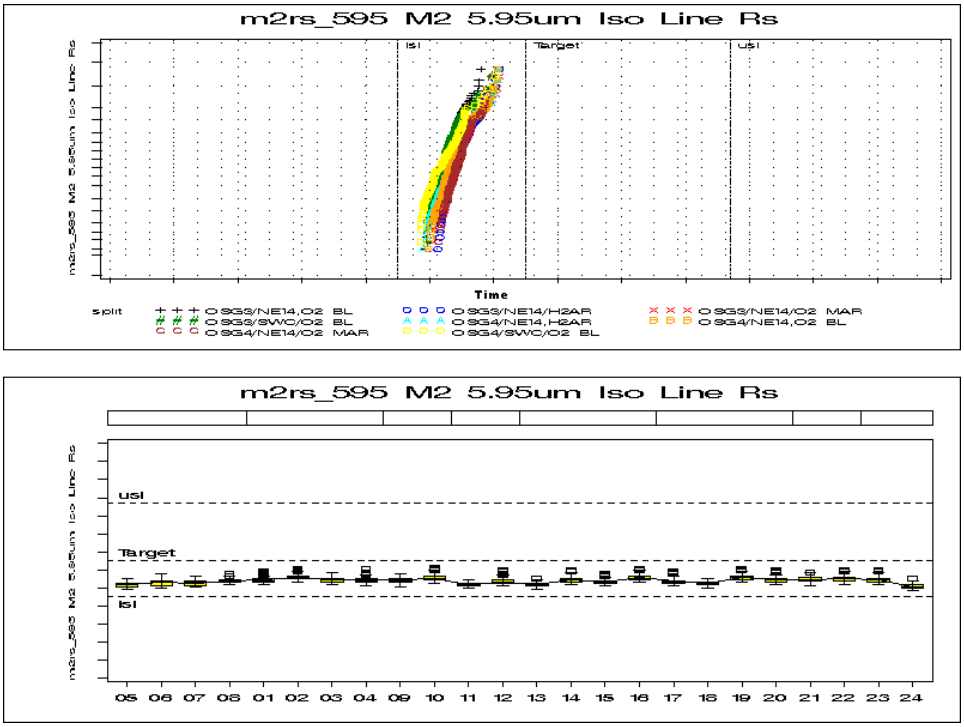

Figure 54. M2 5.95 µm Iso Line Resistance

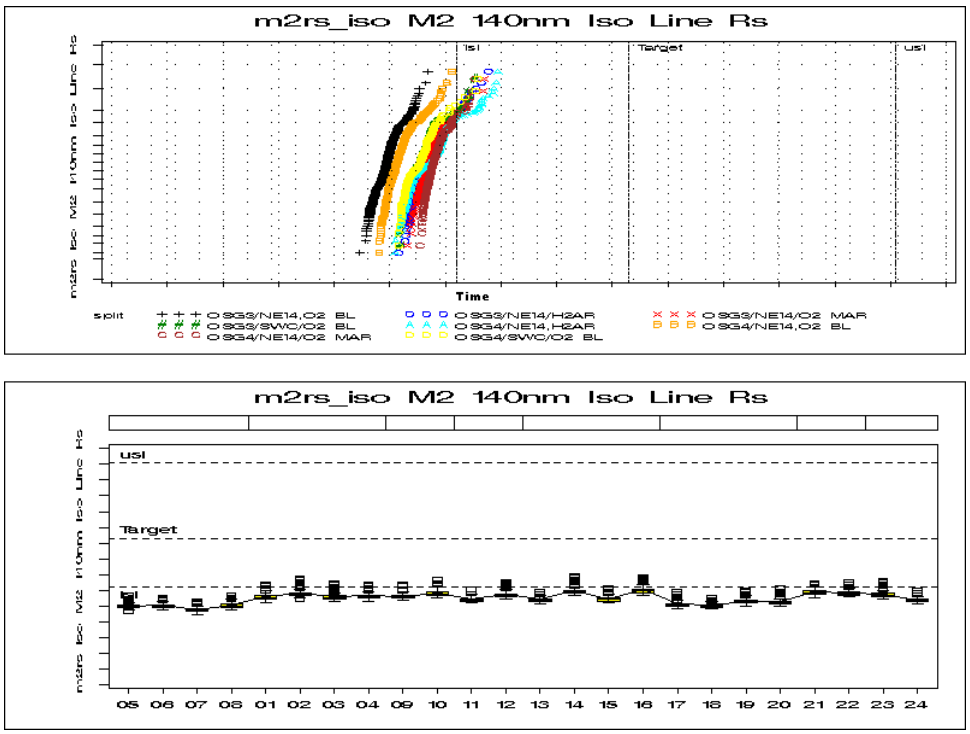

Figure 55. M2 140 nm Iso Line Resistance

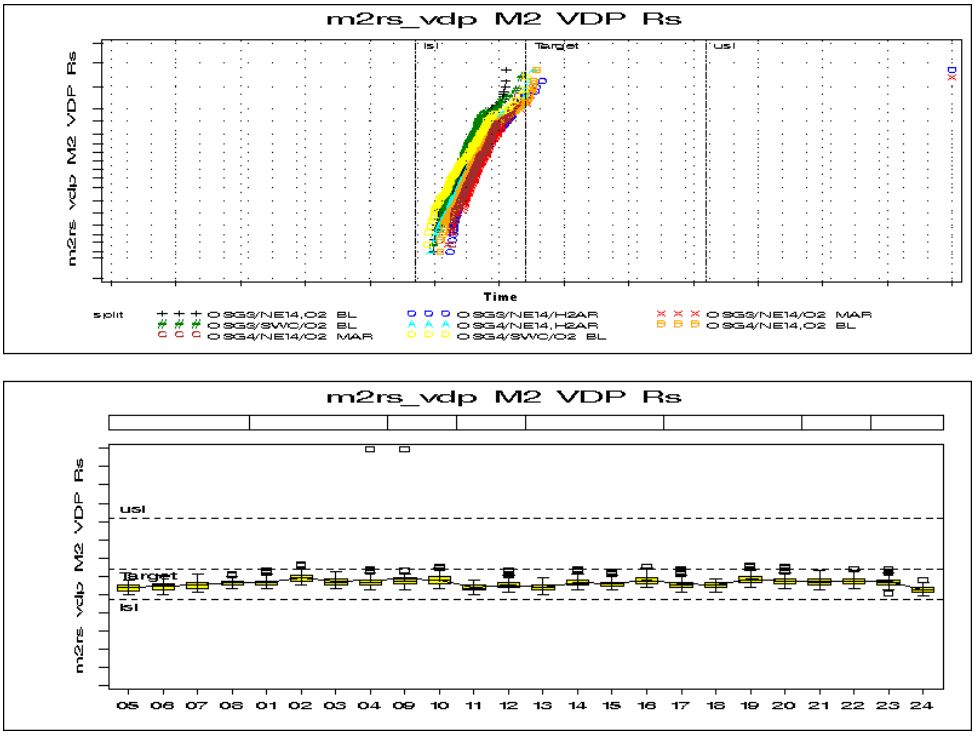

Figure 56. M2 V_{DP} Resistance

Figures 57 through 65 represent various via chain shorts, via chain resistances, and Kelvin square shorts measured through via stress migration tests. These migration tests were performed by placing the wafers inside an oven for a long time to test temperature stresses. Splits 3 and 7 processed with the O_2 margin processes all exhibit zero via yields as expected from the process parameters. In terms of overall yield, splits 1 and 5 processed with H_2Ar plasma processes using OSG3 and OSG4 exhibited the best performance.

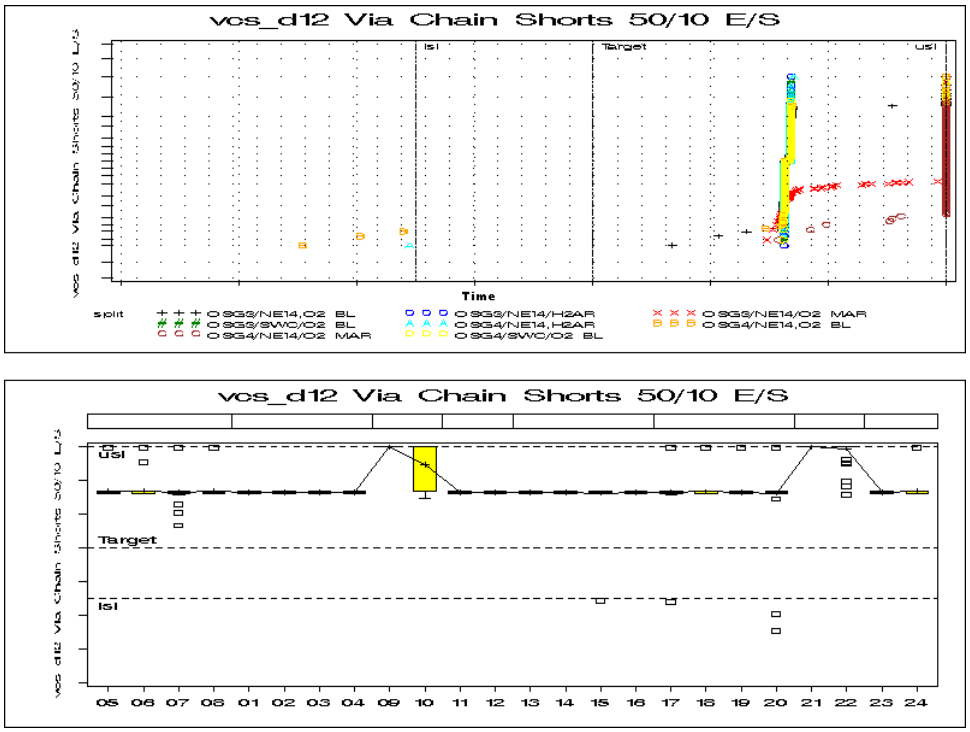

Figure 57. Via Chain Shorts Etch Stop

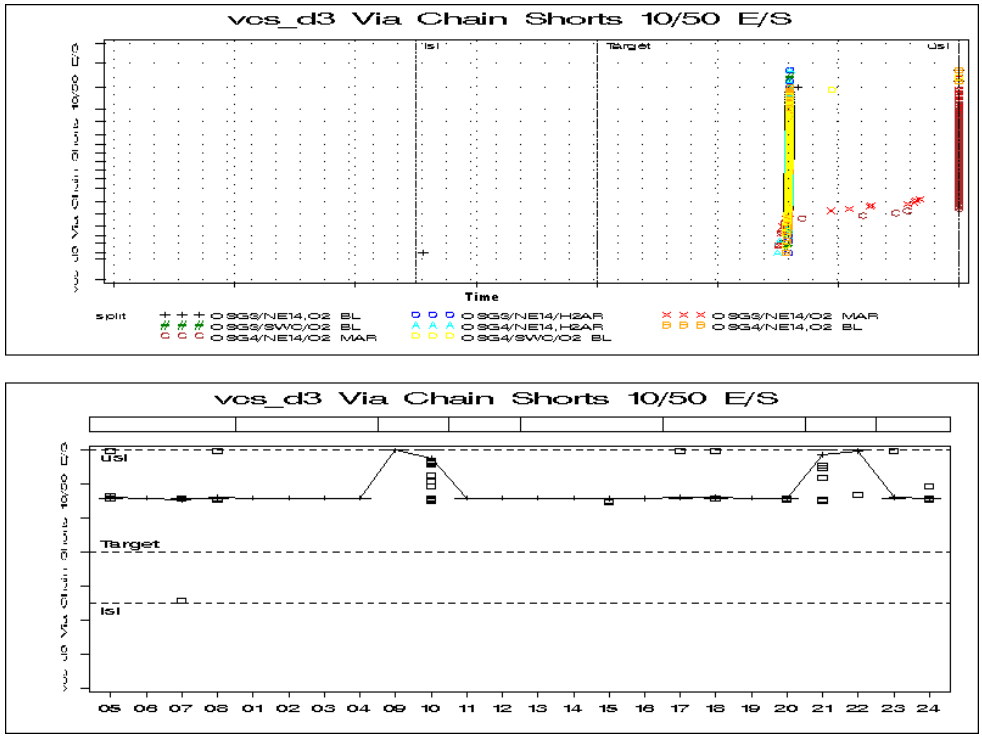

Figure 58. Via Chain Shorts 10nm line/50 nm width

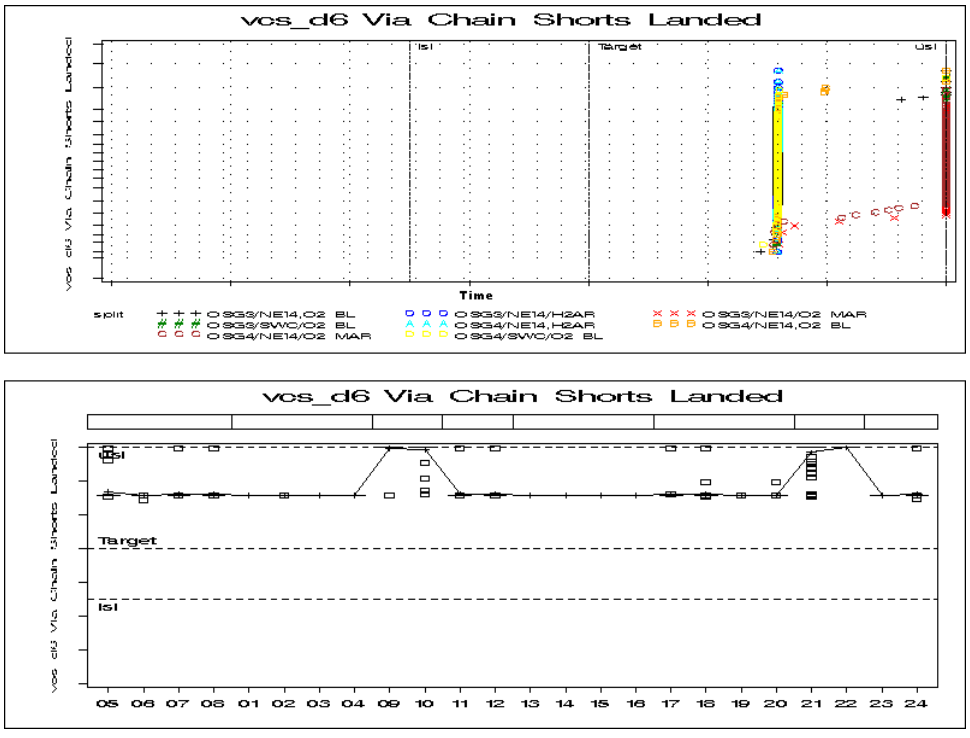

Figure 59. Via Chain Shorts Landed

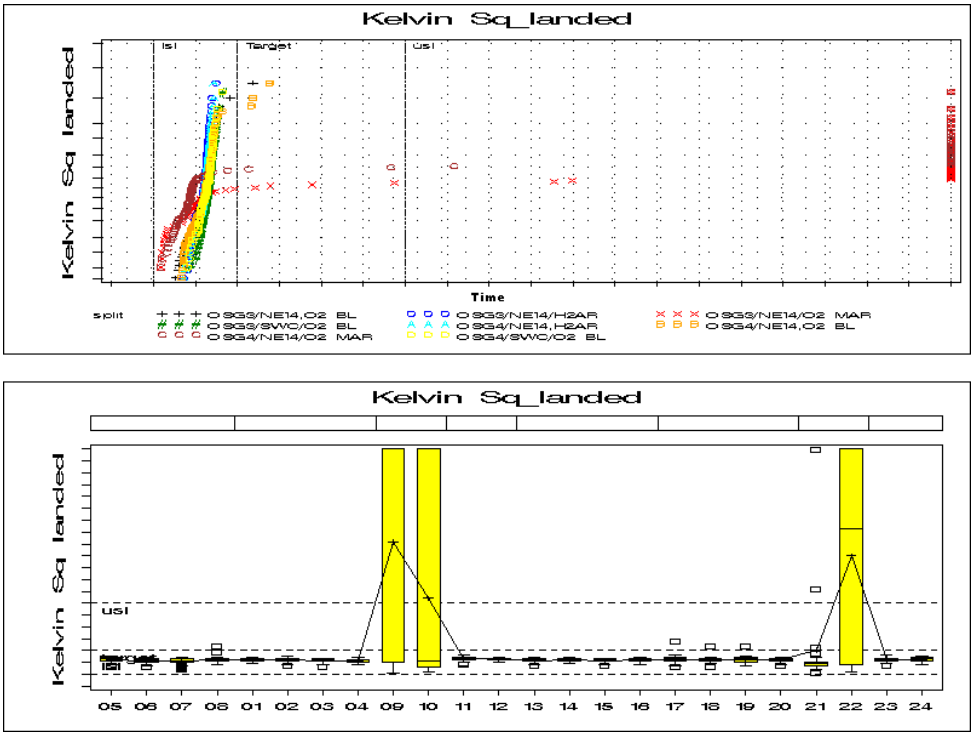

Figure 60. Kelvin Sq Landed

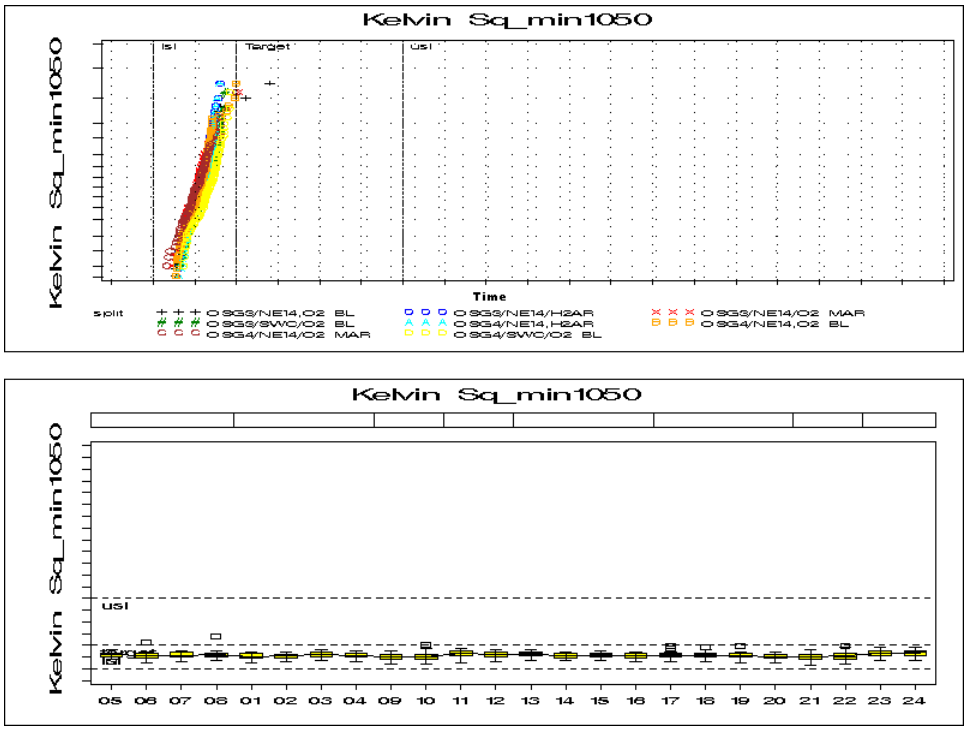

Figure 61. Kelvin Sq 1050 Min

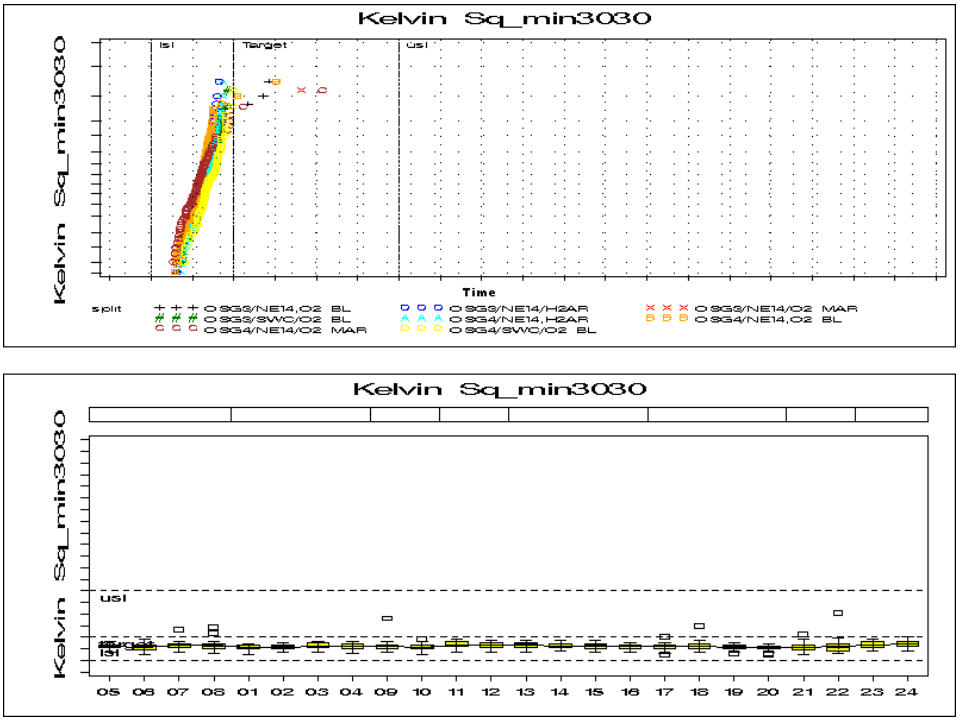

Figure 62. Kelvin Sq 3030 Min

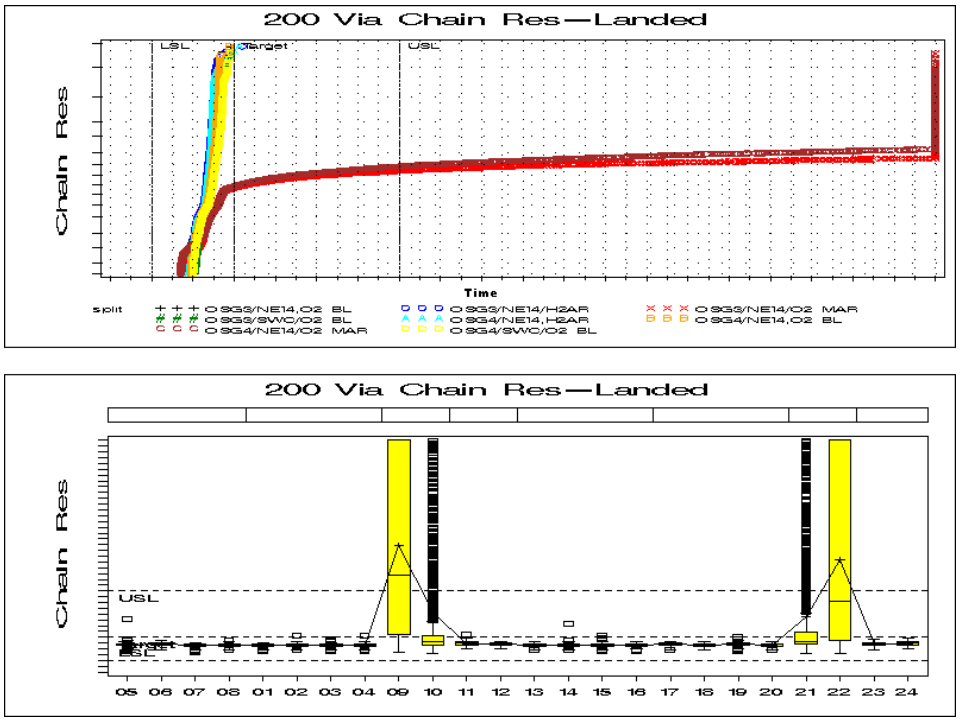

Figure 63. 200 Via Chain Resistance – Landed

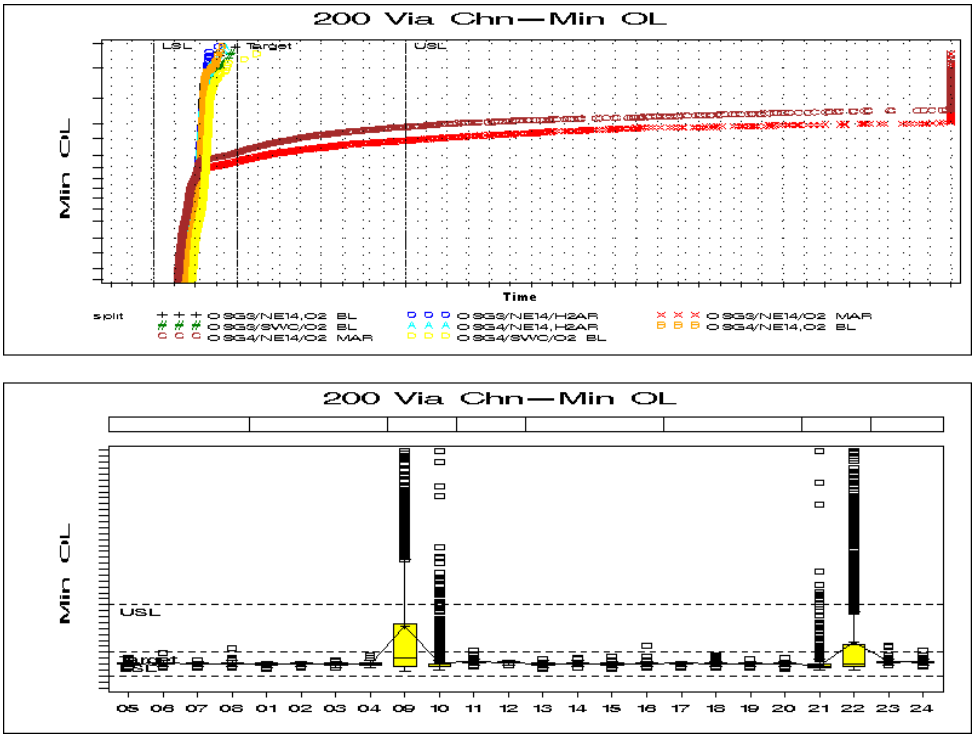

Figure 64. 200 Via Chain – Minimum Overload

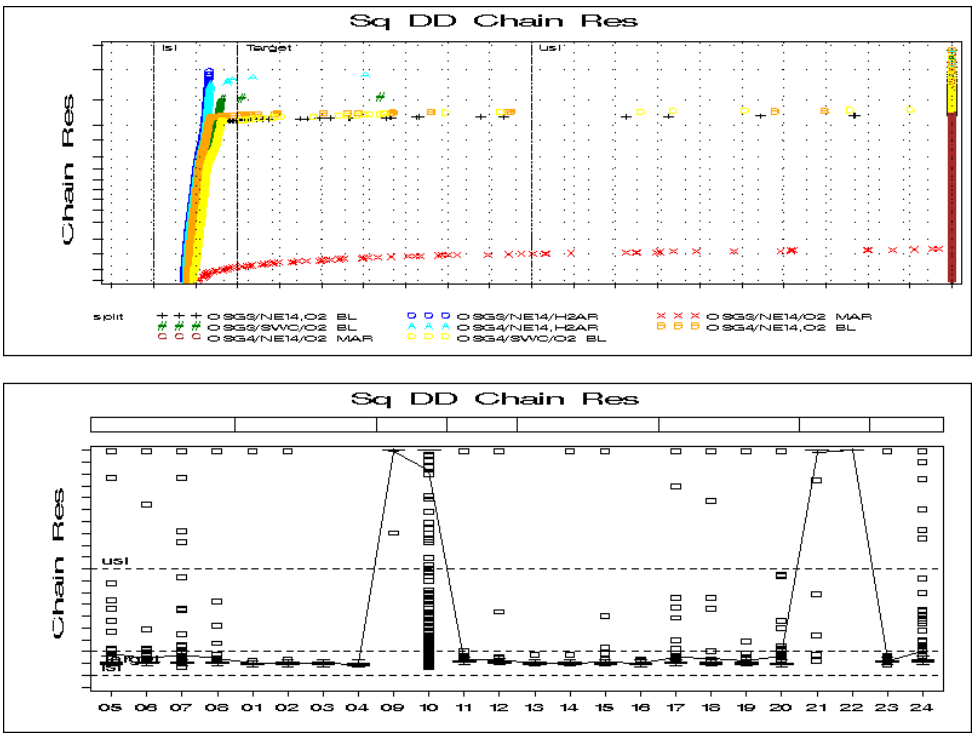

Figure 65. Square Defect Density Chain Resistance

8. Conclusions and Future Investigations

An effective process window for resist stripping on Back End of Line (BEOL) low-k OSG films using H_2Ar and O_2 plasma ash combined with batch clean and single wafer clean has been developed. The quality of OSG film generally compromised during the removal of resist has been observed. Pre- and post-plasma ash OSG film composition has been characterized using FTIR spectrometry, XPS, DSIMS, and SPV on pilot wafers.

A direct correlation between thickness delta between pre- and post-processing versus measured dielectric content has been realized with the use of SPV. FTIR data exhibited less plasma damage using H_2Ar plasma ash compared to O_2 ash for both OSG3 and OSG4 films. XPS data shows that the H_2Ar process was able to maintain over 60% of its carbon content due to less breakage of methyl groups. DSIMS data comparison of atomic depth profiles consisting of carbon, fluorine, silicon, hydrogen, oxygen, and nitrogen has been analyzed. The least amount of carbon depletion was found when processing wafers through H_2Ar ash. The most amount of fluorine content was found after the wafers were batch cleaned. Native oxide thickness also exhibited an increase on OSG wafers processed through O_2 ash.

A lot of test chips was also fabricated and probed at the Metal 1 and Metal 2 levels for serpentine line resistances and comb capacitance measurements to characterize the performance of the OSG film as an ILD. The two highest yielding splits were processed with H_2Ar plasma ash and batch clean. This direct correlation is found across all analytic techniques and test chip yields.

Several new processing possibilities may also be tested in the future by combining single wafer clean with H_2Ar process. This may require fine tuning process conditions to prevent

mechanical breakage. As dielectric values < 2.0 are introduced in the semiconductor industry, novel ways of resist stripping and clean must accommodate this rapid change.

9. References

[1] T. Suemasa et. al. "Low-k Etch/Ash for Copper Dual Damascene," *Proceedings of SPIE*, 2000, pp. 281-286.

[2] S. Savas et. al. "Using an ICP-Based Strip System to Perform Resist and Barrier-Layer Removal in Copper Low-k Processes," *Micro*, Oct/Nov 2004.

[3] S. Savas, "Inductively Coupled Plasmas for Highly Efficient and Low Damage Resist Stripping," American Vacuum Society, 1996, pp. 127-130.

[4] J. S. Tsai et. al. "Effect of Ash Process on Leakage Mechanism of Cu/ELK (k=2.5) Interconnect for 65/45nm Generation," *IEEE*, 2005, pp. 94-96.

[5] E. T. Ryan et. al. "Integration Damage in Organosilicate Glass Films," *IEEE*, 2002, pp. 27-29.

[6] B. White et. al. "Neutral Oxygen Beam Stripping of Photoresist on Porous Ultra Low-k Materials," *IEEE*, 2003, pp. 153-155.

[7] Tokyo Electron Limited, "Process Engineering Manual, Telius 305 DRM," Revision 1.1.1, 2001, pp. 19-49.

[8] P. B. Smith, P. D. Matz. "Damage-free resist resist removal processing for ultra low-k processing," US Patent 7067441, July 2006.

[9] J. Jacques et. al. "Environmental Effects on Crack Characteristics for OSG Materials," *Mat. Res. Soc. Symp. Proc.*, Vol. 875, 2005, pp. O10.6.1-O10.6.6.

[10] H. Cui et. al. "Ultra Low-dielectric-constant Materials for 65nm Technology Node and Beyond," *Mat. Res. Soc. Symp. Proc.*, Vol. 812, 2004, pp. F2.8.1-F2.8.10.

[11] P. T. Liu et. al. "Effective Strategy for Porous Organosillicate to Suppress Oxygen Ashing Damage," *Electrochemical and Solid-State Letters*, Vol. 5., 2002, pp. G11-G14.

[12] A. Y. Du et. al. "The Organic low-k Materials Microstructure Study," *Proceedings of IEEE*, 2002, pp. 179-182.

[13] M. A. Worsley et. al. "The Study of Modified Layers in SiCOH Dielectrics Using Spectroscopic Ellipsometry," *Mat. Res. Soc. Symp. Proc.*, Vol. 766, 2003, pp. E3.29.1- E3.29.5.

[14] P. Hoffman et. al. “Characterization of Chemical Bonding in Low-k Dielectric Materials for Interconnect Isolation: A XAS and EELS Study,” *Mat. Res. Soc. Symp. Proc.*, Vol. 914, 2006, pp. F01-F08.

[15] E. T. Ryan, “Nanoporous Materials Integration Into Advanced Microprocessors,” *Mat. Res. Soc. Symp. Proc.*, Vol. 863, 2005, pp. B2.1.1-B2.1.12.

[16] J. S. Tsai et. al. “Characterization of Strip Induced Damage in Ultra Low-k Dielectric,” *IEEE*, 2005, pp. 183-185.

[17] J. C. Lin et. al. “Via First Dual Damascene Integration of Nanoporous Ultra Low-k Material,” *IEEE*, 2002, pp. 48-50.

[18] E. Niehuis, “Time-of-Flight SIMS,” Surface Analysis, pp. 269-276.

[19] A. Benninghoven, “Chemical Analysis of Inorganic and Organic Surfaces and Thin Films by Static Time-of-Flight Secondary Ion Mass Spectrometry (ToF-SIMS),” *Chem. Int. Ed. Engl.*, Vol. 33, 1994, pp. 1023-1043.

[20] C. Engrand et al., "Chemometric evaluation of time-of-flight secondary ion mass spectrometry data of minerals in the frame of future in situ analyses of cometary material by COSIMA onboard ROSETTA". *Rapid Communications in Mass Spectrometry* **20**: 1361-1368.

[21] Thermal Nicolet Corporation. “Introduction to Fourier Transform Infrared Spectroscopy,” 2001.

[22] Pike Technologies. “Transmission Sampling Techniques – Theory and Applications,” 2005.

[23] Fourier Infrared Spectroscopy. Wikipedia Homepage. 2006. <http://en.wikipedia.org/wiki/Fourier_transform_spectroscopy>

[24] X-ray photoelectron Spectroscopy. Wikipedia Homepage. June 27, 2006. < http://en.wikipedia.org/wiki/X-ray_photoelectron_spectroscopy>

[25] Dieter K Schroder, “Surface voltage and surface photovoltage: history, theory, and applications.” *Measurement Science and Technology*, **12**, 2001, R16-R31.

[26] Surface Photovoltage. Wikipedia Homepage. December 24, 2006. < http://en.wikipedia.org/wiki/Image:Spvapparatus.png>

[27] Leeor Kronik, Yoram Shapira, “Surface photovoltage phenomena: theory, experiment, and applications.” *Surface Science Reports*, **37**, 1999, 1-206.

[28] H. Xu. “Resist Stripping Process Development for Porous Low-k Dielectric Materials,” *IEEE/SEMI Advanced Manufacturing Conference*, 2003, pp. 142-147.